The Effect of Galectin-3 in Experimental Uraemia.

Findlay, Andrew

The Effect of Galectin-3 in Experimental Uraemia

Thesis submitted for the degree of

Doctor of philosophy

Dr Andrew Findlay

Translational Medicine and Therapeutics

William Harvey Research Institute

Queen Mary University of London

2015

Table of Contents

Declaration

I declare that this thesis has been composed by me and that the work of which it is a record has been undertaken by me. Any of the results that were generated in collaboration with others is fully acknowledged. This work has not previously been presented to any institution for a higher degree.

Andrew Findlay

Acknowledgements

I would like to thank my supervisors, Professor Magdi Yaqoob and Dr Steven Harwood who provided invaluable guidance and motivation to complete this work. I am grateful to Julius Kieswich for his mentoring on small animal work including intravital microscopy. I wish to thank Egle Solicito for her help in teaching the methods behind FACS and analysing FACS data. Finally I would like to thank my wife for her enormous support in helping me complete this project.

Presentations associated with this work

1. Is Galectin-3 responsible for microvascular dysfunction and progressive interstitial fibrosis of Chronic Kidney Disease? British Renal Association, Bournemouth, 2013

2. Elevated Soluble and Galectin-3 expressing monocyte levels in experimental uraemia are reversed by anti-Advanced Glycation End products therapy. British Renal Association, Bournemouth, 2013.

3. Leucocyte adherence by intra-vital microscopy, plasma and monocyte Galectin-3 levels are elevated in a model of chronic kidney disease. British Renal Association, Gateshead, 2012.

4. Serum Galectin-3 and leucocyte-endothelial adherence are increased in a murine model of chronic uraemia. American Society of Nephrology, Philadelphia, 2011

Abbreviations

AD	0.25% Adenine diet
ADHF	Acute decompensated Heart Failure
AGE	Advanced Glycation End products
AGE-BSA	Advanced Glycation end product modified Bovine serum Albumin
ALE	Advanced Lipoxidation End products
AMP	Adenine Monophosphate
APRT	adenine phosphoribosyl transferase
ASN	American society of Nephrology
BAL	Broncho-alveolar lavage
BMI	Body Mass Index
BSA	Bovine Serum Albumin
CCL4	Carbon tetrachloride
CCR2	Chemokine Receptor 2
CD11B	Cluster of Differentiation 11B
CD14	Cluster of Differentiation 14
CD16	Cluster of Differentiation 16
CD68	Cluster of Differentiation 68
CHI3l3	Chitinase Like Protein 3
CHO	Chinese Hamster Ovary Cells
CKD	Chronic kidney Disease
CRD	Carbohydrate Recognition domain
CML	Carboxymethyllyseine
CX3CR1	CX3 Chemokine Receptor 1
DNA	2, 8 – dihydroxyadenine
ECM	Extra cellular membrane
eGFR	estimated Glomerular Filtration Rate
ELISA	Enzyme-linked immunosorbent assay
EMT	Epithelial Mesenchymal Transition
FACS	Fluorescence-Activated Cell Sorting

FDA	Federal Drug Administration
Gal-1	Galectin-1
Gal-3	Galectin-3
Gal-3 $^{-/-}$	Galectin-3 knockout mouse
GFR	Glomerular filtration rate
HBA1c	Glycated haemoglobin
HF	Heart failure
HSC	Hepatic Stellate cell
IEG	Immediate Early Gene
IFNγ	Interferon Gamma
IL-12	Interleukin 12
IL-13	Interleukin 13
IL-1β	Interleukin – 1β
IL-2	Interleukin 2
IL-6	Interleukin 6
IL-8	Interleukin 8
IPF	Idiopathic Pulmonary Fibrosis
KDA	kilo Dalton
KDOQI	Kidney Disease Outcomes Quality Initiative
LDL	Low density lipoprotein
LGALs3	Galectin-3 gene
LPS	Lipopolysaccharide
LVEDV	Left ventricular End Diastolic Function
Ly6C	Lymphocyte Antigen 6 C
M1	Classically activated
M2	Alternatively activated
MCP	Modified citrus pectin
MCP-1	Monocyte Chemotactic Protein 1
MDRD	Modification of Diet in Renal disease
MMP2	Matrix metalloprotease 2

mRNA	messenger ribonucleic acid
MSA	Modified mouse serum albumin
NFκβ	Nuclear factor kappa beta
NHANES	National Health and Nutrition Examination Survey
NTproBNP	N-terminal pro-brain natriuretic peptide
NYHA	New York Heart Association
PCR	Polymerase Chain Reaction
PIIINP	aminoterminal propeptide of procollagen 111
PINP	aminoterminal propeptide of procollagen 1
qPCR	real time Quantitative Polymerase Chain Reaction
RAGE	Receptor for Advanced Glycation End products
RANTES	chemokine (C-C motif) ligand 5
RCO	Reactive carbonyl Compounds
Retnla	Resistin like alpha
SD	Standard diet/chow
sGal-3	soluble Galectin -3
SMAD	Similarity to the Drosophila gene Mothers Against Decapentaplegic (MAD)
SR1	Scavenger Receptor 1
T-cell	T lymphocyte
TGFβ	Transforming growth factor beta
TH	T helper
TH1	T helper cell 1
TIMP1	tissue inhibitor of metalloproteinase-1
TNFα	Tumour necrosis factor α

USRDS	United States Renal Registry
UUO	Unilateral Ureteric Outflow Obstruction
WT	Wild Type
αSMA	Alpha Smooth Muscle actin

Abstract

The effect of Galectin-3 in Experimental Uraemia

Gal-3 is a glycoside binding protein elevated in inflammatory and fibrotic disease and highly expressed on cells of a monocyte/macrophage lineage. Elevated leucocyte Gal-3 expression encourages leucocyte-endothelial attachment and tissue transmigration. We demonstrate for the first time plasma soluble and monocyte Gal-3 is elevated in an experimental model of adenine induced uraemia and renal interstitial fibrosis. Galectin-3 knockout mice demonstrate an ameliorated adenine diet phenotype with less weight loss, lower serum creatinine and less severe renal tubular interstitial injury. This ameliorated phenotype is independent of numbers of infiltrating renal interstitial macrophages. Extra-renal leucocyte-endothelial transmigration in the cremasteric microvasculature visualised by intravital microscopy is not reduced in Galectin-3 knockout mice with adenine induced uraemia. The less severe disease phenotype of adenine induced uraemia in Galectin-3 knockout mice is therefore independent of effects on leucocyte-endothelial interactions. We show circulating monocyte subset phenotypic change and renal macrophage differentiation in adenine induced uraemia is altered in Galectin-3 knockout mice with reduced monocyte Ly6C expression and elevated renal macrophage markers of alternative (M2) differentiation. We conclude that Galectin-3 does play a role in chronic kidney disease and the development of renal fibrosis by influencing monocyte and macrophage differentiation towards an inflammatory

phenotype. Strategies to reduce monocyte and macrophage Galectin-3 may benefit progressive renal fibrosis in chronic kidney disease.

List of figures

List of tables

Introduction

Chapter 1

Introduction

1.1 The Galectin Family

1.1.1 Lectins

Lectins are widely conserved proteins that recognise and bind carbohydrate sequences on glycolipids and glycoproteins.[1-3] They are present in vertebrates, invertebrates, plants and protists (sponge and fungus) suggesting carbohydrate-lectin interactions in living organisms are important.[4, 5] The binding of some lectins to carbohydrate sequences can be as specific as antibody-antigen binding.[6] Carbohydrate sequences bound by lectins include the large amount of oligosaccharide glycoproteins and glycolipids on extracellular cell membranes and also circulating glycans including monosaccharides.[7] A small amino acid sequence on animal lectins termed the carbohydrate recognition domain (CRD) facilitates carbohydrate-lectin binding.[5] The CRD frequently commonly binds the terminal, non-reducing carbohydrate sequence of glycoprotein and glycolipids.[2] Lectins can be divided into groups based on CRD amino acid sequences.[5] The requirement of calcium to facilitate CRD binding to carbohydrate sequence is used to discriminate between the two main lectin groups C-type lectins (calcium dependent binding) and S-type lectins (calcium independent binding).[5] The C-type lectins include selectins, collectins and endocytic lectins, S-type lectins consist of galectins.[1, 5, 8, 9]

1.1.2 Galectins

Galectins are lectins that specifically bind β-galactosides present on cell surfaces and the extracellular matrix.[10] A β-galactoside is a molecule with a galactose residue bound to a non-carbohydrate (often a small organic molecule) for example lactose.[11]. β-galactosides are present in the glycoproteins, glycolipids and proteoglycans distributed over cell surfaces within the glycocalx (a glycoprotein-polysaccharide covering the cell membranes of most living cells). [12] Intracellular β-galactosides are less frequently occurring and are limited to proteins containing O-linked N-acetylglucosamine.[13] Most galectin binding to intracellular ligands is by protein-protein interaction rather than involving the CRD. [14] Galectins, by definition, have sequence homology for their CRD- a highly conserved canonical amino acid sequence. [15] The first galectin discovered was galectin-1 (Gal-1), then known as S-type lectin when identified in 1975 from the electric eel. [16] Gal-1 was discovered via its ability to agglutinate red blood cells, which was inhibited by the presence of β-galactosides. Further lectins with β-galactoside binding specificity were discovered independently from sponge, nematode and animal tissue.[17] These lectins had similar properties requiring no metal ion to facilitate binding (unlike C-type lectins), were water soluble and have an acetylated N-terminus. [18] In 1994 the 4 lectins with CRD sequence homology for β-galactosides were grouped together and termed galectins.[1] In time order of discovery they were termed galectin-1, 2, 3, and 4.[1] Galectins were further subdivided into 3 groups based on the number of CRDs per galectin (1 or 2) and whether the CRDs were identical or distinct [Table 1]. [10] Galectins

have either 1 or 2 CRDs within a single polypeptide chain. In contrast to C-type lectins galectins or S-type lectins the polypeptide chain containing the CRD is not attached to a well-defined protein domain. C-type lectins often have several CRDs attached to another protein domain.[19] The 3 galectin groups were termed prototypical, chimeric and tandem repeat [Table-1]. There are 15 known mammalian galectins and 11 of those are present in humans.[20]

Classification	Galectin Family Members	Structure - CRD
Prototypical	1, 2, 5, 7, 10, 11, 13, 14, 15	1 CRD - can dimerise containing 2 identical CRD's
Chimeric	3	1 CRD connected to a non-lectin domain
Tandem Repeat	4, 6, 8, 9, 12	2 distinct CRD's

Table 1 : Classification of the Galectin family by carbohydrate recognition domain (CRD). There are 3 main groups with the subject of this thesis (Gal-3) falling uniquely into its own group. This classification was initially proposed by Hirabyashi in 1993 and is still used to distinguish Galectins into both structural and functional groups.

1.1.2.1.1 The Galectin Carbohydrate Recognition Domain

Membership of the galectin group requires the presence of a conserved CRD amino acid sequence; however, this is not enough by itself. Galectins must also show affinity for β-galactosides.[11] Some molecules termed 'galectin like proteins' have the conserved amino acid sequence but do not bind β-galactosides. [18] Galectin binding to glycoprotein and glycolipids is mediated via specific interactions between the galectin CRD and β-galactoside. [15] The galectin CRD consists of approximately 135 amino acids folded into a β sandwich identified by X-ray crystallography in 1993.[21] Contained within the CRD is a carbohydrate binding site consisting of a 7 amino acid motif termed the carbohydrate binding region. The 2 sheets of the β sandwich are curved with a convex (5 strands) and concave side (6 strands). Between the 2 sheets are 4 sub sites which constitute the carbohydrate binding region.[18] Carbohydrates attach to the concave side which forms a hollow large enough to accommodate a tetrasaccharide molecule.[22] The specific binding is mediated by attachment of β-galactosides on the carbohydrate lying within the convex groove to one or more of the 4 carbohydrate binding region subsites.

1.1.2.2 Galectin β-Galactoside Binding Avidity

Individual galectins have different binding avidities for different β-galactosides influenced by external conditions like temperature and ligand concentration. [12] Most single molecule galectin-ligand binding avidity is less that for protein-protein interactions. [22] Binding avidity may be considerably increased by dimerization or cross-linking of the galectins. For example, monomeric Gal-1 has

a weak affinity for lactosamine residues but is increased in its dimeric form. [23] Galectin-3 (Gal-3) is an example of a galectin whose biological properties are dependent on self-association via its N-terminus into large lattices which greatly increases its binding avidity. [24-26] The N-terminus of Gal-3 does not contain the CRD, therefore when N-terminae self-associate oligomers are formed cross-linking many oligosaccharides within the glycocalx on the extracellular membrane (ECM). [27]

1.1.2.3 Cellular and Tissue Location of Mammalian Galectins

Galectins are synthesized on cytosolic ribosomes and can move from the cytosol to the nucleus, remain in the cytoplasm or move to the cell surface. [18] Post translational modification of galectins appears to be restricted to phosphorylation. [18, 28] Galectins lack a signal peptide and move to the cell surface via a non-classical (non-Golgi, non-endoplasmic reticulum directed) pathway.[29] The ability to move within these intra and extracellular compartments enables galectins to have a wide range of intra and extracellular functions. [30] For example, Gal-3 has the ability to influence nuclear RNA splicing as well as influencing cell adhesion outside the cell. [31, 32] Some galectin members are distributed widely in different tissues and cell types whereas others are more selectively expressed [Table-2]. Galectin 1, 3 and 9 are also stable and biologically active in a soluble form.[33]

Galectin	Cell and Tissue Distribution
1	Muscle, heart, lung, liver, lymph node, thymus, prostate, colon, endothelium, Lymphocytes
2	Small intestine
3	Macrophage, neutrophils, epithelial cells (colon and lung) fibroblasts, limited endothelial expression, urothelium
4	Alimentary tract
5	Erythrocytes
6	Gastrointestinal
7	Skin
8	Liver, kidney, lung
9	Thymus, kidney, circulating leucocytes and lymphatic tissue.
10	Eosinophil, basophil

Table 2: Tissue and cellular distribution of Mammalian Galectins. Gal-3 is expressed on most leucocytes and most epithelial surfaces. In addition to basal expression Gal-3 expression can be increased under inflammatory conditions. Adapted from Than et al.[34]

1.1.2.4 Galectin function –'Optimising molecules'

That galectins are widely present throughout nature suggests an important role in the life of organisms. In vitro data has led galectins to be linked with important roles in inflammation, cancer and developmental biology.[18] The generation of Gal-1 knockout and Gal-3 knockout (Gal-1 $^{-/-}$ and Gal-3 $^{-/-}$) mice has demonstrated absence of one or both genes together does not significantly affect lifespan or fertility of mice under animal house conditions. [35] The specific tissue and cellular distributions of Gal-1 and Gal-3 and their different roles within an organism explain why there is no evidence of functional redundancy regarding these 2 galectins. [18] A review of Gal-1 $^{-/-}$ and Gal-3 $^{-/-}$ mice suggests that galectins may be 'optimising molecules'. This theory would hold that galectins are not required for absolute function but for most efficient function upon encountering a 'hit' like cancer or inflammatory disease.[35] As the role of galectins in disease is elucidated, they present themselves as potential therapeutic targets for translational research. Galectins 1, 3 and 9 are the most researched and described of the galectin family.[36]

1.2 Galectin-3 (Gal-3)

Gal-3 is the only member of the chimeric group of the galectin family, a protein of 29-35 kilodaltons (KDa).[37] Gal-3 was first identified on the surface of murine thioglycollate-elicited peritoneal macrophages.[38] This gave some important initial information, that it is expressed on cells of the monocyte/macrophage lineage and that it was expressed in an inflammatory model. Gal-3 has one carbohydrate recognition domain (CRD) consisting of approximately 130 amino

acids on the C-terminal and is joined to a 110-130 amino acid N-terminal domain with tandem repeats of short amino acid segments.[24] The N-terminal end is rich in proline, glycine and tyrosine residues and is responsible for many of the intracellular biological activities compared to the C-terminus which contains the CRD.[24] The N-terminus is involved in higher order oligomerisation resulting in multivalent Gal-3 molecules with multiple CRDs.[25] The importance of this, as discussed previously, is the ability to increase avidity for β-galactosides in the glycocalx, crosslinking oligosaccharides on cell surfaces.[27] Gal-3 is principally found in endothelial cells, epithelial cells and most immune cells including fibroblasts, lymphocytes, neutrophil and monocytes/macrophages. [39-44] Within these cells it can be expressed on the cell surface, in the cytoplasm, the nucleus as well as cytoplasmic organelles including phagosomes and mitochondria.[45, 46] Gal-3 binds glycoconjugates, like laminin, on the extracellular cell surface and matrix via its CRD.[47] The extracellular biological actions of Gal-3 are dependent on its ability to self-associate into higher order oligomers. [26] Gal-3 oligomers mediate cell-cell and cell-ECM adhesion; acting as a bridge to bind cells together and initiate intracellular signalling. Gal-3 has emerged as a central regulator of both acute and chronic inflammation via its ability to activate, induce migration and regulate apoptosis in immune cells.[36, 37] Gal-3 has often been designated a pro-inflammatory galectin (in contrast to Gal-1), however Gal-3 also provides a role in the resolution of inflammation and tissue repair.[36, 37] Clearance of Gal-3 is predominantly hepatic but is found in the urine, there is no data on renal clearance of Gal-3.[48, 49] The presence of Gal-3 and its secretion from transitional

cell epithelium of the lower urinary tract would make assessment of true Gal-3 clearance difficult unless labelled Gal-3 is used. [50]

1.2.1 Gal-3 and Inflammation

After an early role in the developing embryo Gal-3 has a relatively limited role under resting conditions until inflammation disrupts the basal state. Gal-3 has a role in kidney organogenesis in both murine and human kidneys.[51, 52] Human kidneys express Gal-3 in tissues of the mesonephric duct origin from 5 weeks of age onwards.[51] Once the kidney is mature Gal-3 expression becomes limited to epithelial distal convoluted tubule and collecting duct cells within the nephron and ureter.[51] The Gal-3 $^{-/-}$ mouse is phenotypically identical to a WT mouse of the same background under animal house conditions until 6 months of age apart from subclinical differences in kidney structure and function.[53] Bichara *et al* reviewed differences in renal structure and function between WT and Gal-3 $^{-/-}$ mice.[54] Gal-3$^{-/-}$ mice have approximately 11% fewer glomeruli than WT mice reflecting Gal-3's role in nephrogenesis.[54] Bichara's group found a compensatory kidney hypertrophy in Gal-3$^{-/-}$ mice. These differences were not physiologically relevant under animal house conditions. Gal-3$^{-/-}$ mice and WT mice were found to have similar glomerular filtration rates (GFR), bicarbonate excretion but an increased urinary chloride excretion.[54] Bichara found under low salt conditions there were pathological differences between WT and Gal-3 $^{-/-}$ mice. Gal-3$^{-/-}$ mice fed a chronic low sodium diet developed volume contracture with less extracellular fluid than WT mice.[54] The resting state increased urinary chloride loss also tended to a lower BP in Gal-3$^{-/-}$ mice under standard

conditions.[54] After 6 months of age Gal-3$^{-/-}$ mice develop fatty infiltrates in their livers resembling human non-alcoholic steatohepatitis.[55] underlying Gal-3's role in removing advanced glycation end products (AGE) and advanced lipoxidation end products (ALE).[55] Whilst WT and Gal-3$^{-/-}$ mice are similar prior to 6 months of age under animal house conditions there are significant differences between the two in the generation and resolution of inflammation [Table 3].

Inflammation	
Generation	Resolution
Reduced leucocyte infiltration in murine models of peritonitis and pneumonia in Gal-3 $^{-/-}$ mice	Gal-3 stimulates fibroblasts to produce collagen.
	Gal-3 promotes macrophage differentiation to M2- phenotype.
In vitro Gal-3 promotes adherence of neutrophils to ECM protein – laminin and fibronectin and endothelial cells	Gal-3 $^{-/-}$ mice demonstrate impaired wound healing.
	Gal- 3 safely degrades pro-inflammatory AGE / ALE intermediates.
Gal-3 promotes chemotaxis of monocytes in vivo and macrophages in vitro.	Gal-3 $^{-/-}$ mice demonstrate accelerated diabetic glomerulopathy.
	In vitro Gal-3 binds Klebsiella Pneumonia, Salmonella and E.Coli.
	Gal-3 $^{-/-}$ mice show increased susceptibility to endotoxic shock.
Induces mast cell degranulation	In vitro Gal-3 $^{-/-}$ macrophages have reduced phagocytosis of erythrocytes and thymocytes.
	Gal-3 $^{-/-}$ mice have reduced kupffer cell phagocytosis of red blood cells in a murine model of haemolytic anaemia

Table 3: Gal-3 is involved in the generation and resolution of inflammation. The table above describes the effect of addition of recombinant Gal-3 to leucocytes and Gal-3$^{-/-}$ mice subject to inflammatory models. Generation of inflammation, Gal-3$^{-/-}$ mice have a reduced leucocyte infiltration in models of pneumonia and peritonitis.[56, 57] *In vitro* recombinant Gal-3 promotes adherence of neutrophils to ECM proteins (laminin and fibronectin), and endothelial cells.[47] Gal-3 is a chemoattractant for monocytes and macrophages.[58] Gal-3 induces mast cell degranulation.[59] Resolution, Gal-3 has a role in tissue repair and fibrosis stimulating fibroblasts to produce collagen and promoting macrophage differentiation towards a 'pro-fibrotic' alternate (M2) differentiation.[60] The result is that Gal-3$^{-/-}$ mice exhibit impaired wound healing.[61, 62] Gal-3 also plays a role on the resolution of inflammation by binding and clearing AGE and ALE seen in conditions like diabetes.[63] Gal-3$^{-/-}$ mice in a model of diabetic nephropathy develop worse proteinuria and accelerated glomerulopathy.[64] Gal-3 acts as a pattern recognition receptor (binds Klebsiella, Salmonella and E.Coli) and is a negative regulator of lipopolysaccharide mediated inflammation. [65, 66] Consequently Gal-3$^{-/-}$ mice have an increased susceptibility to endotoxic shock.[65] Macrophage phagocytosis is optimised by Gal-3 and Gal-3$^{-/-}$ mice demonstrate a reduced kupffer cell phagocytosis of red blood cells in experimental haemolytic anaemia.[67]

1.2.1.1 Leucocyte Expression of Gal-3

Most cells involved in the generation and resolution of inflammation express Gal-3. [40, 41, 68, 69] Of the Gal-3 expressing leucocytes only monocytes and macrophages have been documented to have the ability to secrete Gal-3.[70],[71] Most leucocytes can express Gal-3 on their extracellular membrane via 'non-classical' transport and could plausibly secrete Gal-3.[36] Gal-3 leucocyte expression is not a constant and can rapidly change, which is partly regulated at the level of transcription, reflecting Gal-3 role as an immediate early gene (IEG) rapidly responding to changes in the cells local environment.[72]

1.2.1.1.1 Endogenous and Exogenous Gal-3 and Leucocyte Behaviour

This thesis will focus on the effects of Gal-3 and monocyte/macrophage function but an overview below demonstrates that Gal-3 has influence on many leucocyte functions. As discussed previously this influence is not absolute but often as an optimising molecule. Endogenous and exogenous effects of Gal-3 on leucocyte behaviour under inflamed conditions are shown below [Table 4, 5]. Gal-3 does have some pro-inflammatory effects e.g. inducing superoxide production in neutrophils and monocytes. There are also effects that will promote resolution of inflammation e.g., the promotion of macrophage phagocytosis.

Leucocyte	Effect of exogenous Gal-3
T-Lymphocyte	Induces IL-2 production and Ca^{2+} Influx, induces phosphatidylserine exposure and induces apoptosis in activated T-cells
Mast Cells	Induces histamine release
Neutrophils	Induces oxidative burst , Induces IL8 production and L-selectin shedding and protects neutrophils from apoptosis
Monocytes	Induces superoxide anion, Gal-3 acts as a chemoattractant for monocytes

Table 4: Actions of exogenous Gal-3 on Leucocytes, recombinant Gal-3 induces IL-2 production, Ca^{2+} influx and protects activated T cells from apoptosis.[73, 74] In mast cells recombinant Gal-3 induces histamine release.[75] The effects of exogenous Gal-3 on neutrophil function are arguably pro-inflammatory inducing oxidative burst, IL-8 production, L-selectin shedding and protection from apoptosis.[57, 71] Monocytes migrate towards and induce superoxide anion on exposure to Gal-3.[41, 58]

Leucocyte	Effect of endogenous Gal-3
Primary T-cells	Gal-3 necessary for IL-2 dependent cell growth
Macrophages	Gal-3 necessary for phagocytosis of opsonised sheep red blood cells and apoptotic thymocytes through FCR and phosphatidylserine receptors, enhances phagocytosis of apoptotic neutrophils, induces alternative macrophage activation, reduces IL-6, IL-12 and TNFα production on stimulation with LPS
Dendritic cells	Gal-3 suppresses IL-12 production (a Th-1 response cytokine). Hence Gal-3 can modulate Th-response.

Table 5: Actions of Endogenous Gal-3 on leucocytes. Gal-3 is necessary for IL-2 dependent primary T cell growth.[42] Macrophages deficient in Gal-3 have impaired phagocytosis; Gal-3 enhances phagocytosis of apoptotic neutrophils.[58, 76] Gal-3 induces the pro-fibrotic 'alternative macrophage activation and reduces pro-inflammatory cytokine production on stimulation of macrophages by LPS.[65, 77] Gal-3 has a role in modulating Th response in dendritic cells.[78]

1.2.1.1.2 Gal-3 Regulation of Monocyte/Macrophage Subset Phenotype

Monocytes have been known to be a part of the inflammatory response since the 1970's when proliferation in bone marrow of monocytes was observed in inflammatory stimuli resulting in a monocytosis.[79] In 1989 heterogeneity of monocytes was observed for the first time.[80] Both human and murine monocytes can be distinguished into distinct subsets based on surface expression of specific markers. Each monocyte subset has a distinct pathophysiological role. Elevated monocyte levels have been found in various human pathological conditions including cardiovascular disease and CKD.[81-84]

1.2.1.1.2.1 Human and murine monocyte subsets

1.2.1.1.2.1.1 Murine Monocyte Subsets

Ly6c^{high} monocytes are preferentially recruited into inflamed tissue via interaction of chemokine receptor 2 (CCR2).[85] Ly6C^{high} monocytes differentiate to mature inflammatory (M1) macrophages (distinguished by secretion of pro-inflammatory TNF-α, IL6 and contribute to T-cell activation). Ly6C^{low} monocyte subsets secrete the anti-inflammatory cytokine IL-10 on *in vivo* bacterial infection. Upon encountering vascular inflammation they are recruited into tissue and differentiate predominantly into M2 macrophages which secrete anti-inflammatory cytokines and contribute to tissue repair.[86] Because Ly6C^{low} have lower expression of adhesion molecules they are less likely to transmigrate and more likely to patrol the vascular endothelium [Table 6]. Ly6C$^{int\ /mid}$ monocytes

are pro-inflammatory and the human equivalent is the CD14++/CD16+ 'intermediate' monocyte that is found to be elevated in human CKD and significantly associated with adverse cardiac events in both haemodialysis and pre-dialysis CKD cohorts.[81, 87]

Species	Subsets	Surface markers	Chemokine receptors	Role
Human	Classical	CD14++/CD16+	CCR2high/CX3CR1 low	Phagocytosis
	Intermediate	CD14++/CD16+	CCR2mid/CX3CR1high	Pro-inflammatory
	Non-classical	CD14+/CD16++	CCR2low/CX3CR1high	Patrolling
Mouse	Ly6C high	CD11b+/Ly6Chigh	CCR2high/CX3CR1low	Phagocytosis and pro-inflammatory
	Ly6C mid	CD11b+/Ly6Cmid	CCR2high/CX3CR1low	Proinflammatory
	Ly6C low	CD11b+/Ly6Clow	CCR2low/CX3CR1high	Patrolling / tissue repair

Table 6: Human and Murine monocyte subsets, cell surface markers and patho-physiological role.

1.2.1.1.2.2 Gal-3 and Monocyte/ Macrophage differentiation

There is evidence that Gal-3 is important for monocyte/macrophage behaviour. Circulating human monocytes increase expression of Gal-3 as they differentiate into macrophages and Gal-3 is downregulated when they differentiate into dendritic cells.[41, 88] Both monocytes and macrophages can secrete Gal-3 to act in an autocrine or paracrine fashion. Gal-3 can promote monocyte-monocyte attachment leading to polykaron (multinucleate giant cell) formation, a phenotype associated with M2 macrophage activation.[89]

The initial inflammatory response in inflamed tissue is characterised by pro-inflammatory 'classically activated' M1 macrophages. The resolution phase of inflammation is characterised by 'alternatively activated' M2 macrophage accumulation. Macrophages can differentiate into either subset depending on their local micro-environment. M1 macrophage differentiation can be induced by exposure to Th1 cytokines (IFN-λ, IL-12) or microbial agents.[90, 91] M2 macrophage differentiation can be induced by Th2 cytokines IL-4 and IL-13.[92, 93]

1.2.1.1.3 Gal-3 and Leucocyte-Endothelial Interactions

Both *in vitro* and *in vivo* models have suggested that Gal-3 increases leucocyte adherence to endothelium, endothelial transmigration and infiltration into tissues under inflamed conditions.[47, 94-96] These effects appear to be mediated by both CRD-dependent and CRD-independent mechanisms.[47, 96] *In vitro* data includes evidence of Gal-3 promoting neutrophil adhesion to extracellular matrix proteins laminin and fibronectin.[47] Laminin adhesion was partly dependent on

the Gal-3 CRD but binding to fibronectin is independent of the CRD acting by increasing expression of adhesion molecule β-2 integrin.[47] Recombinant Gal-3 mediates human neutrophil attachment to a human endothelial cell line ECV304 monolayer.[94] The same study showed that Gal-3 played a role in β-2 integrin-independent neutrophil extravasation, which occurred during a murine model of alveolar infection with streptococcal pneumonia. Gal-3 can bind major xenoantigen α-gal – expressed on endothelial cells.[96] A neutralising antibody to α-gal prevents human monocyte attachment to porcine endothelium suggesting this as a further mechanism of leucocyte-endothelial adhesion.[96] *In vivo* models of Gal-3's effect on leucocyte infiltration in inflammation are described below [Table-7].

Animal Model	Gal-3 $^{-/-}$ mouse
Thioglycollate induced peritonitis	Reduced macrophage and neutrophil recruitment into peritoneum
Streptococcus Pneumonia	Reduced neutrophil numbers in lungs
Toxoplasma Gondii	Reduced macrophage/ monocyte and CD-8 Infiltration in intestines, liver and brain, but higher parasite burden.

Table 7: Leucocyte recruitment and infiltration in Gal-3$^{-/-}$ mice subject to inflammatory disease models. The Gal-3$^{-/-}$ mouse demonstrates reduced leucocyte recruitment in models of peritonitis, pneumonia and toxoplasma infection.[56, 78, 95, 97]

1.2.1.2 Gal-3 and the Resolution of Inflammation

1.2.1.2.1 Gal-3 as a Scavenger Receptor for AGE

Accumulation of AGE plays a role in the structural and pathological changes associated with diabetes and ageing. AGE are reducing sugars complexed with proteins to form irreversible post-translational modifications. AGE receptors internalize and either degrade or elicit pro-inflammatory pathways (Receptor of AGE (RAGE) receptor pathway). There is evidence of a protective effect of Gal-3 against diabetic nephropathy and lipid induced glomerular injury.[98, 99] The protection may be mediated by the ability of Gal-3 to function as a receptor to internalize and ultimately degrade AGE / ALES's.[100] In 1995 Vlassara *et al*. demonstrated that the 90 kilo Dalton (kDa) AGE receptor had sequence homology with Gal-3 and that Gal-3 could bind AGE modified Bovine Serum Albumin (AGE-BSA).[63] Saturable association kinetics demonstrated an association for free recombinant Gal-3 and stronger association with membrane bound Gal-3.[63] Gal-3 is not a distinct AGE receptor but forms part of a larger AGE receptor complex functionally interacting with AGE-R1 and AGE-R2. Gal-3's role as an ALE receptor was suggested by the interaction with Gal-3 and gp-90/Mac-2 binding protein.[101] The gp-90/Mac-2 binding protein has sequence homology to scavenger receptors that recognise oxidated or acetylated low density lipoprotein (LDL). *Zhu et al* endorsed this hypothesis using Chinese hamster ovary (CHO) cells overexpressing Gal-3.[101] When exposed to labelled I-AGE-BSA the Gal-3 formed a ligand with AGE- BSA, the receptor ligand complex was endocytosed and subsequently underwent lysosomal degradation.[101] The

role of Gal-3 as an ALE receptor and degrader was suggested using CHO cells overexpressing Gal-3 cultured with radioactive labelled acetylated and oxidised LDL where the same degradation process was observed. Cholesterol esters within the CHO cells gave a similar appearance to foam cells. This appearance prompted *Zhu et al* to hypothesize that Gal-3 may be involved in atherogenesis.[101] This is corroborated by Gal-3 acting as scavenger receptor (highly expressed on macrophages) internalising LDL cholesterol in the process of 'Foam Cell' formation.[64] Gal-3 is expressed in human atherosclerotic plaques and inhibition of Gal-3 reduces atherosclerosis in apolipoprotein deficient mice.[102, 103]

Gal-3 is an AGE receptor leading to AGE degradation *in vitro* and Gal-3 is up-regulated in the glomerulus under diabetic conditions.[99] Pugilese *at al* demonstrated early glomerular Gal-3 expression at 2 months with an increasing degree of staining apparent up to 12 months of age in a rat model of experimental diabetes (streptozotosin administration). A non-diabetic control could only show Gal-3 expression after 12 months of age.[100] Other components of the AGE receptor complex (p60 and p90) were up-regulated in a similar fashion in diabetic rats.[100]

Pugilese et al. hypothesized that Gal-3 expression would protect against the renal effects of diabetes (mesangial matrix deposition and other glomerular changes) via its role as an AGE-receptor / degrader. [99] WT and Gal-3 $^{-/-}$ mice were subjected to the streptozotosin model of diabetes and sacrificed at 4 months. Diabetic WT and Gal-3 $^{-/-}$ mice had equivalent metabolic derangement,

growth and serum creatinine. However, renal histology revealed Gal-3 $^{-/-}$ mice had a significantly increased mesangial fractional area (+52%) vs diabetic WT. Diabetic Gal-3$^{-/-}$ mice had significantly raised total AGE levels (+42%) and raised peripheral and mesangial AGE staining vs diabetic WT mice.[99]

Gal-3 $^{-/-}$ mice develop proteinuria when exposed to high levels of AGE, independent of diabetes.[104] N-carboxymethyllsine (CML)-modified mouse serum albumin (MSA) was used by Pugilese's group as an exogenous AGE.[104] Gal-3$^{-/-}$ and WT mice were exposed to this artificial AGE for 3 months giving serum AGE levels equivalent to those in the streptozotosin model.[104] At 7 months the mice were sacrificed, Gal-3$^{-/-}$ and WT mice had equivalent serum creatinine but Gal-3$^{-/-}$ mice had significantly more proteinuria.[104] Gal-3$^{-/-}$ mice had higher circulatory AGE levels, renal tissue AGE expression and kidney Nuclear Factor Kappa Beta (NF-κβ) activity vs WT –CML – MSA exposed mice suggesting a protective role of Gal-3 in AGE mediated disease.[104]

1.2.1.2.2 Gal-3 and Age mediated disease: Type 2 Diabetes

Human Gal-3 is up-regulated in type 2 diabetes and proteinuria correlates to Gal-3 expression.[50, 64, 98] Gal-3 is not expressed under normal conditions in the adult human glomerulus. It is only constitutively expressed in the intercalated cells of the collecting duct.[51] Animal models of renal Ischaemia–reperfusion [105] and mesangial-proliferative glomerulonephritis[106] have shown Gal-3 expression is transiently up-regulated in distal and proximal tubules and expressed in macrophages infiltrating the glomerulus. Kikuchi *et al*. applied anti-human Gal-3 immunohistochemical staining on 37 human renal biopsies (9 - type 2 diabetes, 9

- IgA nephropathy, 6 - membranous nephropathy, 5- minimal change disease and 17 - normal renal tissue from nephrectomies as control specimens).[107] In control biopsies there was no evidence of anti-Gal-3 antibody staining in glomeruli, PCT or interstitium, though weak staining was present in the distal convoluted tubule and collecting duct.[107] Glomerular anti-Gal-3 antibody positive cell infiltration was noted in 12 of the 37 biopsies. (6/9- type 2 diabetes mellitus, 3/9-IgA nephropathy, Mb N- 1/6 minimal change – 0/5). The ratio of glomeruli with Gal-3 + cell infiltration: normal glomeruli were significantly higher in diabetic patients (22.5%). Gal-3 positive cells co-localised on double immunofluorescence with CD68 suggesting the infiltrating cells were macrophages expressing high levels of Gal-3.[107] The degree of proteinuria from diabetic patients correlated with the amount of Gal-3 expression on renal immunohistochemistry ($p<0.001$). The more Gal-3 positive cell infiltration the higher the amount of proteinuria.[107] Baseline measurements of the diabetic patient's glycated haemoglobin (HBA1c) and glomerular filtration rate (GFR) showed no correlation with the amount of Gal-3 positivity. The main histological parameter associated with glomerular Gal-3 positivity was the degree of interstitial fibrosis – significantly higher in Gal-3 positive samples.[107]

Human mesangial cells cultured with rosiglitazone in the presence of AGE up-regulate Gal-3 in a time and dose dependant manner.[108] Rosiglitazone (a peroxisome proliferator-activated receptor agonist) has been shown to ameliorate diabetic nephropathy and reduce circulating levels of serum AGE-peptide. Sun *et al.* investigated the *in vitro* effects of rosiglitazone on human

mesangial cells Gal-3 expression.[108] Human mesangial cells were incubated with different concentrations of AGE modified Bovine Serum Albumin (AGE-BSA) (0, 50,100,200 and 400 mg/l) for different times (0, 24, 36, 48 and 72 hours) and exposed to AGE-BSA in with varying concentrations of rosiglitazone (1, 10, 100 µmol/L).[108] AGE modified-BSA up-regulated Gal-3 expression in cultured mesangial cells in a dose and time dependent manner. Adding rosiglitazone in the presence of AGE-BSA independently increased the mRNA and protein expression of Gal-3 in a dose dependent manner.[108] Interestingly, the use of rosiglitazone is now subject to controversy due to increased cardiovascular risk. Gal-3 has recently been demonstrated to be a novel prognostic marker for heart failure.

Gal-$3^{-/-}$ mice demonstrate accelerated lipid induced glomerular injury.[109] Gal-3 has been shown to act as a receptor for ALE.[109] ALE contributes to disease in a variety of ways including atherosclerosis, pro-inflammatory pathways and can mediate glomerular injury. WT mice fed on a high fat diet increase renal Gal-3 protein expression and Gal-3 mRNA up-regulation.[109] Iacobini *et al*. fed Gal-$3^{-/-}$ mice a high fat diet showed accelerated glomerular injury associated with glomerular cell apoptosis and more pronounced matrix production.[109] Compared to WT controls, serum and kidney ALE/AGE content was raised in Gal-$3^{-/-}$ mice. AGE receptor and Scavenger Receptor expression (except SRA1), systemic and renal tissue oxidative stress and macrophage infiltration was raised in the Gal-$3^{-/-}$ mouse model fed on a high fat diet compared to WT mice fed high

fat diet. The authors speculated that this had important implications for both local renal and systemic disease mediated by ALE's and AGE's.

1.2.1.3 Regulation of Gal-3 under inflammatory conditions

Cellular expression of Gal-3 is regulated at least in part at the level of transcription.[110] Gal-3 signalling pathways are not fully understood despite evidence for different external stimuli regulating cell expression. Soluble Gal-3 is raised in inflammatory conditions associated with raised cytokines and AGE. The mouse Gal-3 gene *(LGALS3)* was described by Rosenburg *et al.* in 1993 [111] and the human Gal-3 gene was described by Kadrofske 1998 [72]. Gal-3 is encoded by a single gene within the human gene on chromosome 14 and is composed of 6 exons and 5 introns over 17 kilobases.[72] There are 2 transcription initiation sequences in the Gal-3 promoter region. The human Gal-3 gene promoter has multiple GC box motifs for binding transcription factor Sp1 in common with constitutively expressed 'housekeeper genes'.[72] When serum starved cells (fibroblasts) are exposed to serum, Gal-3 transcription is increased.[110] In view of this LGALS3 is designated an IEG. IEG are genes which are activated transiently and rapidly in response to a wide variety of cellular stimuli. Several transcription factor binding sites on the Gal-3 promotor have been identified.[72]

1.2.1.3.1 Gal-3 under Cyclic-AMP/ NF-κβ/ Rel control

There is evidence for Gal-3 being a putative gene target for Nuclear Factor Kappa Beta (NF-κβ)/Rel transcription.[73] Hsu et al. demonstrated Gal-3 upregulation in human T-cells infected with HTLV-1 virus.[73] Unlike monocytes, macrophages

and neutrophils Gal-3 is minimally expressed in lymphocytes. Infection of T-lymphocytes with HTLV-1 virus induces gene upregulation via the transactivating factor TAX.[73] TAX itself exerts its effect via 2 transcription pathways CREB/ATF and NFκβ/Rel pathways.[73] Both CREB/ATF and NF-κβ binding sites have been identified within the mouse Gal-3 promoter. [112] Compared to the efficacy of TAX protein to increase Gal-3 expression, CREB/ATF induces a similar expression whilst NF-κβ/Rel did not increase Gal-3 to the same extent.[73] NF-κβ/Rel exerting control over Gal-3 expression would fit with observations of Gal-3 as an IEG with up-regulation in inflammatory conditions.[72] NF-κβ/Rel is a signal transducer in immediate early phases of immune responses and conditions of oxidative stress.[113] Raised AGE in chronic kidney disease can be bound by several AGE receptors including receptor of advanced glycation end products (RAGE) and Gal-3 (designated AGE receptor 3). RAGE is a member of the immunoglobulin superfamily and is expressed on the extracellular membrane on various cell types as well as existing in a soluble form. The RAGE receptor has a cytoplasmic tail which transduces intracellular signalling following AGE binding to the receptor.[114] Membrane bound Gal-3 internalises AGE following binding and detoxifies it without inducing intracellular signalling. However RAGE exerts a cascade of pro-inflammatory signalling following binding including NF-κβ signalling. Given that Gal-3 is potentially under NF-κβ /Rel control and has beneficial opposite effects in AGE scavenging and detoxifying, it could be Gal-3 is upregulated by RAGE via the NF-κβ pathway as a protective feedback. A human immortalised monocytic cell line (THP-1) exposed to AGE (carboxymethyllyseine) modified human serum albumin demonstrated p38 MAPK activation mediating

RAGE induced NF-κβ dependent secretion of pro-inflammatory cytokines.[115] In 2003 another group exposed THP-1 cells to phorbol ester and demonstrated increased Gal-3 expression and inhibited by SB-203580, a specific p38 MAPK inhibitor.[116]

1.2.2 Gal-3 and fibrosis

Fibrosis represents the final common pathway of chronic tissue injury.[117] Chronic inflammation with formation of scar tissue and loss of function is a characteristic of many human diseases and represents a cause of morbidity and mortality worldwide.[118] Quiescent resident tissue fibroblasts become activated to a matrix secreting myofibroblast phenotype. Increased Gal-3 expression has been documented in tissue fibrosis and *in vitro* recombinant Gal-3 induces proliferation of myofibroblasts.[119]

1.2.2.1 Gal-3 and Hepatic Fibrosis

Gal-3 is implicated in and contributes to a murine model of hepatic fibrosis.[120] Henderson *et al*. induced a model of liver fibrosis (CCL-4, carbon tetrachloride) in WT and Gal-$3^{-/-}$ mice.[120] After 8 weeks of CCL-4 treatment Gal-3 was present in periportal and areas of bridging fibrosis in the liver. Control (olive oil treated) animals had Gal-3 expression limited to bile duct epithelium. Liver homogenate showed significantly raised Gal-3 mRNA and protein in CCL-4 treated group.[120] The Gal-$3^{-/-}$ mice given CCL-4 treatment had significantly less collagen deposition and less procollagen-1 mRNA compared to WT CCL-4 treated animals.[120] Gal-$3^{-/-}$ mice treated with CCL-4 had significantly less α-SMA mRNA and protein than WT

treated animals. WT and Gal-3$^{-/-}$ mice had equivalent liver injuries (defined by elevated liver enzymes) after intra-peritoneal administration of CCL4. Liver levels of TNF-α were also similar between the two groups. Macrophages from both WT and Gal-3$^{-/-}$ animals exhibited similar levels of pro-inflammatory cytokines on stimulation with LPS. [120]The hepatic stellate cell (HSC) is the key fibrogenic cell of the liver and after any liver injury HSC's undergo activation to proliferate and phenotypically change into fibrogenic myofibroblasts (with increased expression of alpha smooth muscle actin (α-SMA))Gal-3$^{-/-}$ HSCs proliferate and stain +ve for α-SMA following co-culture with recombinant Gal-3.

1.2.2.2 Gal-3 and Renal Fibrosis

Progressive renal disease is the result of expansion of renal interstitial extracellular matrix leading to nephron loss. Okamura performed unilateral ureteric outflow obstruction (UUO) on WT and Gal-3$^{-/-}$ mice. [121] This model produces progressive fibrosis of the affected kidney without significant rise in creatinine as the unaffected kidney can provide adequate renal function by itself. In the ligated kidney Gal-3 mRNA rises to a peak (95-fold increase) at 7 days post UUO. On immunohistochemistry Gal-3 localised to proximal tubular cells then infiltrating macrophages to the interstitium. In sham operated kidneys of WT and Gal-3$^{-/-}$ mice collagen levels were similar. In kidneys subject to UUO after days 14 and 21 the collagen levels were higher and more disorganised in Gal-3$^{-/-}$ mice suggesting that Gal-3 attenuated fibrosis severity and preserved intact renal tubules in the later stages of the UUO model. Apoptosis (measured by TUNEL staining) of tubular epithelial cells was increased by 123% in Gal-3$^{-/-}$ murine

kidneys 14 days post UUO. Paradoxically despite worse fibrosis severity scores the Gal-3$^{-/-}$ kidneys 14 days post UUO had 80% less fibronectin and procollagen-1 mRNA as determined by real time quantitative polymerase chain reaction (qPCR) and fewer myofibroblasts. The arrangement of collagen fibres was more disorganised in Gal-3$^{-/-}$ mice leading the author's in the paper [121]to conclude that Gal-3 modulates extracellular matrix turnover. Endo-180 is an endocytic receptor for collagen 1 and 4. It is a key receptor for matrix degradation during wound remodelling. During UUO endo-180 mRNA and protein levels rise. Endo-180 deficient mice have significantly worse fibrosis scores after UUO. Gal-3$^{-/-}$ mice have reduced endo-180 levels. Okamura *et al.* speculated that Gal-3 may crosslink α1-integrin (via its CRD) and endo-180 to facilitate collagen endocytosis. Both macrophages and fibroblasts can express endo-180.

In 2008 Henderson *et al.* also investigated Gal-3 regulation of fibrosis in the UUO model of progressive renal fibrosis.[60]. Compared to sham operated animals WT mice with UUO had significantly more Gal-3 in renal interstitium and tubular epithelial cells. Whole kidney qPCR of Gal-3 mRNA showed a significant increase from day 3 to day 7. In contrast to Okamura *et al.* [121] collagen staining of the UUO kidneys in Gal-3$^{-/-}$ mice revealed reduced interstitial collagen accumulation compared with WT mice. Gal-3$^{-/-}$ kidneys subject to UUO also had significantly reduced procollagen-1 and αSMA (a marker of activated myofibroblasts) on qPCR. The authors concluded that the absence of Gal-3 gene protects against renal fibrosis after UUO. Disruption of the Gal-3 gene did not affect macrophage recruitment in the UUO model. Gal-3$^{-/-}$ macrophages have similar cytokine

responses (TNF-α, Interferon-λ) to WT macrophages on stimulation with LPS. The pro-fibrotic effects of Gal-3 were therefore independent of macrophage recruitment and inflammatory cytokine production. Levels of transforming growth factor beta (TGF-β) were similar between Gal-$3^{-/-}$ mice and WT at 3, 7 and 14 days post UUO. The phosphorylated TGF-β ligands SMAD2 and 3 (phosphorylated by TGF beta kinase) were also present in similar amounts. Disruption of the Gal-3 gene blocked renal fibrosis despite similar levels of TGF-β and SMAD 2 and 3. Henderson *et al* demonstrated that Gal-3 positive macrophages could activate renal fibroblasts *in vitro*. As previously shown cultured renal fibroblasts from Gal-$3^{-/-}$ mice were co-cultured with recombinant Gal-3 leading to production of α-SMA, a marker of pro-fibrotic activated fibroblasts.

1.2.2.3 Gal-3 and Pulmonary Fibrosis

Gal-3 secreting macrophages activate fibroblasts to lay down extracellular matrix in human pulmonary fibrosis.[122] Idiopathic Pulmonary Fibrosis (IPF) is characterised by epithelial cell injury with initial accumulation of inflammatory cells followed by deposition of extracellular matrix and fibroblast activation resulting in end stage fibrosis. Nishi *et al.* performed Broncho-Alveolar Lavage (BAL) (obtaining BAL fluid and alveolar macrophages) from 41 patients[122]. Eight patients had diagnoses of fibrotic lung disease, 6 control samples were taken from healthy tissue of lung in patients with lung cancer. The rest had other non-fibrogenic lung pathologies. Gal-3 levels were higher in the BAL fluid from patients with IPF. The source of Gal-3 was secreted by alveolar macrophages that stained strongly positive for Gal-3 on immunofluorescence of BAL. The same

group demonstrated recombinant Gal-3 induced migration and collagen secretion of NIH-3T3 fibroblast cells *in vitro*.[123] The authors suggest macrophage derived Gal-3 acts on fibroblasts and resident macrophages in an autocrine/paracrine manner inducing TNF-α and IL-8 secretion upon recombinant Gal-3 stimulation of a THP-1 macrophage immortalized cell line.

1.2.2.4 Gal-3 and Cardiac Fibrosis

Uraemic cardiac fibrosis contributes to 'stiffening' of the myocardium and diastolic dysfunction associated with CKD. Gal-3 has been implicated in chronic inflammatory disease leading to fibrosis in models of hepatic, lung and renal fibrosis. Gal-3 mediates alternative (M2) macrophage activation, induces proliferation and collagen secretion in quiescent lung and cardiac fibroblasts. Pro-fibrotic and inflammatory multinuclear giant cell formation is associated with monocyte Gal-3 expression. The underlying pathology of Gal-3 mediated cardiac dysfunction is Gal-3 secretion from activated cardiac macrophages. Secreted Gal-3 acts on tissue resident fibroblasts to induce pro-collagen secretion and lay down. Gal-3 was first implicated in heart failure following a microarray analysis of genes from a rat heart failure model.[119] Gal-3 mRNA was expressed 5-times greater in failing myocardium vs compensated left ventricular hypertrophy. In the failing rat heart myocardial tissue section, Gal-3 co-localised with macrophages amongst areas of fibrosis. Human myocardial biopsy similarly showed correlation between presence of Gal-3, a lower ejection fraction on echocardiography and left ventricular hypertrophy. Sharma *et al.* went on to demonstrate that Gal-3 was not just a marker of myocardial fibrosis and

dysfunction but directly implicated in its pathophysiology by studying intra-pericardial infusion of Gal-3 into normal rat hearts. The Gal-3 infusion resulted in a decreased ejection fraction, increased heart mass and an abundance of collagen 1, compared with rat hearts subjected to placebo infusion.

1.2.2.4.1 Clinical evidence implicating Gal-3 in human heart failure and cardiac remodelling

The first human clinical evidence of Gal-3 being associated with heart failure was published in 2006 [124], Gal-3 and NT pro-BNP (a cardiac dysfunction biomarker) levels were measured in 599 patients attending the emergency department with dyspnoea. 35% of these patients had Acute Decompensated Heart Failure (ADHF). Area under the curve analysis showed Gal-3 to be inferior to NT pro-BNP as a diagnostic biomarker of ADHF but it was superior as a prognostic marker (predictor of death or death/recurrent HF at 60 days in a multivariate adjusted analysis of the 209 subjects with HF). 240 patients from the DEAL-HF study with stable heart failure (New York Heart Association (NYHA) grade 3 and 4) had Gal-3 measured and allocated to quartiles based on soluble plasma Gal-3 concentrations.[125] Patients were followed up for a mean 4.0 years for all-cause mortality. Progressively higher levels of Gal-3 were associated with increased age, worse renal function, lower body mass index (BMI) and higher NT pro-BNP levels. Overall, Gal-3 remained an independent predictor of mortality in these stable HF patients (Gal-3 hazard ratio 1.24, 95% confidence interval 1.03–1.5 after adjustment for age, gender, renal function and NT-pro BNP). This study also investigated associations between ventricular remodelling and Gal-3. In the 240

patient cohort serial echocardiograms were performed at baseline and 3 monthly during follow up. At baseline mean left ventricular end diastolic volume (LVEDV) was measured and patients divided into 3 groups based on subsequent changes in their LVEDV. Those patients with increasing LVEDV over time had significantly higher plasma Gal-3. Multivariate linear regression analyses revealed that Gal-3 was positively correlated to change in LVEDV (p=0.01).

Serum Gal-3 is associated with markers of cardiac extracellular matrix turnover in heart failure patients.[126] A total of 106 patients with a mean NYHA class of 2 were recruited to have serum galectin-3, extracellular matrix including type I and III aminoterminal propeptide of procollagen (PINP and PIIINP), matrix metalloproteinase-2 (MMP-2), and tissue inhibitor of metalloproteinase-1 (TIMP-1) assessed. After adjusting for age, sex, smoking status and NYHA functional class, the relationship between Gal-3 and PIIINP or MMP-2 remained significant. Gal-3 has been also been examined in healthy subjects for its ability to predict subsequent heart failure. 3353 of the Framingham community based cohort had Gal 3 levels measured at the 6th examination (1995-8). [127] All prevalent heart failure patients were excluded (n=40), plasma Gal-3 was measured and patients divided into quartiles based on Gal-3 value. In multivariate analysis Gal-3 was positively associated with age, hypertension, BMI and negatively associated with estimated GFR. During a mean follow up of 8.1 years 5.1% of patients experienced first heart failure events. The crude incident heart failure rates increased with increasing Gal-3 quartiles. After multivariable adjustment Gal-3 remained predictive of heart failure risk and an independent predictor of all-

cause mortality. Plasma Gal-3 is now a federal drug administration (FDA) approved blood test for clinical use in the USA.

1.3 Gal-3 and Chronic Kidney Disease

1.3.1 Chronic Kidney Disease

Chronic Kidney Disease (CKD) is a major worldwide public health problem. [128] In 2002 the Kidney Disease Outcomes Quality Initiative (KDOQI) of the National Kidney Foundation defined CKD as either kidney damage or Glomerular Filtration Rate (GFR) below 60 ml/min/1.73m^2 for 3 or more months with or without evidence of kidney damage, irrespective of the cause. [129] Estimates of GFR have been used for epidemiological purposes including the Cockcroft Gault and the Modification of Diet in Renal Disease (MDRD) equations. Based on the (MDRD) formula the estimated GFR (eGFR) is now commonly used to describe GFR.[130] The United States Renal Registry (USRDS) collects annual epidemiological data on Chronic and End Stage Kidney Disease. Between the years 2005-2010, a prevalence of 6.7% of the USRDS data collection population had an eGFR of < 60mls/min/1.73m^2. However the frequency increases with age, from a prevalence of 0.2% (age 20-39), 2.2% (aged 40-59) and 24% (aged 60+).[131] 5 stages of CKD have been defined based on eGFR. Prevalence of each stage in the study population used to get USRDS data – the National Health and Nutrition Examination Survey (NHANES) population is shown below from 2003 [Table 8].[132]

Stage CKD (and definition)	GFR (ml/min/1.73m2)	Prevalence %
1 (Persistent albuminuria with a normal GFR).	Normal (>90)	3.3
2 (persistent albuminuria with a GFR of 60 to 89 mL/min/1.73 m).	60-89	3
3	30-59	4.3
4	15-29	0.2
5	<15	0.2

Table 8: Prevalence of Chronic Kidney Disease by Stage. Data taken from 2003 NHANES population

The majority of people with stage 1-3 CKD will not progress to end stage (stage 5) renal failure but will suffer an increased cardiovascular risk.[133] Three aspects of CKD are pertinent to research in Gal-3. The first is the disproportionate cardiovascular risk associated with CKD, the second is renal tubulointerstitial fibrosis in progressive CKD and the third is elevated AGE and ALE in CKD.

1.3.2 Evidence of Elevated Circulating Soluble Gal-3 in Human CKD

Evidence for changes in soluble Gal-3 levels in human CKD can be taken from data in human studies of Gal-3 and heart failure that collected baseline kidney function measurements. Six published papers have shown a significant inverse correlation between renal function and Gal-3 [Table 9].

Paper	Cohort Number	Significant inverse correlation	Spearman's R (where available)
Shah R *et al.*	115	Yes	r = −0.42, p=<0.001
Lok *et al.*	232	Yes	r = −0.619, p=<0.001
Felker *et al.*	895	Yes	
De Boer *et al.*	7968	Yes	
Van Der Velde *et al.*	1329	Yes	
Gopal *et al.*	119	Yes	r=-0.82, P<0.001

Table 9: Human studies showing significant inverse correlation between sGal-3 and creatinine clearance or GFR. Data is taken from heart failure trials which collected plasma Gal-3 data and measured renal function.[125, 134-138]

In 2012 plasma Gal-3 was measured on baseline blood samples of 7968 patients from the Prevention of Renal and Vascular End-stage (PREVEND) cohort. Plasma Gal-3 was significantly associated with several clinical and biochemical characteristics. Multivariate analysis revealed gender, age-squared, BMI, triglycerides, Creatinine, Cystatin-C and C - reactive protein as independent correlates of plasma Gal-3.[136] Despite clinical evidence of an inverse correlation between kidney function and soluble Gal-3 there has been no published data as to why Gal-3 is raised or its source in CKD. The relationship between raised soluble Gal-3 with CKD and heart failure was investigated Gopal *et al*. in the

Journal of the American Heart Association in 2012.[138] Gopal *et al*. noted that published heart failure data to date had not included a cohort of patients with CKD and without heart failure. Gopal's study measured plasma Gal-3 by ELISA in 6 groups including a group with CKD but no heart failure. The mean soluble Gal-3 in study Group 6 (CKD without heart failure) was significantly higher than the control or the 4 other heart failure groups. A strong inverse relationship between kidney function and soluble Gal-3 existed and was unaffected by the presence or absence of heart failure. Gopal *et al.* commented on the uncertainty aetiology of raised soluble Gal-3 in CKD, speculating whether it is a result of decreased renal clearance or increased renal synthesis.

1.3.1.1 Cardiovascular Risk in CKD

CKD has been identified as a significant cardiovascular risk factor from early stages.[133] Proteinuria itself without evidence of impaired GFR is an independent risk factor for cardiovascular disease. As CKD progresses through stages 1-5 there is a rise in cardiovascular mortality.[133] The CKD population have traditional cardiovascular risk factors but also atypical cardiac risk factors [Table 10]. Whether Gal-3 is an atypical or 'non-traditional' risk factor for CKD cardiovascular disease is still debated.

Traditional Cardiac Risk Factor	Non-traditional Cardiac Risk Factor
Older age	Albuminuria
Male sex	Homocysteine
Hypertension	Dyslipidaemia
Higher LDL cholesterol	Anemia
Lower HDL cholesterol	Abnormal calcium/phosphate metabolism
Diabetes	Extracellular fluid volume overload
Smoking	Electrolyte imbalance
Physical inactivity	Oxidative stress
Menopause	Inflammation (C-reactive protein)
Family history of CVD	Malnutrition
LVH	Thrombogenic factors
	Sleep disturbances
	Altered nitric oxide/endothelin balance

Table 10: Cardiovascular risk factors in CKD.[139] Gal-3 is a potential non-traditional risk factor for cardiovascular disease in CKD.

1.3.1.1.1 Myocardial fibrosis in CKD

Cardiac remodelling with left ventricular hypertrophy, diastolic dysfunction and myocardial fibrosis are characteristics of CKD induced cardiovascular disease. Myocardial biopsies of patients with CKD frequently show evidence of cardiomyocyte hypertrophy, myocardial fibrosis, and thickening of the intramural arteries and arterioles.[140] Putative factors in the development of cardiac remodelling in CKD are shown outlined in Table 11. Gal-3, with a role in both human and animal models of cardiac fibrosis, as well as elevated soluble Gal-3 in CKD present it as a potential contributor to uremic cardiac fibrosis. [119, 134]

Myocardial Stressors in CKD leading to fibrosis	Pathological Effect
Haemodynamic overload, oxidative stress, Inflammation, Cytokines, cardiotrophin 1, TGFβ, Anaemia, Hyperphosphataemia, hyperparathyroidism, vitamin D deficiency, Uremic Toxins	Accumulation of collagen type I fibres, exaggerated synthesis by cardiac fibroblasts and myofibroblasts, unchanged or depressed degradation by extracellular matrix metalloproteinases

Table 11: Causes of Myocardial Fibrosis in CKD.[141]

Diastolic dysfunction is the clinical effect of myocardial fibrosis and altered cardiac remodelling.[142] Diastolic dysfunction is present on echocardiographic assessment in 46% of patients with stage 2+3 stage CKD and 62% of patients with stage 4+% CKD. [142] The implication of developing diastolic dysfunction is serious with mortality from diastolic heart failure higher than mortality from systolic heart failure in CKD patients.[143]

1.3.1.1.2 Monocyte subset phenotypic change in CKD as a cardiovascular risk factor

There is an association between monocyte count and cardiovascular disease found in large epidemiological studies.[144-146] There is also a distinct monocyte

subset – the 'intermediate' subset that correlates with adverse cardiovascular events in CKD and dialysis patients.[81, 87] Gal-3 is known to influence macrophage differentiation, if Gal-3 has a role in directing monocyte subset change it could be implicated in the formation of the 'intermediate' monocyte subset in CKD.[77] This thesis will examine circulating monocyte subsets in relation to experimental CKD and Gal-3.

1.3.1.2 Progressive interstitial fibrosis in CKD

This thesis has previously described Gal-3 in fibrotic disease. Gal-3 is implicated in the progression of fibrotic disease including models of CKD. The final common pathway of progressive CKD is renal fibrosis regardless of initial cause.[147] Renal fibrosis includes glomerulosclerosis, tubulointerstitial fibrosis and changes to renal vasculature. Tubulointerstitial fibrosis found on kidney biopsy is a predictor of a progression towards irreversible loss of kidney function and eventually end stage renal disease.[117] Despite considerable research and understanding about the mechanisms underlying tubulointerstitial fibrosis there are no effective therapies to disrupt and halt this process.[147] Renal tubulointerstitial fibrosis is a complex process involving exposure of the renal interstitium to insults and the host response to these insults [Table-12]. Given the described data implicating Gal-3 in fibrotic mechanisms, the described elevated plasma Gal-3 in human CKD this thesis will review the association of Gal-3 and CKD fibrosis in experimental uraemia.

Tubulo-Interstitial Insult	Renal Interstitial Cellular Response
Glomerular Proteinuria	Tubular epithelial cell apoptosis
Chronic interstitial hypoxia	Epithelial to mesenchymal transition
Glomerular hyperfiltration	Activation of fibroblasts
Tubular Protein leakage	Fibroblast transition to myfibroblast
Direct toxic insults	Influx and proliferation of lymphocytes, macrophages, fibrocytes, fibroblasts
Drug exposure	

Table 12: Overview of precipitants and inflammatory responses leading to renal interstitial fibrosis.[148] This thesis will review whether Gal-3 is implicated in a murine model of experimental CKD and tubulointerstitial fibrosis.

1.3.1.3 AGE and ALE in CKD

This thesis has described Gal-3 as an AGE receptor and that renal Gal-3 expression is elevated in the presence of excess AGE/ALE.[63, 64, 109] The author will now describe CKD as a disease of AGE/ALE excess. AGE products such as pentosidine and carboxymethyllyseine (CML) have been consistently demonstrated in normoglycaemic patients with end stage renal failure[149, 150] on renal replacement therapy and throughout progressive chronic kidney disease.[151] Uraemia is also associated with ALE product accumulation. [79] Proteins can be modified by carbohydrates but also by lipids peroxidation

derivatives like malondialdehyde to form irreversible ALE.[151] In CKD patients ALE levels rise concomitantly with AGE suggesting a common genesis.[151] AGE and ALE are usually albumin adducts and hence do not undergo glomerular filtration and renal clearance. The raised AGE and ALE in uraemia is therefore unlikely to be due to reduced renal clearance.[150] AGE and ALE are both formed by carbonyl amine chemistry between protein residues and reactive carbonyl compounds (RCO).[151] In health RCO are formed constantly by metabolism of carbohydrates, lipids and amino acids.[150] In haemodialysis patients the levels of several lipid and carbohydrate derived RCO's are elevated [Table 13]. [152-154]

Reactive Carbonyl Compounds derived from carbohydrates - (yield AGE)	Reactive Carbonyl Compounds derived from lipid peroxidation of fatty acids - (yield ALE)
Glyoxal,	Glyoxal,
Methylglyoxal,	Malondialdehyde,
Arabinose,	Hydroxynonenal,
Glycoaldehyde,	Acreolin
3-deoxyglucosone,	
Dehydroascorbate	

Table 13: Reactive carbonyl compounds derived from carbohydrates and fatty acids forming AGE and ALE. The underlined RCO are those found elevated in CKD.[150]

The cause of raised RCO in CKD is likely to be either due to decreased clearance or increased production. Uraemia is a condition of oxidative stress with raised levels of Reactive Oxygen Species (ROS) and lower levels of anti-oxidants. [154] ROS can directly modify proteins by oxidation of amino groups [155] or indirectly increase levels of RCO's which leads to generation of AGE and ALE.[156] However, whilst oxidative stress may contribute to a raised RCO production in uraemia there are ROC that are formed by oxidative stress including 3-deoxyglucosone and methylglyoxal. [157] Another explanation for increased levels of RCO in uraemia could be reduced enzymatic detoxification of RCO. RCO can be detoxified by different enzymatic pathways (e.g. aldose reductase, aldehyde dehydrogenase and glycoxylase).[157] These detoxification pathways utilise the redox co-enzyme glutathione. The RCO - glyoxal and methylglyoxal react reversibly with the thiol group of glutathione before further metabolism by Glyoxalases I and II into lactate and glutathione. This effectively lowers RCO levels. In the uraemic state there is abrogation of the activity of serum glutathione dependent enzymes.[158] [159] A third consideration is whether there is reduced renal clearance of RCO. RCO have low molecular weights and could be filtered at the glomerulus and undergo subsequent renal clearing.

1.4 Gal-3 as a therapeutic target in CKD

The investigation and safety profiles of Gal-3 antagonists were initially researched in the field of haemato-oncology. Gal-3 is overexpressed in many cancers and has roles in tumour transformation, apoptosis, angiogenesis, cancer cell adhesion and cancer metastasis.[160]

1.4.1 Modified Citrus Pectin

In 1992 Modified Citrus Pectin (MCP) was developed with observation of potential anti-metastatic properties, initially without knowledge of its Gal-3 antagonism.[161, 162] Subsequently MCP has been demonstrated to be effective *in vivo* and *in vitro* against prostate cancer,[162, 163] colon cancer,[164, 165] breast cancer,[165] melanoma,[161, 165] myeloma[166, 167] and lymphomas. Citrus pectin is a complex water-soluble, indigestible polysaccharide obtained from the peel of citrus fruits. It can be modified by high temperature and Ph. treatment to yield a substance rich in β-galactose.[161] The main mechanism of action of MCP was to bind to Gal-3 (a β-galactoside) and inhibit Gal-3 mediated interactions in cancer.[168]

Human trials of MCP demonstrated safety and dosing strategies in an oncological setting. The emerging *in vitro* and *in vivo* role of Gal-3 in fibrotic disease led to interest in MCP being a therapeutic role in chronic fibrotic conditions of which CKD was one.

1.4.2 GCS-100

In October 2012 an open label single group assigned phase 1 study of weekly administration of GCS-100 in patients with CKD was started (Clinical Trials.gov identifier - NCT017172480). The purpose was to evaluate the safety of GCS-100 as a treatment for chronic kidney disease. The GCS-100 was administered once a week intravenously. Subjects were aged between 18-75 years old and had a stable eGFR (defined by CKD EPI) between 15-45 ml/min/1.73m^2. The study was completed in June 2013 but no results have been made available.

In April 2013 a phase 2a placebo controlled, randomised, single-blind study of weekly doses of GCS-100 in CKD was started (Clinical Trials.gov identifier NCT01843790). The primary objective of this study was to compare changes in eGFR from baseline to Week 8 between placebo and GCS-100 treatment. The secondary objective was to determine the safety and tolerability of GCS-100 administered for 8 weeks relative to placebo. In addition, the study measured the effect of GCS-100 on circulating Gal-3 and other markers of disease activity. The study arms included a low dose GCS-100, a high dose GCS-100 and placebo arm. This trial is ongoing but has stopped recruiting. The results from this study were presented at a poster session in the November 2014 American Society of Nephrology (ASN) annual meeting. The abstract suggested a significant improvement in eGFR for the 1.5mg/m^2 GCS-100 group vs placebo after 8 weeks treatment, p=0.45. This significant improvement was still present 5 weeks after treatment stopped. However, there was no significant improvement in the higher dosing GCS-100 group (receiving 30mg/m^2). The abstract also suggested a

sub-group analysis demonstrated diabetic CKD patients were particularly protected by GCS-100 at the 1.5mg/m^2 dose.

In December 2014 a phase 2b placebo-controlled, randomized, double-blind, multi-centre study of GCS-100 in patients with CKD caused by diabetes was established (Clinical Trials.gov identifier NCT02312050). This study had a longer follow up and consisted of 4 arms – a placebo arm and 3 GCS-100 arms at 1 mg, 3mg or 9 mg push injections. This trial is currently recruiting. The primary endpoint was a change in eGFR from screening to measurements taken at week 26.

In 2015 the pharmaceutical company La Jolla Pharmaceuticals® discontinued further recruitment into the trial after the US Food and Drug Administration (FDA) requested further analytical studies of GCS-100. There were no patient safety or pre-clinical toxicology issues raised by the FDA. There are ongoing clinical trials of Gal-3 antagonists in the settings of liver fibrosis, CKD and idiopathic pulmonary fibrosis [Table 14].

Clinical Trials identifier	Disease	Gal-3 Antagonist	Status	Results
NCT01717248	CKD	GCS-100	Completed	Unpublished
NCT02421094	Liver Fibrosis	GR-MD-02	Not Yet recruiting	Unpublished
NCT01899859	Liver Fibrosis	GR-MD-02	Completed	Unpublished
NCT01843790	CKD	GCS-100	Active not recruiting	Unpublished
NCT02257177	Lung fibrosis	TD-139	Recruiting	Unpublished
NCT01960946	Hypertension	MCP	Recruiting	Unpublished
NCT02312050	CKD	GCS-100	Recruiting	Unpublished
NCT02333955	CKD	GCS-100	Withdrawn	Unpublished

Table 14: Clinical trials of Gal-3 antagonists in human fibrotic disease as of 2015.

1.5 Introduction Summary

sGal-3 is elevated in human CKD and is undergoing clinical trials with the endpoint of ameliorating chronic interstitial fibrosis. There is no data as to why Gal-3 is elevated in CKD, whether the useful effects of Gal-3 (AGE scavenging) reflect the elevation of Gal-3 as an appropriate physiological response in uraemia or a pathological pro-fibrotic mediator of systemic renal and cardiovascular disease. This thesis will attempt to address some of these themes.

1.6 Hypothesis and Aims

The author hypothesizes that soluble Gal-3 is elevated in a murine model of subacute uraemia and interstitial fibrosis (Adenine Diet) and that the source of Gal-3 is monocyte derived. In view of the data described before showing Gal-3's role in fibrotic disease a further hypothesis is that Gal-3 knockout mice will be protected against the renal interstitial fibrosis associated with the AD. Finally we hypothesize that the protection that is inferred by absence of Gal-3 will be mediated by fewer leucocytes infiltrating the kidneys reflecting Gal-3's role in promoting leucocyte-endothelial attachment and transmigration.

1.6.1 Aims

1) To perform the Adenine diet and optimise age of mice and duration of diet to enable incorporation of Gal-$3^{-/-}$ mice.

2) To measure both plasma soluble and solid organ Gal-3 in WT mice fed AD

3) To measure circulating monocyte Gal-3 and monocyte subset phenotype in both WT and Gal-$3^{-/-}$ mice fed AD.

4) To measure differences in weight, plasma Cr, histological tubulointerstitial injury and markers of fibrosis between WT and Gal-$3^{-/-}$ mice fed SD and AD.

5) To measure differences in leucocyte-endothelial interactions between WT and Gal-3-/- mice in the cremasteric microcirculation and renal interstitial monocyte/macrophage accumulation.

Gal-3 expression in an experimental model of uraemia

Chapter 2

Chapter 2: Gal-3 expression in an experimental model of uraemia

2.1 Background

Whilst soluble Gal-3 (sGal-3) has been demonstrated to increase in human CKD there is little animal data to suggest a similar pattern in experimental chronic uraemia.[125, 134-138] The cause of elevated sGal-3 in human CKD is not understood but already Gal-3's association with fibrotic disease has led to human trials of Gal-3 antagonists (Introduction, section 1.5.).[138] There are data on renal interstitial Gal-3 expression in a rat model of acute kidney injury (renal ischaemia/reperfusion injury) but there is none in relation to plasma soluble Gal-3 in uraemia.[105] Progressive renal interstitial fibrosis is the histological endpoint of the majority of human chronic kidney disease (CKD) regardless of aetiology.[169] A non-uremic animal model of progressive obstructive renal fibrosis (the unilateral ureteric obstruction model (UUO)) has been published examining Gal-3's role in the promotion of renal fibrosis and suggested that the absence of Gal-3 ameliorates the fibrotic effect of ureteric obstruction.[60, 121] It is not known how the addition of the uraemic milieu affects renal and systemic Gal-3 expression and renal interstitial fibrosis. This chapter presents data on plasma sGal-3, circulating monocyte Gal-3 concentrations and solid organ Gal-3 expression in experimental uraemia using the AD model.

2.1.1 Chronic Kidney Disease: Adenine Diet (AD).

The AD model of CKD is well established in rodents.[170] The AD is a model of nephrolithiasis with intraluminal tubular crystal deposition and a model of florid renal tubulointerstitial fibrosis and progressive uraemia.[171]

2.1.1.1 Adenine Phosphoribosyl transferase deficiency.

A direct human correlation to the accumulation of 2, 8 – dihydroxyadenine (DHA) crystals within the nephron is limited to a rare autosomal recessive condition called adenine phosphoribosyl transferase deficiency (APRT deficiency).[172] The largest case series of APRT deficiency was published from Japan and estimated that up to 1% of the population carry an APRT mutation as a heterozygote.[173] Few patients are diagnosed with APRT deficiency compared to the prevalence of the mutation, suggesting it is underdiagnosed.[174] The clinical presentation in human APRT mutation homozygotes is variable in the age at presentation and severity of disease phenotype. This is due to differences in the ability of an individual to saturate urinary DHA.[175] Some homozygotes are asymptomatic whilst others have significant childhood and adult nephrolithiasis which progresses to end stage renal failure.[175] Recurrence of DHA crystals in renal transplants of APRT deficient patients is also described.[176, 177] Treatment of APRT deficiency with allopurinol, if diagnosed prior to significant nephrolithiasis, can prevent and even reverse long term renal damage.[178]

2.1.1.2 Renal interstitial macrophage infiltration and fibrosis in the AD.

The AD model in mice reflects a rare human nephrolithiasis, but it is the renal macrophage infiltration, tubulointerstitial inflammation and fibrosis elicited by DHA nephrolithiasis that makes it more comparable to human CKD including diabetic nephropathy, IgA nephropathy and lupus nephritis.[179-182] As a model of renal interstitial macrophage infiltration, progressive tubulointerstitial fibrosis and uraemia it correlates with advanced CKD. Renal interstitial fibrosis is accompanied by leucocyte interstitial infiltration with chemokine and cytokine generation from these cells.[183, 184] Tamura *et al*. sought to define macrophage and chemokine pathways leading from DHA tubular stone formation to progressive renal interstitial fibrosis.[170] At day 7 of feeding 0.25% AD to C57B/6 WT mice birefringent crystals of DHA were observed in harvested renal tubules. At 14 days AD there was a marked infiltration of macrophages into the renal interstitium. Renal tissue mRNA levels of macrophage associated chemokines and cytokines -chemokine receptor 2 (CCR2), monocyte chemotactic protein-1 (MCP-1), Interleukin – 1β (IL-1β) and chemokine (C-C motif) ligand 5 (RANTES) were significantly elevated from day 7 of the diet and increased up to 28 days of feeding. Gal-3 expression was not undertaken in this study. Tamura *et al*. concluded that localised intraluminal tubuloepithelial inflammation elicited by physical damage from DHA crystals results in tubuloepithelial release of MCP-1 and (transforming growth factor beta TGF-β). This local inflammatory response is then amplified by the subsequent influx of monocyte/macrophage lineage cells inducing collagen laydown by activated interstitial fibroblasts.[170]

Tubuloepithelial expression of MCP-1 and accompanying macrophage infiltration are elevated in the UUO model of progressive interstitial fibrosis.[185] In the UUO operated kidney infiltrating macrophages secrete humoral factors TGF-β, TNF-α and fibroblast growth factor that attract and activate renal fibroblasts to produce collagen and propagate fibrosis.[186, 187] Proximal tubular cells can undergo epithelial-mesenchymal transition (EMT) which potentiates fibrosis and is established in the UUO model of renal fibrosis. EMT has not been defined in the AD model.[187, 188] The AD has an advantage over the UUO model by generating uraemia with interstitial fibrosis and allowing the interaction of uraemia and fibrosis to be observed. This is useful whilst studying Gal-3 because a hypothesis for this thesis is that elevated Gal-3 in CKD is derived from circulating monocytes and the observed monocyte subset phenotypic change in CKD promotes renal interstitial fibrosis.

2.1.1.3 Pathophysiology of the AD: the Polyamine Pathway.

Mammals produce adenine endogenously as a result of the polyamine pathway. Adenine and 5-phosphoribosyl-1-pyrophosphate are salvaged by the purine enzyme APRT to adenine monophosphate (AMP), which is not harmful. When functional APRT is absent, adenine becomes a substrate for xanthine dehydrogenase which oxidises adenine into 2, 8-dihydroxyadenine (DHA) [Fig 1]. Rodent APRT deficiency can be absolute, in a knockout model described by Stockelmen *et al.*, or functional in any WT rodent given sufficiently high oral administration of adenine.[172] DHA has a low solubility and precipitates in renal tubules having been filtered through the glomerulus. Rodents lacking APRT and

AD treated animals demonstrate nephrolithiasis with extensive tubular dilatation, inflammation, tubular necrosis, interstitial fibrosis and accompanying renal failure. C57B/6 mice fed 0.25% AD over 4 weeks demonstrate progressive macrophage and fibroblast infiltration into renal interstitium from 1-2 weeks. Infiltrating macrophages respond to increased expression of chemokines and cytokines including MCP-1, CCR-2, and TGF-β from renal tubular epithelium damaged by crystals. Tubular epithelial cells are physically stimulated by DHA crystals to produce the above cytokines and chemokines resulting in progressive peri-tubular fibrosis.[189] Biochemical and clinical data from a 0.2% AD in C57B/6 mice has been described recently confirming a severe weight loss, elevated serum creatinine with polyuria and a systemically inflamed circulating cytokine expression [Table-15].[190] The AD is not a hypertensive model unlike the majority of human CKD which is associated with hypertension [Table 15]. The other noticeable effect of AD on *WT* C57B/6 mice is a weight loss phenotype which is seen often in advanced CKD.

The polyamine pathway.

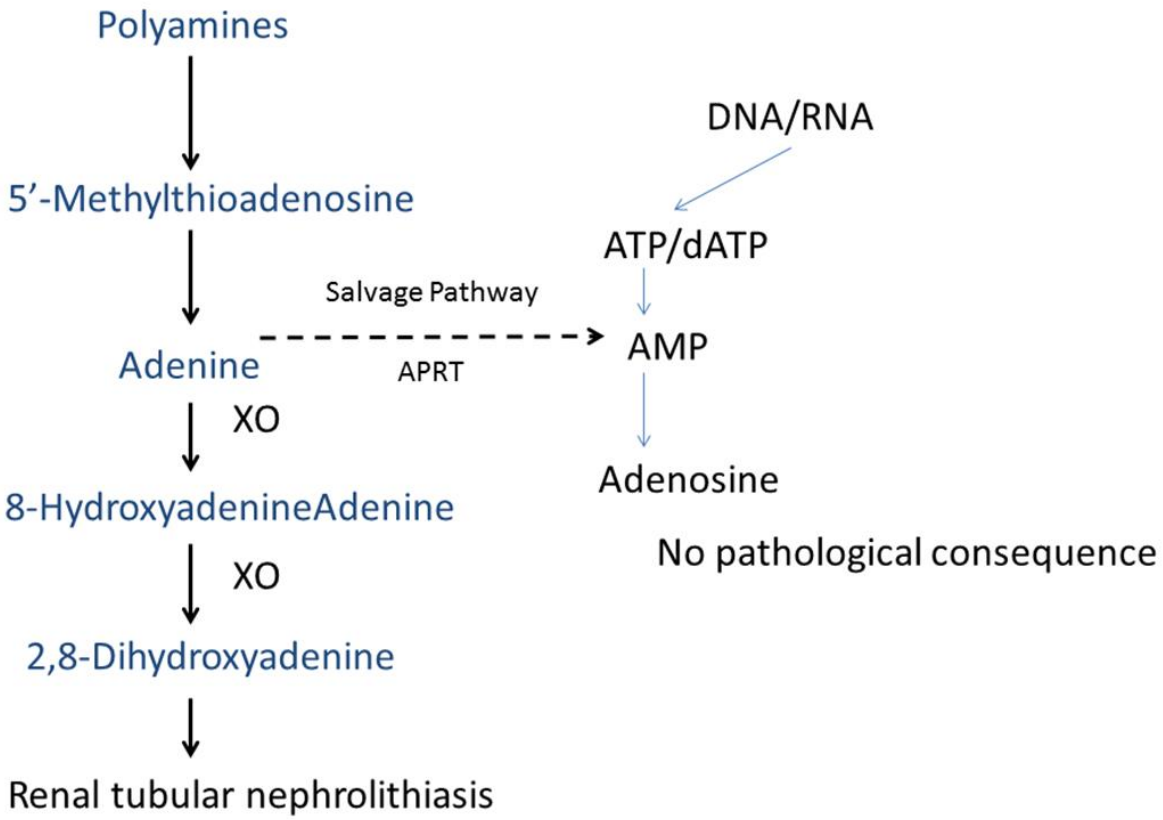

Figure 1: The polyamine pathway. Mammals endogenously produce adenine which is safely converted to AMP without consequence by APRT. When APRT is absent or overwhelmed (in the case of the adenine diet) adenine is metabolised to 2, 8-Dihydroxyadenine with resultant crystal deposition in renal tubules eliciting a brisk renal interstitial nephritis and subsequent interstitial fibrosis

Mean (SEM)	Sham Diet (n=10)	0.2% Adenine Diet (n=10)	P<0.05
Weight (g)	29.4 (0.3)	19.7 (0.5)	*
Food Intake (g/day)	4.9 (0.1)	3.3 (1.1)	NS
BP (mm/Hg)	79.7 (2.9)	84.2 (1.3)	NS
Urine Volume (uL/24hr)	680 (44)	1620 (148)	*
Creatinine (uM/L)	30.05 (2.65)	76.9 (2.65)	*
TNF-α (pg/ml)	0.8±0.1.	21.9 (8.0)	*
IL-1β (pg/ml)	13.2±5.1	57.8 (23.5)	*
IL-6 (pg/ml)	4.8±2.7.	145.8 (19.7)	*
IL-4 (pg/ml)	0.4±0.1	0.2 (0.1)	
IL-10 (pg/ml)	4.1±0.8.	24.3 (12.3)	*

Table 15: Adapted from Santana *et al*.[191]Clinical and biochemical data from WT C57B*l*6 mice fed a 0.2% AD over 6 weeks compared to standard diet (SD).The 0.2% diet induces uraemia with significantly elevated serum Cr, and a pro-inflammatory serum profile with significantly elevated TNF-α, Il-1β, IL-6 and IL-10 compared to SD controls.

2.1.1.4 AD: Experimental protocols.

There are publications using different strengths and durations of AD exposure in mice. Trial of a lower strength (0.2%) AD fed to C57B/6 WT mice over 6 weeks still yields significant weight loss.[191] Ting *et al*. set to optimise the AD in mice to overcome the significant weight loss and suboptimal duration of uraemia.[192] Prior to this paper most AD protocols had been optimised in rats and thereafter extrapolated to mice. Mice have an aversion to consuming adenine containing chow. Ting *et al*. included casein in the AD which reduces the adenine taste and smell in chow. An 8 week protocol was used with 10 day induction phase (0.3% AD + casein) followed by a maintenance phase of 46 days (alternating 0.15% and 0.2% AD). This protocol has significant benefit compared to the 4 week 0.25% AD model because murine models of CKD need 8 weeks to develop CKD associated pathology like vascular calcification.[193] Mice subject to the eight week casein protocol had a rapid weight loss in the first 10 days of induction with 0.3% AD but had a stable weight during the remaining 46 days of alternating between the 0.2 and 0.15% diet. During periods fed 0.15% AD there was a fall in measured urea and PTH indicating that there could be a washout period.

Gal-3 is expressed by most leucocytes and epithelial cell surfaces.[39-41, 68, 69, 194] The human and murine epithelial and leucocyte Gal-3 expression is frequently basal but can be increased in inflammatory disorders and cancer.[195] CKD is an inflammatory disorder with systemic effects and renal specific effects. The AD model creates a uraemic milieu in which circulating leucocytes will be exposed to pro-inflammatory mediators whilst the kidney will have intra-luminal DHA crystal

deposition and secondary leucocyte infiltration.[170, 190] This chapter seeks to define both systemic and renal Gal-3 expression for the first time in experimental chronic uraemia.

2.2 General Methods

2.2.1 Animal Husbandry

All animals were kept in accordance with the Animals Scientific Procedures Act 1986 under project licence no. 707055. Mice were housed 6 to a cage at a fixed temperature of 21±2^{o}C with 40% humidity and 12 h light /dark cycle. All animals had free access to drinking water and standard rodent chow. The standard chow (SD) was obtained from Special Diet Service ^{TM} UK RM-1 diet (product number 801002). Mice were the only animals used in the experiments contained in this thesis because of the availability of a Gal-3 knockout mouse. Any morbidly ill animals identified after experimentation were euthanized according to protocol. Murine anaesthesia, intravital microscopy (IVM) and AD supplementation was performed by myself with supervision from Julius Kieswich.

2.2.1.2 Anaesthesia during Experimentation

Anaesthesia for murine experimentation was performed by intra-peritoneal injection of Xylazine (7.5mg/kg body weight) and Ketamine (150mg/kg). Following injection the level of anaesthesia was assessed and Xylazine/Ketamine (X/K) intra-peritoneal boluses were given until an adequate level of anaesthesia was established.

2.2.1.3 Adenine Diet administration

10 week old male WT mice were fed 0.25% AD or SD over 4 weeks. All AD fed mice were otherwise kept in identical conditions as mice fed SD. Baseline demographic data including weight of the mice and weight of diet consumed were recorded each week. At weekly intervals mice were harvested and blood was taken by cardiac aspiration for plasma creatinine, Gal-3 ELISA and Flow Cytometry. The 0.25% AD was obtained from Special Diets Service (Company Number: 4225846, Product Number 823742). The AD was identical to standard chow (SDS RM1) apart from being pelleted as opposed to expanded and containing 0.25% adenine by weight. All diet was used within the expiry date of 3 months or discarded.

2.2.2 Murine Plasma Preparation

Murine plasma was used for analysis rather than murine serum. Plasma is the liquid portion left from non-clotted blood once cells have been removed by centrifugation. Serum is the liquid portion left after removal of clotted blood and does not contain clotting factors. Mice from experimental and control groups were anesthetised and underwent cardiac aspiration into a 1 ml heparinised syringe via a 25 gauge needle. Approximately 100-500 µl of whole blood was obtained and kept on ice. Whole blood was centrifuged at 1000 rpm for 10 min at 4^{o}C. Samples were inspected for turbidity or haemolysis. If there was evidence of turbidity the sample was centrifuged for a further 10 min and discarded if haemolysed. Acceptable clear plasma supernatant was pipetted into sterile 1.5

ml collection tubes and frozen at -20^{o}C for future analysis. Samples were analysed within 2 weeks of collection.

2.2.3 Plasma Creatinine Assays

A commercial plasma Creatinine (Cr) assay was used in accordance with manufacturer's instructions (BioAssay Systems, QuantiChrom™ Creatinine Assay Kit: Product number BA_DICT-500). Absorbance values were determined on an 'MRX-2' plate reader (Dynex Technologies Ltd, Worthing UK). Data was analysed with 'Revelation' software by Dynex Technologies Ltd. OD values were determined by reading the absorbance at 450 nm as the primary wavelength and 650 nm as the reference wavelength. Blank wells were subtracted from the sample well value. Intra and inter-assay coefficient of variation from samples was measured and is presented in appendix [Table A1].

2.2.4 Plasma Gal-3 ELISA

Plasma concentrations of Gal-3 were measured by ELISA in accordance with the manufacturer's instructions from age sex matched WT mice fed either SD or AD. The commercial ELISA kit used was Gal-3 (R&D Systems- Europe Ltd. Catalogue number DY1197).The Gal-3 ELISA required dilution of the murine plasma samples with reagent buffer. The Gal-3 plasma samples were assayed in duplicate in a 96 well plate pre-coated with the appropriate detection antibody. Plates were analysed immediately on a Dynex Technologies Ltd, Worthing UK MRX 2 plate reader and analysed with 'Revelation' software by Dynex Technologies. OD values were determined by reading the absorbance at 450 nm as the primary wavelength and 650 nm as the reference wavelength. Blank wells were

subtracted from the sample well value. Standard curves were generated by plotting mean absorbance against each concentration of recombinant standard. The concentration of protein in samples was calculated from the standard curve and multiplied by dilution. Inter and intra-assay Coefficient of Variation (CV) of the Gal-3 (and Gal-1) ELISA plates contributing to results is described in the appendix [Table A2, A3]. The mean CV of the Gal-3 ELISA is higher than ideal (less than 15%). The ability of Gal-3 to self-associate could contribute to a high degree of variance. Gal-3 ELISA plasma sample results with a CV greater than 20% were not included in this work. Plasma Gal-3 levels were raised beyond expected values in haemolysed plasma samples appearance, indicating a release of intracellular Gal-3 from disrupted cells. This was confirmed by centrifuging mouse blood samples at a high speed (> 800 *g*) [Table A4]. To reduce the chance of capturing intracellular Gal-3 data on ELISA any haemolysed appearance was documented and excluded from data analysis. Care was taken to reduce trauma to the integrity of the whole blood sample. Plasma sGal-3 concentrations included in this thesis were similar to published data [196].

2.2.5 Real time quantitative PCR

The details below are attempting to satisfy MIQE guidelines on minimum data requirements for publishing results for real time quantitative PCR (qPCR) [197].

2.2.5.1 Total RNA isolation from solid organs

qPCR was performed on WT murine kidneys. Following appropriate anaesthesia organs were retrieved in a sterile operating field. The kidneys were retrieved by laparotomy. A whole kidney was ‘snap frozen’ in liquid nitrogen. The estimated

time from effective anaesthesia to snap freezing the kidneys was less than 2 min. Kidney specimens were transferred to storage at -80^{o}C for use within 6 months.

2.2.5.2 Nucleic acid retrieval

Each sample was processed individually to yield mRNA in accordance with commercial manufacturer's instructions (Qiagen RNeasy Mini kit: Cat no 74104). There were 2 techniques used for homogenising tissues in commercial buffer (RLT buffer).

1- Pestle and Mortar; frozen kidneys were taken from -80^{o}C storage into liquid nitrogen. A whole kidney was crushed by pestle and mortar until a fine powder. 30mg of powder was transferred to a 2.0 ml syringe containing 600µl of RLT buffer with 1% β-mercaptoethanol. The buffer and powdered tissue were passed through a 20-gauge (0.9 mm) needle attached to a sterile plastic 5–10 times or until a homogeneous appearance of lysate was achieved.

2- Ultrasonication by commercial tissue disrupter; frozen kidneys were taken from -80^{o}C storage into liquid nitrogen. A whole kidney was cut into quarters then placed in 2 ml of RLT buffer and given 3 pulses of 30 sec with a 15 s rest on ice to prevent overheating. This was performed until a homogenous appearance of lysate. Subsequent steps were identical between the 2 methods of tissue homogenisation.

The resulting lysate was centrifuged at full speed (800*g*) for 3 min. Supernatant was pipetted into another 2 ml eppendorf™ tube and the pellet discarded. 1 volume of 70% ethanol was added to the supernatant and mixed gently by

pipetting. 700µl of the ethanol/supernatant was placed in an RNeasy spin column in a 2 ml collection tube and centrifuged for 15 s at 10,000 rpm. The collected flow through was discarded. 700 µl of RW1 buffer (Qiagen RNeasy mini Kit) was added to the RNeasy spin column and centrifuged for 15 seconds at 10,000 rpm. Follow through was again discarded. The spin column membrane was then washed by adding 500 µl of RPE buffer (Qiagen RNeasy mini kit) and centrifuging for 15 seconds at 10,000 rpm. The collection tube was emptied and a further 500 µl of RPE buffer was added to the spin column and centrifuged for 2 min at 10,000 rpm. A new collection tube was then added to the spin column and centrifuged at full speed for 1 min. Finally a 1.5 ml sterile collection tube was placed on the spin column and 40 µl of nuclease free water was added to the spin column, which was then centrifuged for 1 minute at 10,000 rpm. The collected RNA in nuclease free water was stored at -80^{o}C until required.

2.2.5.3 Nucleic Acid quantity and quality assessment.

The quality and concentration of RNA was assessed using a commercial spectrophotometer (Nanodrop ND-1000, NanoDrop Technologies, DE, USA). Nucleic acid purity was measured against a sample of genetic grade water as a baseline control [Table 16]. The concentration of RNA was measured in ng/µl from the absorbance at 260nm. 260/280 and 260/230 ratios were recorded to demonstrate RNA quality. The ratio of absorbance at 260 and 280 nm is used to assess RNA purity, and a ratio > 2.0 is accepted as pure for RNA. All samples used for PCR in this thesis have achieved this, however the 260/230 ratio were lower. The ratio of absorbance at 260 nm and 230 nm is a secondary measure of purity

and should be around 2. Lower 260/230 ratios could indicate the presence of a contaminant absorbing at 230. Possible contaminants include carbohydrates, phenols and EDTA. The RNeasy Mini kit does not contain phenolic compounds. A 260/230 ratio of >1.8 is generally acceptable. Genomic DNA contamination is claimed unlikely using RNeasy spin since the silica-gel–membrane, spin-column technology efficiently removes the majority of the DNA without DNase treatment. However a DNase step in reverse transcriptase would reveal possible contamination.

	RNA concentration (ng/µl)	Absorbance Ratio	
		260/280	260/230
Gal-3 -/-			
s1	3000	2.02	2.24
s2	3401	1.97	2.18
s3	2009.6	2.98	1.83
a1	3189.3	1.99	2.18
a2	3899.3	1.8	1.98
a3	-2	-5.95	-0.14
a4	3430.6	1.95	2.13
a5	2523.7	2.06	2.15
WT			
s1	2766.9	2.05	2.09
s2	1117.4	2.11	1.36
s3	4001.9	1.74	1.79
a1	3267.6	1.98	2.14
a2	2831	2.04	2.17
a3	3054.9	2.01	2.14
a4	3191.5	1.99	2.13
a5	2674.8	2.05	2.19

Table 16: RNA quality and quantity assessment of kidney specimens used for PCR in this thesis.

2.2.5.4 cDNA synthesis.

RNA was quantified and equilibrated for all samples to 1000ng total per sample to be reverse transcribed into cDNA. The following steps followed manufacturer's instructions for Superscript (II) Reverse transcriptase by Invitrogen (Cat no 18064-014).To a nuclease-free microcentrifuge tube the following were added; 1µl of random primers, 1 µl dNTP Mix [10mM], RNA volume (variable to equilibrate) and genetic grade water to make up the volume to 12 µl. The samples were then placed in a G-Storm thermal cycler and the contents heated to 65^{o} C for 5 min. Samples were removed, chilled on ice and then briefly centrifuged. The following was then added to each microcentrifuge tube; 4µl of 5x First-Strand buffer, 2µl of DTT (0.1M) and 1µl of RNaseOUT to a total volume of 19 µl per sample. The samples were placed back in the G-storm thermic cycler and incubated at 25^{o}C for 2 min. At this point the heating cycle was paused, the lid of the cycler was opened and 1 µl of Superscript 2 Reverse Transcriptase was added to each tube and mixed by gently pipetting up and down. The cycler lid was then closed and the 25^{o}C program continued for 10 min, 42 ^{o}C for 50 min and finally the samples were inactivated by heating to 70 ^{0}C for 15 min. This yielded a 20µl volume to which 80µl of nuclease free water was added. The resulting cDNA samples were then stored at -80 ^{o}C until ready to be used for qPCR.

2.2.5.5 Real Time Quantitative PCR

qPCR was performed with Absolute qPCR Mix (AB-1139). A mastermix was generated for each gene of interest. 10 µl samples were manually pipetted in

0.1ml Corbett style strip tubes. The house keeper gene was 18s (TaqMan® Ribosomal RNA Control Reagents - catalogue number 4308329), the probe was conjugated to a VIC fluorophores designed to detect ribosomal 18s RNA. The probe on the Gal-3 probe was FAM (6-carboxyfluorescein). Both fluorophores are TaqMan™ probes with VIC being detected on the yellow channel and FAM on the green channel of the Corbett 6000 thermal cycler. All samples were performed at least in duplicate. Once prepared the samples were placed in the Corbett 6000 thermal cycler and the following thermal cycling profile used. Samples were held before cycling at 50^{o}C for 2 min then 95^{o}C for 10 min before undergoing 50 cycles of 95^{o}C for 15 sec and 60^{o}C for 60 s.

2.2.5.6 Primers and Probes

Gene of interest Primers and Probes were purchased from Sigma-Aldrich and sequences shown below. All primers and probes were stored at -20^{o}C. For qPCR they were diluted to 100µM. Primers were used at 500nM and Probes at 250 nM.

Target Gene	Gene Name	Chromosome	Gene Accession number
Mouse Gal-3	*Lgals3*	14	NC_000080.6 (47373860..47386167)
Mouse α-SMA	*Acta2*	19	NC_000085.6 (34240336..34255585)
Mouse Pro-collagen (I)	*Col1a1*	11	NC_000077.6 (94936270..94951867)
Mouse TGF-β	*Tgfb1*	7	NC_000073.6 (25687002..25704996)
Mouse CD 68	CD68 antigen	11	NC_000077.6 (69664213..69666646
Mouse CHI 313	Chi3l3	3	NC_000069.6 (106147548..106167564)
Mouse Retnla	*Retnla*	16	NC_000082.6 (48842552..48844461)

Table 17: qPCR target genes of interest used during this thesis showing gene names, chromosome and gene accession number. Chapter 2 gives results for Gal-3 and CD 68 PCR data. Data from fibrosis genes (*Pro-collagen (1), TGF-β, α-SMA*) and Macrophage subset differentiation genes (*CHI-313* and *Retnla*) are presented in Chapter 3 of this thesis.

Oligo name	Sequence (5'-3')	Purification
Mouse procollagen probe	[6FAM]ATGGCTGCACGAGTCACA[TAM]	HPLC
Mouse α-SMA probe	[6FAM]TCCAAATCATTCCTGCCCA[TAM]	HPLC
Mouse Galectin-3 probe	[6FAM]CGGTCAACGATGCTCACCYACTGCA[TAM]	HPLC
Mouse TGF-Beta probe	[6FAM]CAACTATTGCTTCAGCTCCACAGAGAACTG[TAM]	HPLC
Mouse Procollagen Fwd	TTCACCTATACAGCACGCTTGTG	DST
Mouse Procollagen Rev	GATGACTGTCTTGCCCCAAGGTT	DST
Mouse alpha-SMA Fwd	TCAGCGCCTCCAGGTTCCT	DST
Mouse alpha-SMA Rev	AAAAAAAACCACGAGTAACAAATCAA	DST
Mouse Galectin-3 Fwd	TTGAAGCTGACCACTTCAAGGTTG	DST
Mouse Galectin-3 Rev	AGGTTCTTCATCCGATGGTTG	DST
Mouse TGF-beta fwd	CACCGGAGAGCCCTGGATA	DST
Mouse TGF-beta rev	TGTACAGCTGCCGCACACA	DST

Table 18: Commercial Primer / probe sequences purchased from Sigma Aldrich. Commercial primers and probes purchased from Sigma-Aldrich, TaqMan probes were used exclusively for PCR.

2.2.5.8 Agarose gel of amplicons from qPCR

Agarose gel electrophoresis of products from the housekeeper (18S), α-SMA, TGF-β, Procollagen (1) and Gal-3 PCR was performed to exclude contaminants in the amplification process. All genes showed a single band excluding significant RNA contamination in the amplification process [Fig 2]. Agarose gels for CD-68, CHI-313 and Retnla genes were not performed due to time constraints.

2.2.5.8.1 Agarose gel methodology

Agarose gel electrophoresis was performed by Julius Kieswich. 10µl volumes from qPCR reactions were mixed with commercial gel loading buffer (Sigma Cat no: G2526) and separated on 2% agarose gel. The gel was then stained with Gel Red (Cambridge Biotechnology Cat no: BT41003) for 30 min before photographing over an Ultra-Violet (UV) light (UVIP).

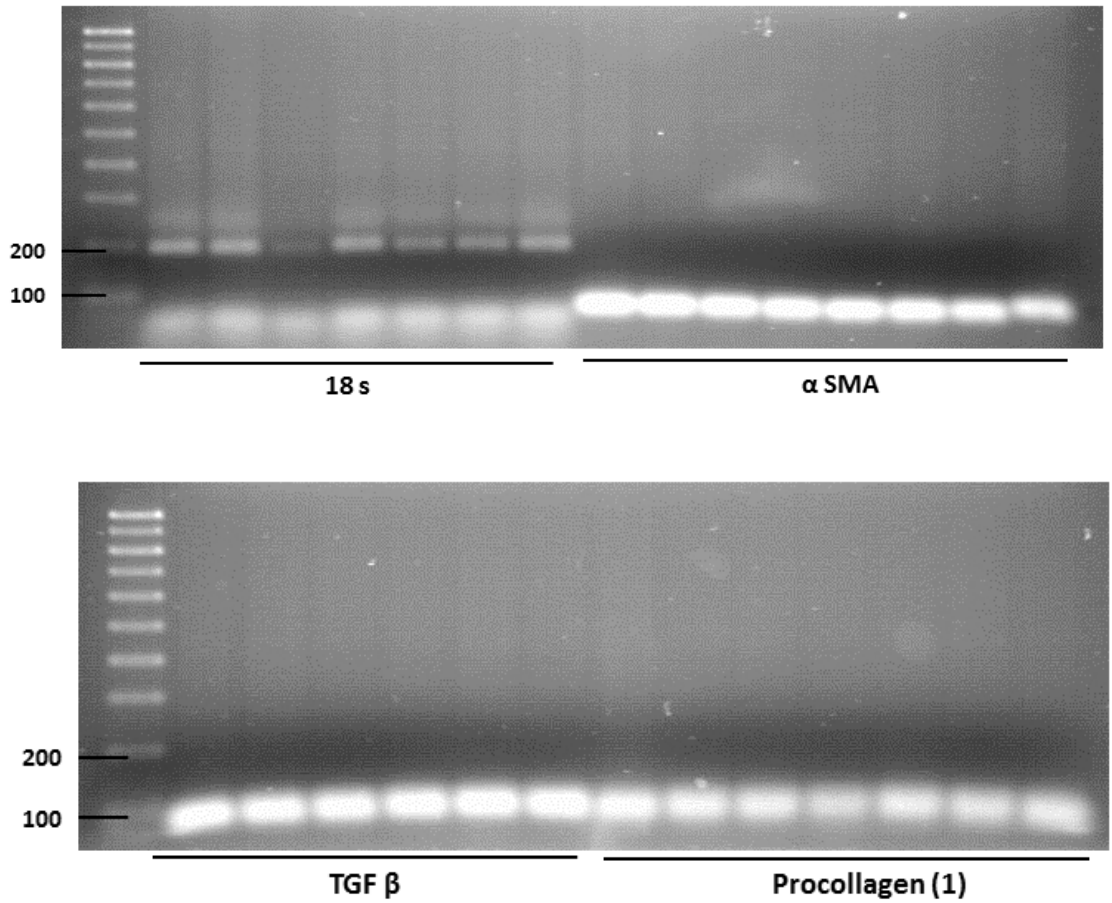

Figure 2: Gel of housekeeper (18s), α-SMA, TGF-β and Procollagen (1) amplicons after qPCR. There is a single band for each gene at the appropriate amplicon length for the 18s housekeeper and genes of interest. Amplicon length of 18s = 187bp, α-SMA = 68 bp, TGF-β = 72bp and Procollagen (1) amplicon = 65 bp. There are no differences between lanes because this is taken after 40 cycles at the linear phase of amplification.

2.2.5. qPCR Data analysis

qPCR was performed in the investigators laboratory and data interpreted by the investigator. Comparative quantitation was used to compare data and unlike the delta-delta CT method this does not require assessment of reaction efficiencies before analysis. Analysis was conducted on the Corbett 6000 software and exported to Microsoft Excel. Only data with low standard deviation between samples (<0.7) were included in results. For analysis no template controls (NTC) and reverse transcriptase controls (RTC) were switched off. Samples were performed at least in duplicate and preferably in triplicate. Because TaqMan™ primers and probes were used melt curve analysis could not be performed.

2.2.6 Leucocyte Fluorescence-Activated Cell Sorting

2.2.6.1 Fluorescence-Activated Cell Sorting (FACS) analysis of circulating leucocytes

WT and Gal-3 $^{-/-}$ fed SD or AD had FACS analysis of their circulating leucocytes from whole blood samples obtained after anaesthesia. Mice were underwent cardiac puncture to obtain approximately 200-500 µl of whole blood into a heparinised syringe. Erythrocytes were lysed using 10 mL 1x lysis buffer per blood sample (RBC lysis Buffer 10x, eBioscience, Cat no: 00-4300-54). The sample was agitated for 30 s until clear. 5 mL of ice-cold PBS was then added to each sample to halt lysis. Samples were centrifuged at room temperature at 300 *g* for 10 min. The supernatant of lysis buffer and lysed erythrocytes was discarded and the cell pellet of leucocytes was suspended in 100 µL of Phosphate Buffered Saline (PBS) +0.1% Bovine Serum Albumin (BSA). The cell suspension was plated

onto a 96 well plate and washed twice with 100 µL of PBS (+0.1% BSA). The washing step involved adding 100 µL of PBS (0.1% BSA) to each well, centrifuging at 1000 rpm at 4^{o}C for 8 min then discarding the supernatant and repeating the step. Care was taken to agitate the cell pellet during the washing by pipetting up and down to adequately wash the cells. Suspended cells were then incubated for 10 min with FC block (anti-mouse CD16/CD32) on ice in the dark [Table 19]. 2 wash steps were repeated and the cells were incubated with cell surface antibodies on ice in the dark for 30 min. The cells were then washed twice again then fixed by adding 100 µL of fixation buffer per well and samples were incubated at room temperature for 20 min in the dark (IC Fixation Buffer, eBioscience, Cat no: 00-8222-49). Following fixation 200 µL of permeablisation buffer (PB) was added to each well and then washed twice more in PB (Permeablisation Buffer 10x, eBioscience, Cat no: 00-8333-56). The cells were then incubated at 4^{o}C in the dark for 45 min with intracellular antibody or isotype control in PB. Following incubation cells were washed 2 more times in PB and left in 100 µL of pure PBS. Samples were kept on ice in the dark until analysis.

2.2.6.2 FACS analysis of peritoneal macrophages

WT mice fed SD and AD were used for FACS analysis of resting peritoneal macrophages. The peritoneum was not inflamed prior to analysis which has been described in WT and Gal-3 $^{-/-}$ mice previously. In contrast to harvesting whole blood, mice were not anaesthetised by IP injection of X/K but underwent cervical dislocation to minimise peritoneal trauma and inflammation prior to analysis. After cervical dislocation 5 mL of peritoneal lavage solution (PBS + 0.25% BSA

and 2 mM Ethylenediaminetetraacetic acid EDTA) was injected into the peritoneal cavity. The abdomen was gently manipulated for 2 min. After 2 min the lavage solution was aspirated from the peritoneal cavity into a 5 mL syringe. An erythrocyte lysis step was not undertaken and following this all steps were performed as outlined in section 2.2.6.1.

2.2.6.3 Flow Cytometry controls and data analysis.

CD 11B, Gal-3, Ly6c were optimised at different concentrations to use the minimum concentration necessary to achieve acceptable results [Fig 4]. All antibodies were used in conjunction with isotype controls at the same concentration. An isotype control is a flourochrome of the same antibody class as the primary conjugated antibody but lacks the binding epitope. Isotype controls demonstrate how much non-specific binding there is. Unstained controls were also used in conjunction with isotype controls to discern a true fluorescent effect above baseline.

All samples were analysed on the same Beckton-Dickinson fluorescence activated cell sorter (FacsCalibur A). Voltage and compensation parameters were set for each experiment to achieve the optimum reading of sample against its isotype. All FACS data were analysed using Flo-Jo^{TM} software (version 7.6.5). Leucocyte sub-populations were gated by a combination of size (forward scatter – fsc), granularity (side scatter – ssc) and positivity for cell-markers CD11b and Ly6c (monocytes) ly6g (granulocytes) and CD-68 (macrophages). Compared to SD fed WT leucocytes after 3 weeks of diet, AD fed WT leucocytes showed increased auto-fluorescence, and increased susceptibility to permeabilisation – which

reduces side scatter characteristics. The data had to be analysed taking this into account. The use of an isotype controls reduced concern over the contribution of auto-fluorescence to the final results [Fig 3, Table 19].

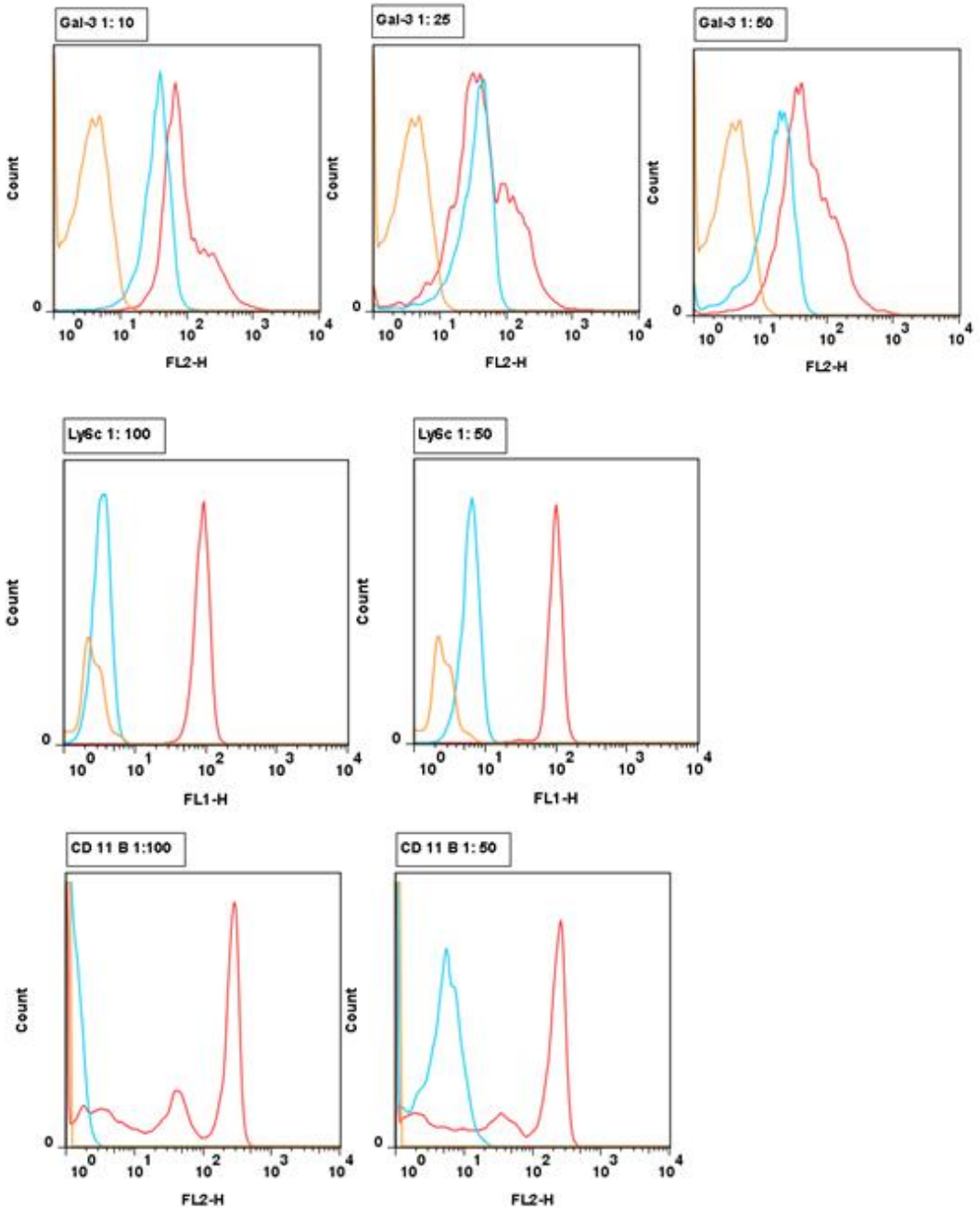

Figure 3: Optimisation of antibody concentrations used in flow cytometry. All antibodies used in flow cytometry were fluorochrome conjugated primary antibodies. Each antibody was assessed against an unstained sample and isotype control. Different concentrations of antibodies were tested to give an optimal fluorescence separation from its isotype control. Panels show unstained sample (orange line), isotype control (blue line) and primary fluorochrome associated antibody (red line).

Antibody	Use	Fluorochrome	Dilution	Company	Catalogue number
Cell Surface Antigen					
Rat anti-mouse Ly6c	Monocyte marker	FITC	1 : 100	Abcam	Ab15686
Rat anti-mouse Ly6g	Granulocyte marker	FITC	1 : 10	Abcam	Ab25024
Intracellular Antigen					
Rat anti-human/mouse Gal-3	Protein of interest	PE	1 : 50	eBioscience	12-5301-82
Rat anti-human/mouse CD 11b	Monocyte marker	PE	1 : 75	Biolegend	101208
Rat anti-mouse CD68	Macrophage	FITC	1 : 50	Novus Biologicals	NB100-63984
Isotype Controls					
Rat-anti mouse IgG2a κ	IC for Gal-3	PE	1 : 50	Biolegend	400508
Rat-anti mouse IgG2b κ	IC for CD 11-B	PE	1 : 75	Biolegend	400607
Rat-anti mouse IgG2a κ	IC for Ly6c	FITC	1 : 100	Biolegend	400505
Block					
Anti-mouse CD16/CD32	Fc- Block	N/A	1 : 50	Biolegend	101301

Table 19: Commercial antibodies used in FACS of murine whole blood in this thesis.

2.2.7 Histopathology

All samples collected for histology were washed briefly in 0.9% normal saline, and then placed in 10% formalin for 48 h. After this they were placed in 70% ethanol before being embedded in paraffin. Histology was performed by the William Harvey institute Cancer Pathology services. Briefly 4 µm thick tissue sections were cut from organs mounted on paraffin blocks. Histological scoring was by performed by myself blinded to the treatment of the animal and scoring randomly assessed and agreed with a Consultant Histopathologist, Professor Sheaff, using ImageJ software.

2.2.7.1 Renal Gal-3 immunohistochemistry

The primary anti-Gal-3 antibody was optimised to a 1:250 dilution using mouse lung as a positive control (Goat anti-mouse Gal-3, R+D systems, Cat no: BAF1197) [Fig 4]. Secondary HRP conjugated antibody was a polyclonal rabbit anti-goat biotinylated used at a dilution of 1:100 (Rabbit anti-goat, Dako, Cat no: E0466). Non-specific secondary antibody staining was assessed by using secondary antibody incubation alone without primary antibody.

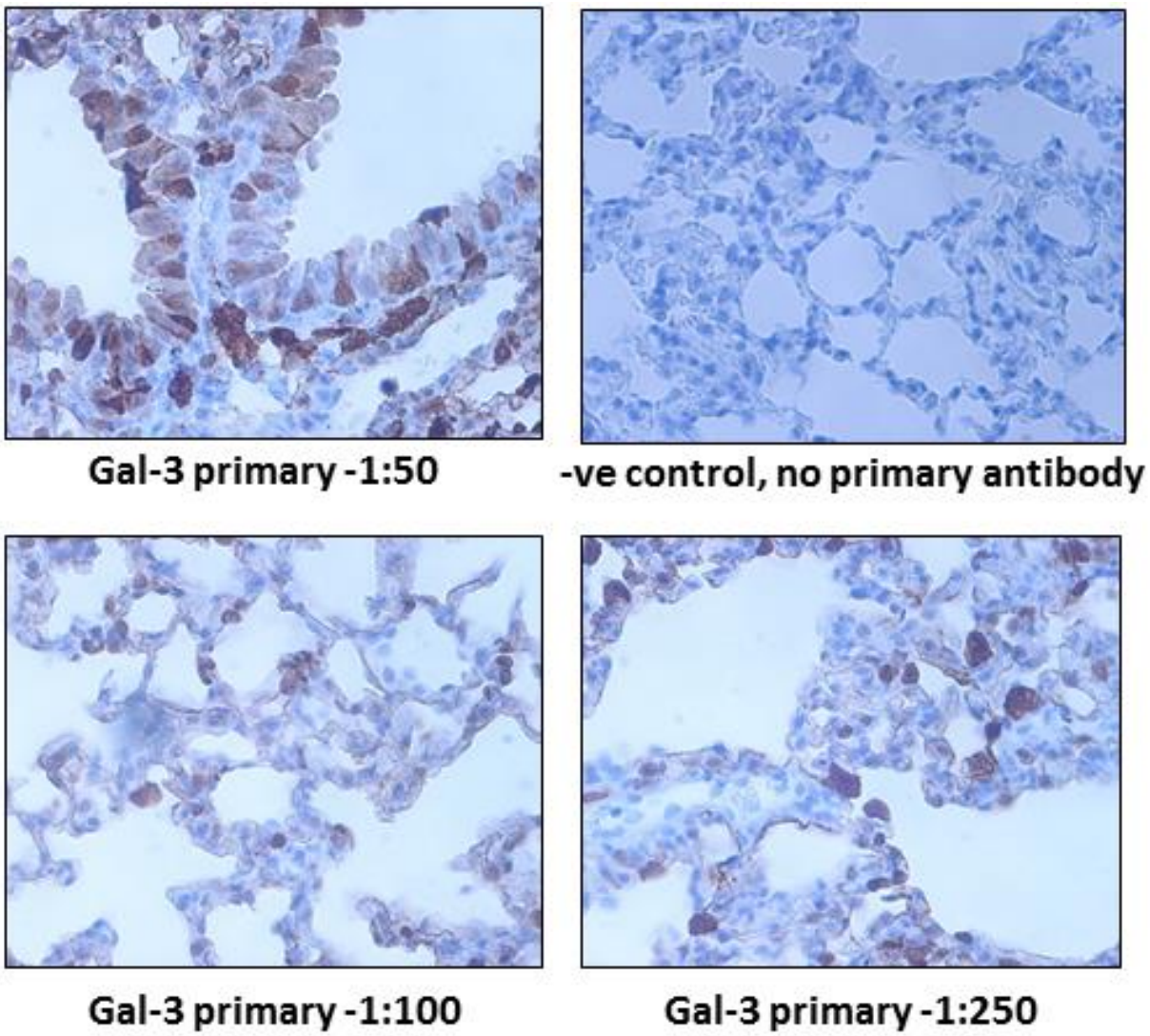

Figure 4: Immunohistochemistry, Gal-3 antibody optimisation using mouse lung as a positive control. Gal-3 was optimised to a dilution of 1:250 which eliminated the majority of background non-specific immunoperoxidase staining.

2.2.7.2 Macrophage (F4/80) immunohistochemistry

4µm kidney sections were stained with a rat anti-mouse F4/80 primary antibody (F4/80, IgG2b T-2008, BMA Biomedicals) at 1:100 dilutions. An isotype control (ABD Serotec IgG2b Negative Control -MCA1125) was also used to demonstrate non-specific staining at the same dilution.

2.2.7.3 Histopathological scoring

The number of F4/80 +ve cells per x40 field was used to quantify renal interstitial macrophage number. 6 x40 cortical images were used per animal. The mean number of cells per image was calculated and compared between groups [Figure 5].

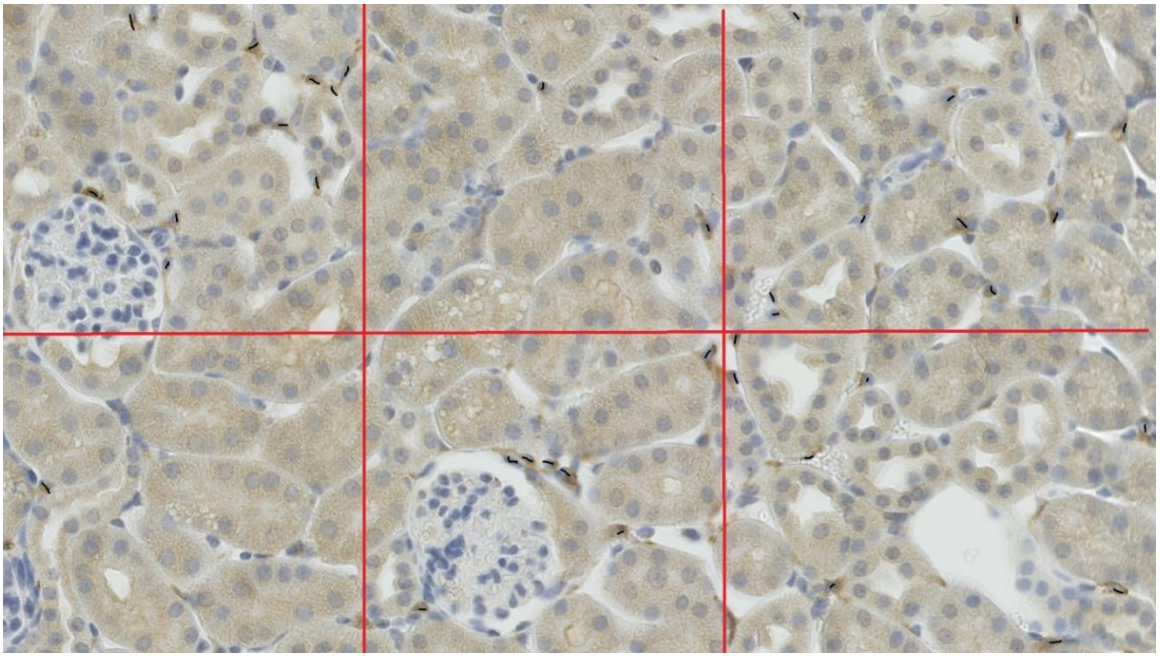

Figure 5: Histological F4/80 positive cell scoring of x 40 magnification image of mouse renal cortex. A x40 image was divided into 6 areas and F4/80 +ve cells marked with a black line. The cells were counted per square then added to get an overall number of F4/80 +ve cells per x40 image. 6 images per cortex were scored for each animal and a mean of the numbers of cell was generated per animal.

2.3 Results

2.3.1 Characterisation of optimum duration of AD-CKD in mice.

AD diet induces renal failure and weight loss in WT mice

7 week old WT mice were allocated to SD or AD and harvested at 1, 2, 3 and 4 weeks duration of diet. Body weight and plasma Cr was measured in each animal at weekly intervals [Table 20]. AD fed mice had increased mean plasma Cr at 1 week of diet compared to SD mice at 1 week. After 2 weeks of AD the Cr rose significantly compared to SD mice, indicating significant kidney impairment. AD fed mice continued to develop progressive uraemia over the 3rd and 4th week. Mortality was high at the 4th week and optimal duration of diet was felt to be 3 weeks for subsequent experiments. 10 week old WT mice harvested at 3 weeks demonstrated similar plasma Cr differences between AD and SD fed mice and tolerated the diet better [Fig 7]. For all subsequent AD experiments 7 week old mice were used for 3 week duration to maximise efficiency and reduce expense.

2.3.1.1 Determination of optimum age of AD-CKD mice

WT mice lose weight over 4 weeks of AD.

WT AD fed mice rapidly lose body weight over the 4 weeks [Table 20, Fig 6a]. At 4 weeks there was a significant mortality with just under 25% of mice dying in the last week (data not shown). The second experimental group had less weight loss comparatively to the first group but a similar mortality. The 7 week old WT mice were not weighed each week, only at harvest, so mean weight over time does not reflect weights from the same individuals. Data of weight changes

within the same group of 10 week old WT mice fed AD or SD was subsequently collected [Fig 6b]. Collecting data sequentially on the same group of individuals rather than different individuals each week demonstrated a more consistent weight loss with a lower mean weight each week [Fig 6b]. 10 week old WT animals were heavier than the 7 week old animals and had a lower mortality at 4 weeks. The amount of diet consumed by 10 week old animals was assessed by distributing a set weight of both SD and AD to each cage every week. Before the next food refill the remaining feed was re-weighed and the total weight of diet consumed was recorded. This remained constant over time and equivalent between the WT SD and AD fed mice (Chapter 3, section 3.3.1). The AD is pelleted and SD expanded so it is possible the pelleted diet, being smaller, could fall between food trough bars, not consumed. The implication being that AD could fall into the cage without being consumed so the weight of leftover AD would not therefore indirectly correlate with consumed AD feed.

	Standard Diet				Adenine Diet			
Duration of Diet (Wks)	1	2	3	4	1	2	3	4
Number of animals	8	8	7	6	7	6	7	7
Plasma Cr (μM/L)	8.97 (6.72)	14.39 (2.81)	15.96 (7.93)	19.46 (4.04)	24.78 (12.08)	48.09 (11.28)	55.28 (16.99)	55.76 (25.02)
Mean Wt (g)	20.64 (0.98)	21.06 (2.75)	24.29 (1.09)	24.52 (3.01)	17.69 (1.73)	13.26 (0.83)	13.79 (1.83)	13.29 (2.12)

Table 20: Plasma Cr and body weight data for 7 week old WT mice fed SD or AD diet over 4 weeks. Plasma Cr and body weights are shown as mean (± standard deviations) values. At 1 week SD vs AD there is a significant increase in mean plasma Cr in the AD group, p= 0.071 (unpaired t-test). The mean plasma Cr continues to increase over the duration of diet whilst SD fed mice have no statistical increase in their plasma cr. Body weight also falls significantly at 1 week AD compared to SD fed mice, p=0.0012 (unpaired t-test).This table refers to WT animals only. At 4 weeks AD animals had significant mortality and body weight lost. Further experiments used mice fed AD for 3 weeks only for better survival and subsequently greater consistency of data.

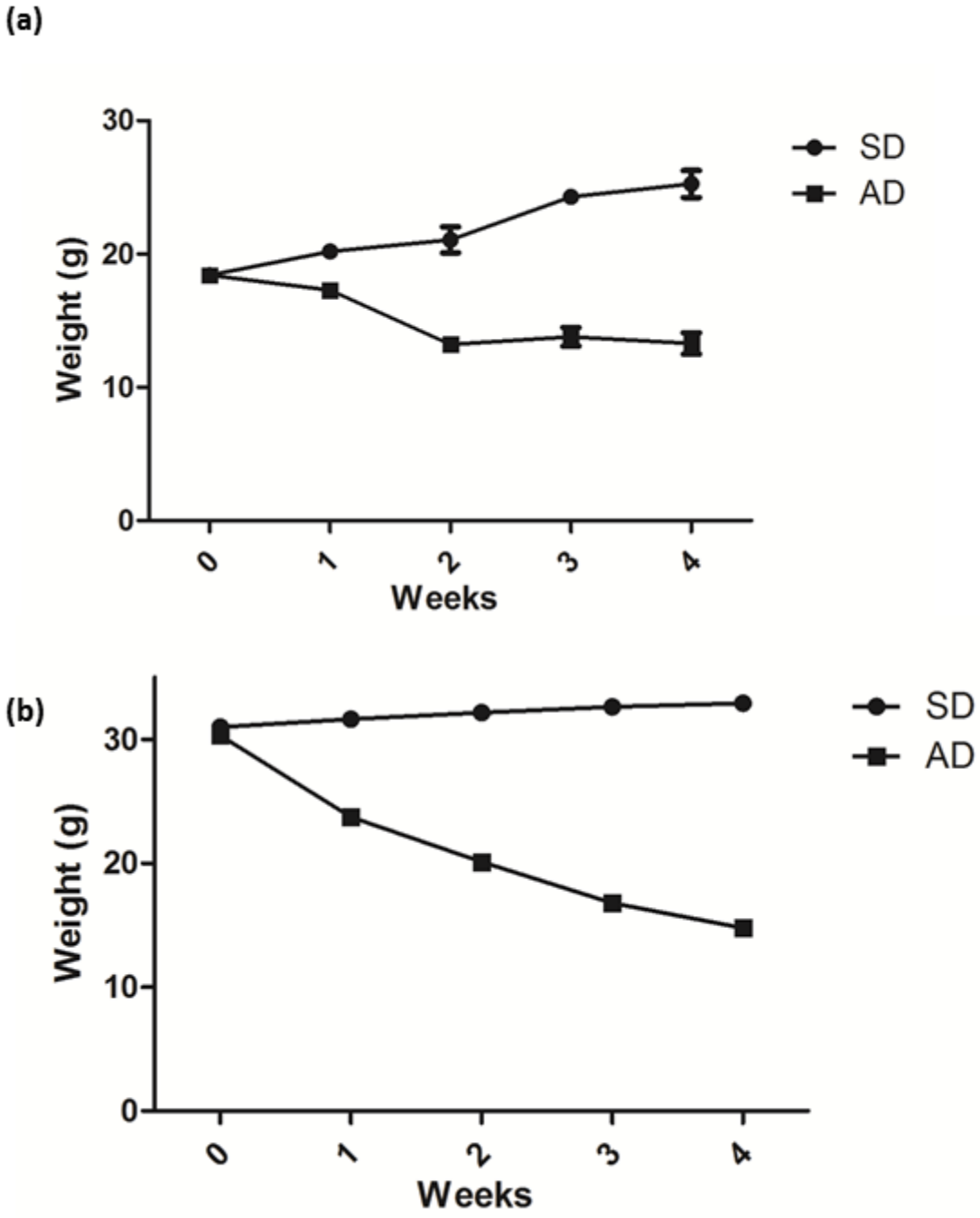

Figure 6: Body weight data Mean (SEM) from 2 different age groups of WT mice fed AD or SD over 4 weeks**.** (a) Body weights from 7 week old mice. SD fed mice body weight is significantly greater than AD fed mice from 1 week diet p=0.0356 (Mann Whitney). (b) Body weights of 10 week old mice again show a significant difference in weights between SD fed mice and Ad fed mice from 1 week diet p=0.0317 (Mann Whitney)

(a)

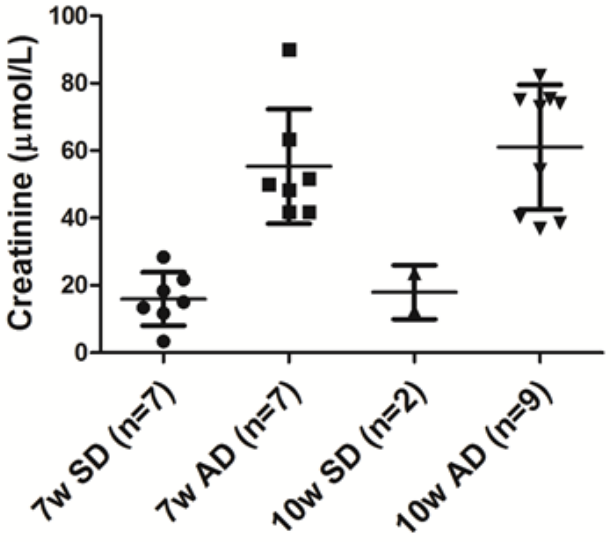

(b)

	7 Week Old		10 Week Old		p=<0.05
	WT SD	*WT* AD	*WT* SD	*WT* AD	
Number of Animals	7	7	2	9	
Plasma Cr (µmol/L)	15.96 (7.93)	55.28 (17)	17.99 (8.0)	61.04 (18.49)	(NS)

Figure 7: Plasma Cr at 3 weeks AD diet in different age groups of mice. (a) Scatter plot of plasma Cr with individual results amongst groups with error bars displaying mean and standard deviation values (b) Mean (Standard Deviation) values of plasma Cr data from 7 week old vs 10 week old WT mice taken at 3 weeks of AD. Plasma Cr was not significantly different (NS) between the 7 week old AD fed WT vs 10 week old AD fed WT mouse groups, Cr = 55.28 µmol/L (±17) vs. 61.04 µmol/L (± 18.49) p=0.53.

2.3.2 Soluble Gal-3 in experimental uraemia

2.3.2.1 Plasma sGal-3 concentration is elevated from 1 week in AD treated WT mice.

47 WT mice o were used to assess sGal-3. Plasma sGal-3 was measured by ELISA in duplicates. 25 mice were assigned to SD (10 had sGal-3 measured at 1 week diet, 8 measured at 2 weeks SD and 7 measured at 3 weeks). 22 mice were used in the AD group (10 had sGal-3 measured at 1 week AD, 7 mice had sGal-3 measured at 2 weeks AD and 5 mice at 3 weeks AD). The lower numbers in the week 3 AD reflecting the significant mortality at this point. Of those 47 measurements only 16 SD fed mice and 16 AD fed mice had duplicate plasma sGal-3 values with a CV < 20%. Any sample with a duplicate CV > 20% was excluded from analysis.

Plasma sGal-3 rose within a week of commencing the AD, compared to SD fed mice (19.05 vs 16.24 ng/ml) [Fig 8a]. This reached statistical significance after 3 weeks of diet and there is a significant positive correlation between plasma Gal-3 and plasma Cr [Fig 8b]. sGal-3 levels are equivalent to concentrations seen in pathological human disease including CKD.[138] The sGal-3 increases in the AD only reached significance at 3 weeks so it was decided to examine Gal-3 expression in circulating leucocytes at this time point on the diet.

Plasma Gal-3 (ng/ml)				
Week	Nos of Mice (SD vs AD)	SD	AD	p=<0.05
1	(4 vs 6)	16.24 (4.43)	19.05 (4.32)	NS
2	(6 vs 6)	12.55 (4.39)	18.57 (7.47)	NS
3	(6 vs 4)	11.04 (1.61)	23.57 (8.44)	*

(a)

(b)

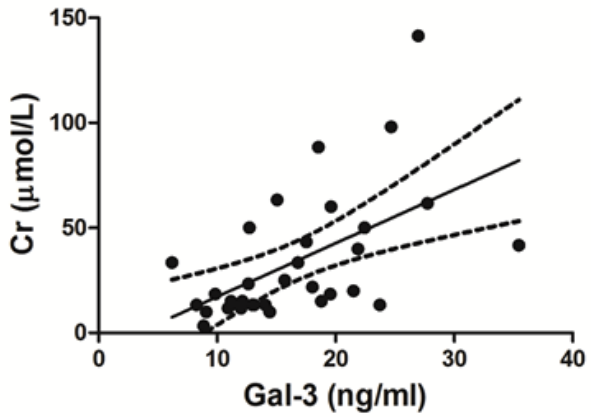

Figure 8: sGal-3 in the AD over time in WT mice. (a)Plasma sGal-3 ELISA over 3 weeks SD or AD in 7 -10 week old WT mice. Table shows median sGal-3 values (standard deviation). Median plasma Gal-3 rose in a time dependent manner in AD fed animals. This only reaches significance at 3 weeks AD, p=0.0095 (Mann Whitney U). Though SD fed mice have a reducing median plasma sGal-3 over 3 weeks this does not reach statistical significance. (b) Linear regression of plasma Cr vs plasma sGal-3 in 32 WT mice fed either SD or AD. Line shows best fit with dashed lines the 95% confidence intervals. There is a significant positive correlation between plasma Cr and sGal-3 with Pearson's r = 0.55, p=0.0012.

2.3.3 Circulating leucocyte Gal-3 expression in the AD

2.3.3.1 Circulating monocyte Gal-3 expression is increased at 3 weeks AD.

12 WT mice were used to analyse circulating monocyte Gal-3 staining by flow cytometry. 5 mice were placed on SD for 3 weeks, 5 mice were given 1 week of AD and 5 mice given 3 weeks of AD. Only 2 of the SD fed mice had suitable processing for FACS analysis. The 1 week AD animals were an important control. At 1 week of AD we had determined that plasma Cr was not significantly elevated from SD fed mice, that body weight was not significantly and that plasma sGal-3 was not significantly different from SD fed animals. Therefore the 1 week AD fed group would enable us to see if there was a direct adenine effect on monocytes independent of uraemia and weight loss that would come with a longer dietary duration. Because the SD number was low and plasma Cr, body weight and plasma sGal-3 were not significantly different between SD fed mice and 1 week AD the FACS results for both these controls were grouped together to enable appropriate statistical comparison

All mice were harvested on the same day for flow cytometry. Permeablised monocytes were gated from live events by size and granularity characteristics (ssc/fsc) and positivity to the monocyte marker Ly6c [Fig 9 a+b]. The median Gal-3 MFI and % of events gated as monocytes were recorded per animal. Mice fed an AD had equivalent numbers of monocytes but there was significant monocytosis evident at 3 weeks of AD feeding [Fig 9c]. A median 25.65% (±2.19) of the total events were gated as monocytes in the SD fed mice, 19.9% (±2.45) in

the 1 week AD fed mice and 48.2% (±9.87) in the 3 weeks AD group [Table 21]. Of those gated monocytes Gal-3 Median Fluorescence Intensity (MFI) was significantly greater in 3 week AD fed mice compared to both SD fed mice and 1 week AD fed mice, 797.4 (±36.84) vs 519.5 (±68.5) and 402.6 (±24.42) respectively [Table 21].

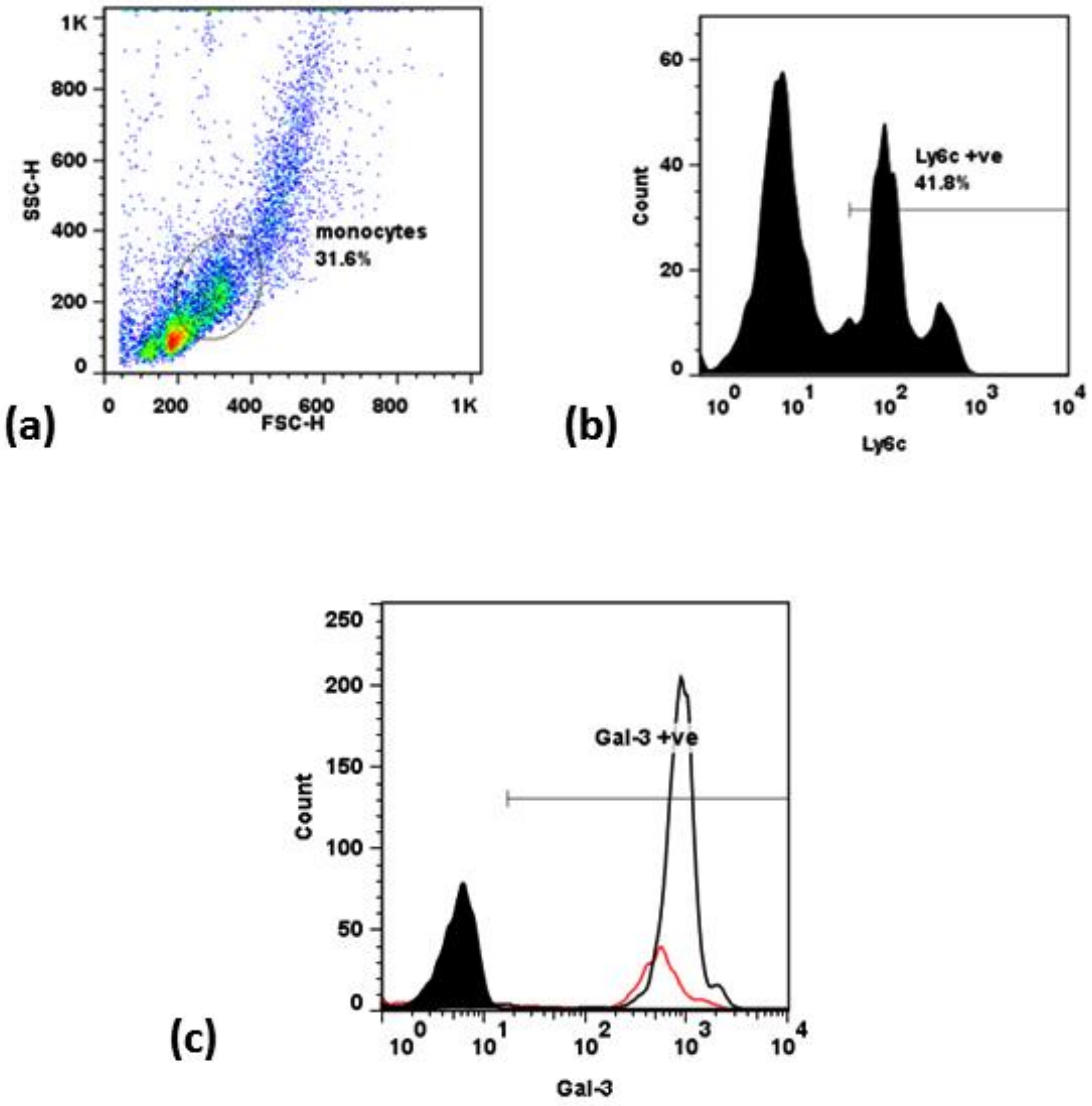

Figure 9: Circulating monocyte gating and Gal-3 expression in cells isolated from animals fed with an AD compared to those on a SD. Cells with side scatter and forward scatter characteristics compatible with monocytes are sorted (a). (b) Cells within this grouping (based on size and granularity) had the monocyte marker (ly6C) median fluorescence intensity measured to select monocytes. (c) Gal-3 MFI and cell count from a representative WT mouse fed SD (red line) compared to a WT mouse fed 3 weeks SD (black line). This demonstrates the marked monocytosis that adenine fed animals develop at 3 weeks AD and increased Gal-3 expression by MFI (a Gal-3 isotype control is shown by a filled in black histogram).

(a)

	SD	1Wk AD	3 Wk AD
No of Animals	2	5	5
% Monocytes	25.65 (2.19)	19.9 (2.45)	48.2 (9.87)
Gal-3 MFI	519.5 (96.87)	432 (54.61)	797 (82.39)

(b)

	Controls (SD + 1Wk AD)	3 Wk AD	p=<0.05
No of Animals	7	5	
% Monocytes	20.7 (3.4)	48.2 (9.87)	p= 0.0025
Gal-3 MFI	442 (82.5)	797 (82.39)	p=0.0025

Table 21: FACS analysis of monocyte proportion of gated event and monocyte Gal-3 expression (as median fluorescence activity (MFI)). (a) Median Gal-3 MFI and % events gated as monocytes increases at 3 weeks but not 1 week of AD in WT mice compared to SD fed WT mice. (b) The SD and 1 Wk. AD fed mice are control groups with equivalent Cr, body weight, plasma sGAl-3, % monocyte proportion and monocyte Gal-3 MFI. The 2 control groups were combined to test for statistical significance. The 3 Wk. AD fed group had a significantly greater proportion of gated events identified as monocytes and a significant increase in monocyte Gal-3 expression (Mann Whitney).

2.3.4 Solid Organ Gal-3 expression in the AD fed mice

2.3.4.1 Renal but not cardiac, lung, or aortic Gal-3 is elevated at 3 weeks AD.

Solid organs (heart, aorta, lung and both kidneys) were harvested from 5 mice fed SD for 3 weeks and 5 mice fed AD for 3 weeks. The organs were snap frozen then homogenised and assayed for protein content and Gal-3 content on ELISA. Only one kidney from each animal was used for Gal-3 ELISA, the contralateral kidney was harvested for immunohistochemistry. Gal-3 ELISA was performed in duplicates and where duplicates had a CV > 20% they were excluded for analysis. Kidney homogenate data had 2 samples excluded because of excessive CV values. There were no significant differences in Gal-3 values after 3 weeks AD or SD for heart, lung or aortic tissue homogenate [Table 22]. As previously documented lung Gal-3 content is very high (38.2 ng/mg tissue) and is often used as a positive control in immunohistochemistry. The aortic Gal-3 level was higher than expected (10.82 and 10.61 ng/mg tissue). This is likely because of the very low levels of protein measured from the aortic samples. Cardiac Gal-3 is not elevated on tissue ELISA which was validated on Gal-3 immunohistochemistry [Appendix]. The only organ assayed to show a significant increase in Gal-3 expression after feeding an AD was the kidney [Table 22]. There is a concern that the SD fed kidney Gal-3 value is unexpectedly low since murine kidneys express Gal-3 in distal convoluted tubular epithelium and transitional cell epithelium. However an increase in kidney Gal-3 at 3 weeks of AD compared to SD is further validated by immunohistochemical and PCR data [Fig 10 +11].

Gal-3 (ng/mg Tissue)				
Tissue	**No of Mice SD vs AD**	**SD**	**AD**	**P<0.05**
Heart	5 vs 5	3.30 (0.9)	3.55 (1.28)	NS
Lung	5 vs 5	38.2 (16.83)	38.22 (10.58)	NS
Aorta	5 vs 3	10.82 (7.22)	10.61 (10.81)	NS
Kidney	4 vs 5	0.38 (0.11)	3.44 (0.54)	*

Table 22: Summary table of Gal-3 content of different solid organs in 7 week old WT mice after 3 weeks AD by ELISA. Murine tissue was homogenised and a BCA assay performed to assess protein content of the samples. Tissue homogenate in buffer was then subject to commercial murine Gal-3 ELISA. The Gal-3 value from ELISA was divided by the protein concentration of the tissue sample to correct for discrepancies in amount of tissue present. All Gal-3 samples were performed in duplicate and where the CV of duplicates exceeded 20% the sample was not included in the results. * Kidney homogenate median Gal-3 corrected for protein content of tissue in SD = 0.38 ng/mg (±0.11) vs AD mean Gal-3 of 3.44 ng/mg (±0.54) p= 0.016 (Mann Whitney).

2.3.4.2 Renal cortical and medullary Gal-3 is increased in tubular epithelial cells and interstitial cells at 3 weeks AD.

3 kidneys from SD fed mice and 5 kidneys from AD fed mice were processed for immunohistochemistry using a Gal-3 primary antibody. Morphometric analysis of the Gal-3 immunoperoxidase positive area was performed on 6 x cortical and 6 x medullary images (x40 magnification images) per animal. The mean % area quantified as Gal-3 positive was recorded and compared between SD and AD fed mice. The immunoperoxidase stain demonstrated an increase in Gal-3 expression in renal tubular epithelial cells and Gal-3 positive infiltrating leucocytes [Fig 10a]. Medullary and cortical Gal-3 expression measured as % area positive for Gal-3 was significantly elevated [Fig 10b].

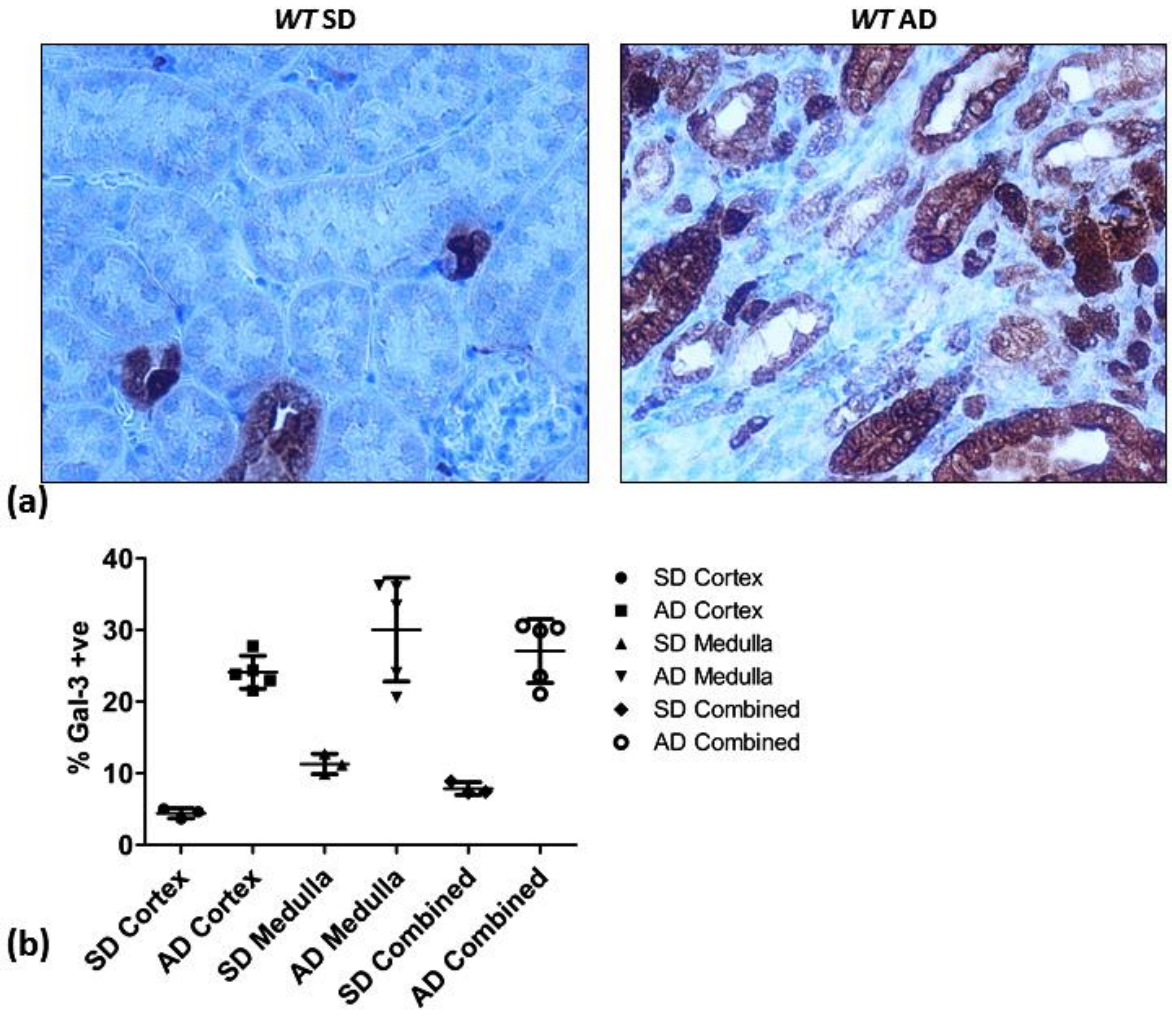

Figure 10: Renal gal-3 expression on immunohistochemistry in WT mice fed AD or SD. x40 image of renal cortex with anti-Gal-3 primary antibody and secondary immunoperoxidase stain. (a) Representative x40 images of renal cortex in SD and AD fed mice. Renal tubular epithelial expression of Gal-3 is limited to collecting duct epithelia, and distal convoluted tubule in SD fed WT mice. AD fed mice develop Gal-3 positive cell infiltrates and increased Gal-3 expression in tubular epithelium. (b) Quantitative assessment of mean Gal-3 +ve area of x40 images (6 per mouse) showing significant increase in x40 image area +ve for Gal-3 by morphometric analysis p = 0.036 (Mann Whitney). SD = 3 mice AD = 5 mice

2.3.4.3 Gal-3 gene expression is significantly increased at 3 weeks AD.

qPCR analysis of Gal-3 gene expression was undertaken from the kidneys of 5 mice fed SD for 3 weeks and 6 fed AD for 3 weeks. RNA was extracted from the kidneys and qPCR was performed using a Gal-3 primer and probe and 18s as a housekeeper gene. Comparative quantitation analysis showed all 6 AD fed mice had a higher Gal-3 gene expression compared to SD fed mice [Fig 11].

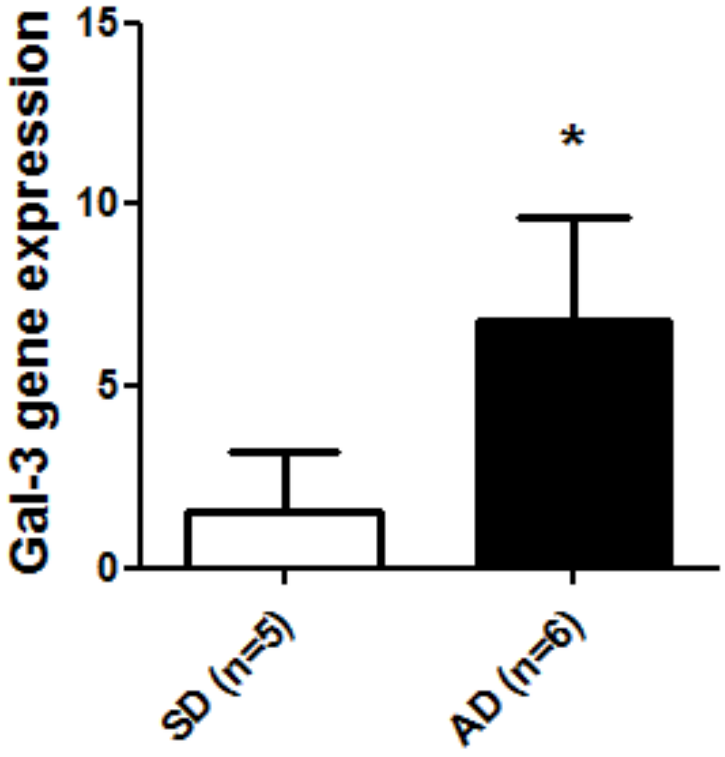

Figure 11: Quantitative real time PCR of 10 week old WT SD and AD kidney homogenate for Gal-3 mRNA. Results of comparative quantitation analysis of WT SD and WT AD Gal-3 mRNA divided by a 18s housekeeper gene. Relative expression of WT AD compared to WT SD using the WT SD as a calibrator gene with an expression of 1. * Relative expression of Gal-3 mRNA/18s housekeeper in WT SD vs WT AD 1.58 (±0.91) vs 6.82 (±2.3) p= 0.0135 Mann-Whitney

2.3.5 Renal and Peritoneal macrophage in the AD

2.3.5.1 Renal interstitial macrophage (F4/80) numbers are elevated in WT Kidneys in mice fed AD at 3 weeks compared to SD fed controls.

7 week old WT mice fed SD or AD for 3 weeks were harvested and kidneys processed for immunohistochemistry using an F4/80 primary antibody and HRP conjugated secondary antibody. 6 images of renal cortex per animal were taken (x40 magnification). The number of F4/80 cells was counted per x40 image and averaged per animal. The median values were then compared between SD and AD fed mice. The quality of staining meant that only 2 SD and 3 AD fed mice were included. All AD fed mice had greater numbers of F4/80 positive cells (representing macrophages), median 113.5 (±38.42) F4/80 +ve cells vs 35.84 (±3.3) [Fig 12a +b]. The lack of SD numbers meant statistical significance could not be tested.

2.3.5.2 Renal CD-68 (Macrophage) relative gene expression is significantly elevated in the AD.

Kidneys from 5 SD fed WT mice and 6 AD fed mice aged 10 weeks were harvested and had RNA extracted for qPCR using a CD-68 primer and probe and 18s housekeeper. Comparative Quantitation analysis of relative gene expression using a SD fed kidney as a calibrator gene demonstrated a significant increase in CD-68 gene expression in AD fed mice 2.25 (±0.66) vs 1.0 (±0.02) p=0.0067 (Mann Whitney) [Fig 12c].

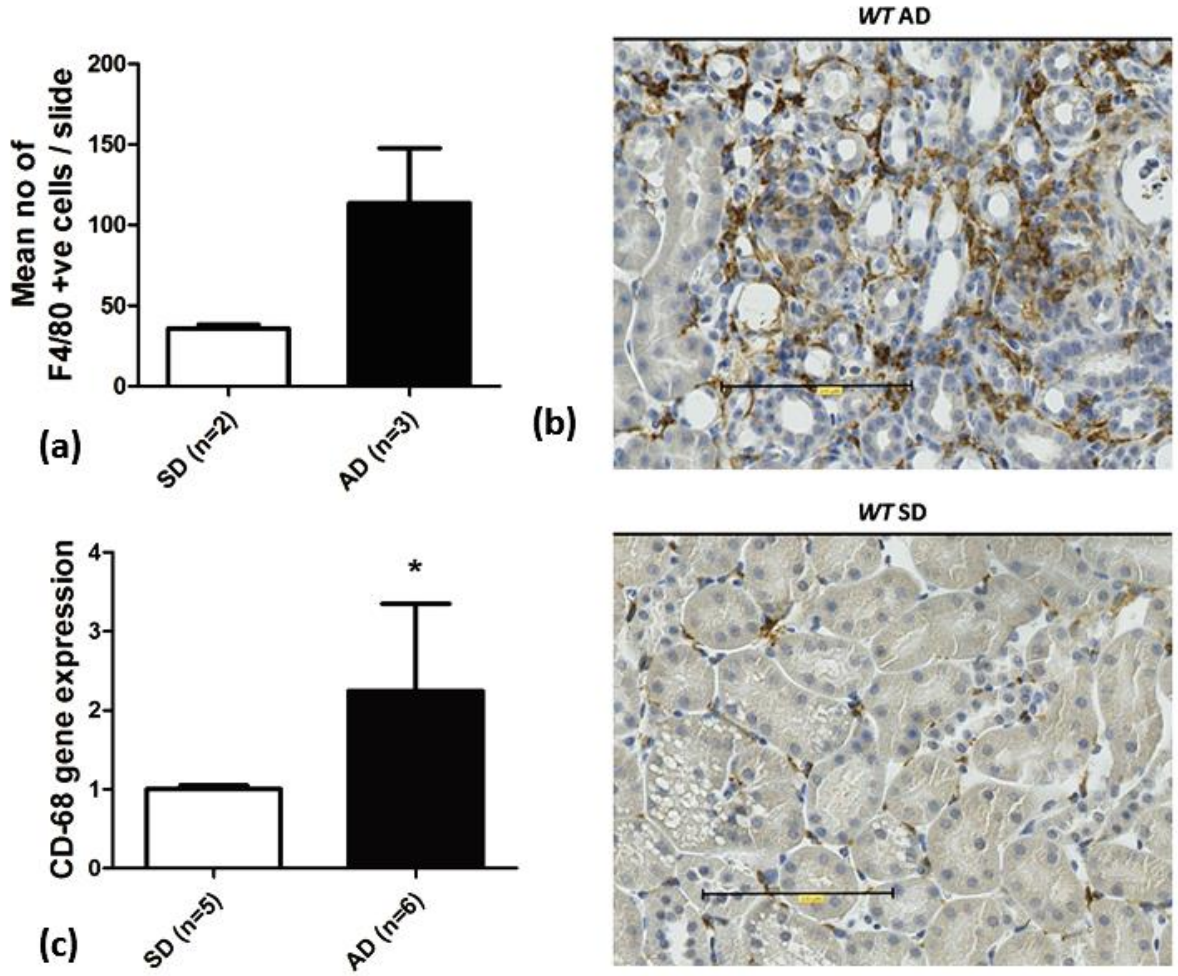

Figure 12: Renal interstitial macrophages at 3 weeks AD vs 3 weeks SD in WT mice by immunohistochemistry and qPCR. 6 slides of renal cortex per mouse were scored for numbers of F4/80 cells. (a) Bar chart of median and range of mean numbers of cells per animal. WT AD fed mice (n=3) at 3 weeks had greater numbers of F4/80 positive cells than WT SD fed mice (n=2), median number of F4/80 +ve cells per slide = SD- 35.84 (± 3.3) vs AD 113.5 (± 38.42). (b) Representative x40 images of renal cortex from WT mice fed AD (top) and SD (bottom). (c) bar chart showing median and range of CD-68 relative gene expression by qPCR from kidney homogenate of WT mice fed SD or AD for 3 weeks.CD-68 expression was significantly higher in AD fed mice 2.25 (± 0.66) vs 1.0 (± 0.02), p=0.0067 (Mann-Whitney).

2.2.5.2 Peritoneal macrophage numbers and Gal-3 expression are equivalent at 3 weeks AD compared to SD fed WT mice.

To assess whether Gal-3 expression was increased in a macrophage population remote from the kidneys peritoneal macrophages were isolated. This experiment again used SD fed mice and 1 week AD fed mice as controls. 5 mice were fed SD, 5 were fed AD for 1 week and 5 were fed AD for 3 weeks. All mice were harvested on the same day. Peritoneal lavage and aspirate was performed and cells within the aspirate analysed by flow cytometry. Macrophages were defined (gated) by SSC and CD-68 positivity [Fig 13 a +b]. The percentage of macrophages from the total number of events was equivalent in all 3 groups [Fig 13 c + d]. Gal-3 MFI of the defined macrophages was also equivalent between SD fed mice and AD fed mice at 1 and 3 weeks [Fig 13 c+d].

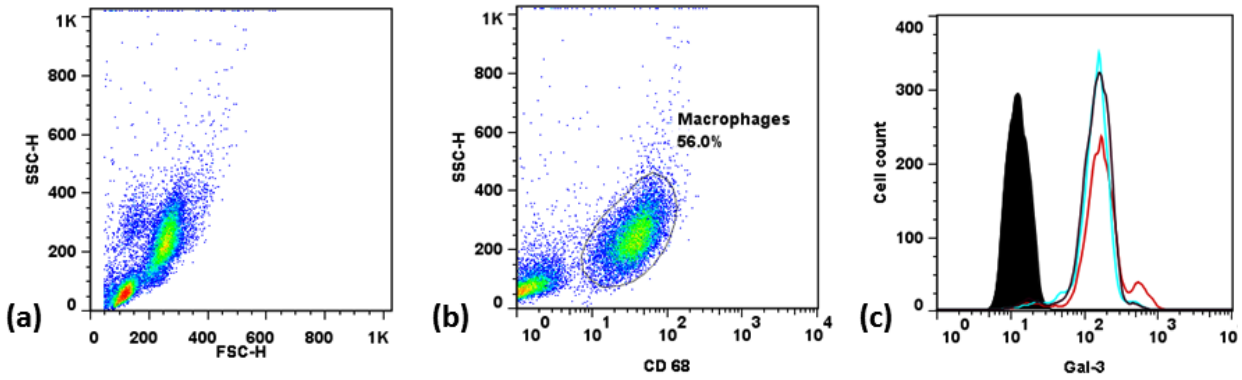

(d)

Peritoneal Macrophage (CD-68)	SD	1 Wk AD	3 Wk AD	p=<0.05
Number of animals	5	5	5	
Weeks of Diet	3	1	3	
% Macrophage of gated events	34 (5.5)	29.9 (8.91)	45.2 (17.15)	NS
Gal-3 MFI	170 (28.87)	136.4 (40.23)	150.2 (27.41)	NS

Figure 13: FACS data for Gal-3 expression of peritoneal macrophages in WT mice fed SD and AD at 1 and 3 weeks. Gating of macrophages from peritoneal aspiration (a) shows forward and side scatter, (b) macrophages are identified by side scatter characteristics and positivity for CD 68 (Fl-1 flourochrome)(c) Representative FACS histogram**,** WT peritoneal aspirate demonstrates equivalent numbers of macrophages and permeablised Gal-3 (fl-2) MFI at 1 and 3 weeks of AD compared with SD fed mice at 3 weeks. The solid black histogram is an Fl-2 isotype control, red histogram = SD fed mouse, blue histogram = 3 week AD fed mouse, black histogram = 1 week AD fed mouse. (d) Krushkal Wallis one way analysis of variance demonstrates no significant difference in median Gal-3 MFI between groups or the percentage of gated events that are defined as macrophages by SSC and CD-68 positivity (p=0.1479, p=0.8781 respectively).

2.4. Discussion

2.4.1 Elevated sGal-3, monocyte Gal-3 and renal Gal-3 in the AD.

sGal-3 is elevated in the AD model of experimental uraemia and renal fibrosis in a time dependent manner reaching significance at 3 weeks. The cause of elevated sGal-3 in murine plasma is not known. Gopel *et al*. hypothesised elevated sGal-3 in human CKD could be as a result of reduced renal clearance or increased production.[138] Gal-3 is detected in the urine, however the expression of Gal-3 on transitional cell epithelium means that measured urinary Gal-3 is not necessarily filtered through the glomerulus but may be from a source lower in the urinary tract. The main clearance of sGal-3 is thought to be hepatic.[49, 50] We attempted to measure urinary Gal-3 in WT mice fed AD compared to SD over 3 weeks but the ELISA proved difficult to perform on urine specimens with large standard deviations and coefficient of variations in measured Gal-3 [Appendix Table]. A plausible cause of elevated sGal-3 in the AD is secreted Gal-3 from monocytes. Monocytes and macrophages have the highest leucocyte expression of Gal-3 and monocytes are the only documented leucocyte to secrete Gal-3.[70, 71]

FACS analysis of monocytes subjected to the AD demonstrated a significant circulating monocytosis at 3 weeks of diet compared to controls. Similar levels of monocytosis have also been demonstrated in the UUO model which suggests the monocytosis may be independent of uraemia. Our data demonstrated a significant increase in Gal-3 expression of monocytes at 3 weeks of AD compared to controls. The monocytes were permeablised so this is a total Gal-3 expression

rather than cell surface specific expression. Tissue resident macrophages in the non-inflamed peritoneum did not demonstrate any increase in numbers or Gal-3 expression. This may be due to the relative protection of the peritoneum from the uremic milieu. Other organs, the heart, lungs and aorta did not demonstrate increased Gal-3 expression on ELISA. The only solid organ to demonstrate significant increased Gal-3 expression was the kidney. In the AD the kidney is the focus of inflammation. Immunohistochemistry suggested that Gal-3 expression was not only due to an increase in the expression of tubular epithelial cells but also there was the presence of interstitial Gal-3 in infiltrating leucocytes. Unfortunately dual staining was not performed but these are likely to be infiltrating cells of monocyte / macrophage lineage. WT AD fed mice at 3 weeks did have more F4/80 positive cells in renal cortex and a significantly elevated CD-68 expression on qPCR. These data indicate a source of elevated sGal-3 could be monocyte derived, that renal infiltrating monocytes and macrophages are also a source of Gal-3 which could potentiates the interstitial fibrosis seen in the AD. Gal-3 is known to facilitate leucocyte-endothelial attachment and transmigration. A hypothesis generated from my data is that elevated sGal-3 and monocyte Gal-3 facilitates renal monocyte transmigration from blood to renal interstitium. Increased monocyte transmigration leads to increased renal interstitial macrophage numbers and renal fibrosis via macrophage– fibroblast interactions. Chapter 3 will examine this hypothesis by performing the AD in a constitutive Gal-3 $^{-/-}$ mouse.

2.4.1 AD model as a comparator to human CKD

The protocol for AD used in this thesis is too short (4 weeks) to demonstrate some of the pathologies of CKD. The 4 week AD should be regarded as a subacute model and is more relevant to the study of a human tubulointerstitial nephritis mechanism rather than a true CKD model. The weight loss demonstrated by mice fed 0.25% AD is a significant confounding factor to interpretation of the results. Mice have an aversion to eating AD and a model of starvation is unethical and unhelpful when considering human CKD. To gain reassurance that the mice were consuming the AD I weighed the diet used over a week which was equivalent to mice fed SD and AD. The AD is pelleted, however, which is more compact and smaller than the expanded SD. Thus the AD would be more likely to fall between the bars of the food cage and I can't confirm a reduction in diet mass weighed at the end of a week directly corresponded to diet consumed. Gavage was considered but murine adenine gavage has a high mortality and is not recommended.[192] The severity of weight loss meant there was a high mortality at the end of 4 weeks of AD of approximately 25%. Results in the 4th week of diet were more variable and the mice frail which made anaesthesia and cardiac puncture difficult as well as giving a reduced amount of plasma for analysis. For these reasons it was decided to analyse further work on mice at 3 weeks of diet when mortality was reduced and when a better blood volume for analysis could be achieved. This was particularly important for whole blood flow cytometry, which relies on good yields. Whilst analysing mice at 3 weeks of 0.25% AD reduced the morbidity and mortality, it further reduces the

application of this model to human CKD. In future the 8 week AD protocol using a casein chow mixture should be applied but this protocol was not available until 2013 and was not on our group Home Office licence. WT week 3 AD mouse has a reduced body weight, is polyuric and normotensive which contrasts significantly from overweight, hypertensive patients which have become the norm in human advanced CKD.

2.4.2 AD as a reliable model of subacute uraemia and tubulointerstitial nephritis

All mice used and fed AD demonstrated weight loss, elevated creatinine and renal histological changes of tubulointerstitial nephritis. In WT mice a reduction in body weight and elevated creatinine could be seen after 1 week AD in all animals. Weight loss and elevation in Cr persisted reliably until 3 weeks of AD, in the final week results were more variable.

2.4.3 Measuring renal function in the AD

Serum creatinine and blood urea nitrogen reflect glomerular filtration rate (GFR) poorly in mild and moderate renal impairment.[198] Serum Cystatin-C is the gold standard for measuring underlying GFR in mouse experiments but unavailable to use in these experiments. Cystatin-C is more accurate than creatinine and shows earlier GFR impairment than serum urea in murine I/R and 5/6nx than serum creatinine.[199] In this thesis plasma creatinine was used as a measure to infer changes in GFR. Cr is influenced by GFR but also muscle bulk which is reduced in 3 week AD fed mice. The observation of reduced muscle bulk is subjective by my

inspection on laparotomy and thoracotomy. Therefore, it may be plasma Cr is an underestimate of the reduction in GFR that mice fed AD demonstrate. Whilst the plasma Cr can be used as an indicator of GFR, it should be interpreted with caution. The use of histological assessment of kidneys in conjunction with an appreciation of plasma creatinine allows a more confident comparison of renal impairment between groups of mice. Cr divided by body weight has been advocated as more reliable than Cr alone in assessing renal function in the 8 week AD as it reflects urea levels more precisely.[192] A further more accurate way of evaluating GFR would be to calculate Cr clearance on paired urine Cr and plasma Cr from metabolic cages. Unfortunately the resources for accurate metabolic cage collection of urine in mice were not available.

2.4.4 Concluding Remarks

Despite the limitations of the murine AD CKD model these experiments suggest that circulating sGal-3 levels are increased in CKD with an increased monocyte and renal tissue Gal-3 expression compared to controls. This interesting observation is further explained in the next chapter.

The adenine diet induced uraemic phenotype in Gal-3 $^{-/-}$ mice

Chapter 3

Chapter 3: The Adenine diet induced uraemic phenotype in Gal-3 $^{-/-}$ mice.

3.1 Background.

3.1.1 Gal-3 and Monocyte/Macrophage tissue infiltration in fibrotic disease

WT plasma Gal-3 and circulating monocyte Gal-3 are elevated in mice fed an AD (Chapter 2, section 2.3.2.1, 2.3.3.1) and kidneys from WT AD fed mice demonstrate macrophage accumulation (Chapter 2, give heading). Furthermore leucocyte-endothelial attachment and transmigration is abrogated in experimental inflammation in Gal-3 $^{-/-}$ mice (heading ref). However the main leucocyte studied in a model of bacterial infection (*Streptococcus pneumonia*e) was neutrophil-endothelial interactions and transmigration.[94, 95] There is evidence that shows that elevated monocyte expression of Gal-3 could facilitate monocyte-endothelial adhesion and transmigration.[96, 200] *In vitro* data suggest monocyte migration is driven by soluble or immobilised Gal-3 in a dose dependant manner and that monocyte migration is driven by interactions with ECM proteins laminin and fibronectin.[200] Migratory interactions between monocyte Gal-3 and ECM proteins are via the CRD.[200] The same study also documented macrophage migration in response to Gal-3.

Macrophage organ infiltration and M2 differentiation propagate fibrotic disease.[92] Whilst there is theoretical *in vitro* data available to hypothesize that a reduction in macrophage accumulation in fibrotic models on Gal-3$^{-/-}$, there is no *in vivo* data to support it.[56, 60, 120, 121] Gal-3 $^{-/-}$ mice do have an ameliorated fibrotic disease phenotype compared to WT controls in a model of renal

fibrosis.[60, 121] A hypothesis to be tested on Gal-3 $^{-/-}$ mice is that they may have an ameliorated disease phenotype after being fed an AD due to reduced monocyte transmigration, renal infiltration and renal macrophage accumulation.

3.3.2 M2 macrophage differentiation promoted by Gal-3.

A secondary hypothesis would be that of the effect of absence of Gal-3 on monocyte and macrophage differentiation phenotype. M1 classical differentiation of macrophages occurs in the initial inflammatory cascade and is promoted by Th1 cytokines (IFN-γ and IL-12).[90, 91] M2 'alternative' macrophage differentiation predominates, and is implicated in, chronic fibrotic disease.[77] M2 differentiation of macrophages can be induced by Th2 cytokines (IL-4 and IL-3) and M2 differentiated macrophages display characteristic markers including Ym1/CHI313 and Fizz1/Retnla.[92, 93, 201-203] *In vitro* Gal-3$^{-/-}$ murine macrophages show classical activation on stimulation with LPS but do not demonstrate M2 markers (CHI313 and Retnla) upon stimulation with Th2 cytokines IL-4 and IL-13.[77] *In vivo* m stimulation of macrophages with Th2 cytokines induces secretion of Retnla and CHI313.[204-208]

3.3.3 Monocyte Phenotypic change in CKD

There are conflicting data about the relative importance of Ly6C^{high} and Ly6C^{low} monocyte populations in fibrosis and a recent discovery of a Ly6C^{int} group in a model of uraemia.[209, 210] Monocyte phenotype in fibrotic disease has been studied using a bleomycin model of pulmonary fibrosis. Monocytes and macrophages are not involved in the initial inflammatory phase but during the pro-fibrotic phase monocyte phenotype and alternative macrophage

differentiation are important determinants of progression.[210] Depletion of circulating monocytes reduced the numbers of tissue resident macrophages at 24 h and reduced the markers of alternative macrophage activation.[210] Ly6C^{high} monocytes exacerbated lung fibrosis and promoted an increase in CHI313 positive (alternatively activated) macrophages.[210] In a murine model of AKI (bilateral renal pedicule clamping) tissue infiltrated and resident CD11B+Ly6C^{high} cells predominated during the initial inflammatory phase, a CD11B+Ly6C^{int} group during the initial resolving period and Ly6C^{low} during the fibrotic phase of renal recovery.[209] Markers of 'alternative macrophage' activation were increased with the expression of CD11B+Ly6C^{low} cells. This paper did not look at circulating monocyte phenotype, only the tissue resident CD11B cell populations. In the AD model of progressive renal fibrosis both Ly6C and Ly6G (granulocyte) +ve cells were elevated compared to those fed SD, again this did not look at circulating monocyte populations.[211] This chapter presents data on the AD uraemic phenotype in Gal-3$^{-/-}$ mice looking at renal macrophage numbers within the kidney, circulating monocyte phenotype and macrophage differentiation markers.

3.2 Methods.

3.2.1 Generation of Gal-3 $^{-/-}$ mice

Jackson Laboratories create *Gal-3*$^{-/-}$ mice using the following methodology: For the Lgals3 targeted mutation allele; a targeting vector containing neomycin resistance and herpes simplex virus thymidine kinase genes was used to disrupt 3.7kb of sequence that includes exons 2, 3 and 4. The construct was electroporated into 129/Sv and C57BL/6 and SJL derived WW6 embryonic stem (ES) cells. Correctly targeted ES cells were injected into outbred MF-1 blastocysts. The resulting chimeric male animals were crossed to 129 female mice. Heterozygotes were crossed to generate homozygotes. The single targeted mutation lines were subsequently crossed to generate a double mutant. The double mutant strain was then backcrossed to C57BL/6 for 5 generations prior to arrival at The Jackson Laboratory. WT mice used were 6 week old male C57BL/6 mice purchased from Charles River. Animals of the two strains were age-matched but were not littermates. Gal-3$^{-/-}$ mice used in experiments were genotyped on a randomised basis (section 2.2.4.9) to confirm absence of the Gal-3 gene.

3.2.2 Genotyping Gal-3 $^{-/-}$ mice

3.2.2.1 Gal-3 $^{-/-}$ genotyping: DNA extraction

Mouse kidneys from WT and Gal-3$^{-/-}$ mice were taken from -80^{o}C storage. DNA was extracted by proteinase K digestion buffer (DB). 2 mm samples of kidney tissue were placed in microcentrifuge tubes with 500 µl of DB. The tubes were

incubated at 55^{o}C with gentle mixing overnight. The proteinase K was denatured by 10 min incubation at 94^{o}C and samples centrifuged at 16,000 *g* for 15 min.

3.2.2.2 Gal-3 $^{-/-}$ genotyping: Polymerase chain reaction

A standard polymerase chain reaction was carried out in a 50 µl reaction mixture containing 2 µl cDNA. Buffer and Taq Polymerase were purchased from Life Technologies, Paisley, U.K. Briefly, a mastermix containing buffer, dNTP mix, MgCl2 and dH_2O and Gal-3 primers were added. A second mastermix containing Buffer, Taq Polymerase and dH_2O was prepared and added to individual cDNA samples. Finally the two mastermixes for each sample were combined. PCR was performed using the G-Storm model GS1 machine, (KAPA Biosystems, Somerton Biotechnology Centre, U.K.).

3.2.2.3 Gal-3 $^{-/-}$ genotyping: Gel analysis of amplified samples

20 µl of PCR products were mixed with Gel Loading Buffer (Sigma Cat no: G2526) and separated on a 2% agarose gel, which was then stained with Gel Red (Cambridge Biotechnology, Cat. no: BT41003) for 30 min before photographing over UV light (UVIP) [Fig 14].

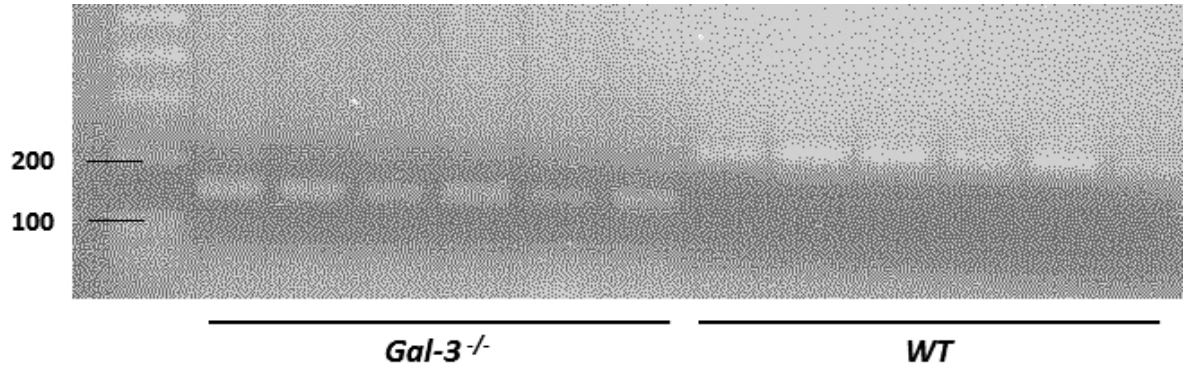

Figure 14: Agarose gel of amplified cDNA products from WT and Gal-3 $^{-/-}$ kidneys. Double Gal-3$^{-/-}$Mutant=~150 base pairs (bp), Heterozygote = ~150 bp and ~220 bp, Wild type=~220 bp. This gel confirms all samples from purchased Gal-3$^{-/-}$ mice are true knockouts.

3.2.3 qPCR – markers of fibrosis and M2 macrophage differentiation.

Methodology for conducting qPCR is covered in detail in Chapter 2 (section 2.2.5). Samples were analysed by comparative quantitation using a WT SD fed animal kidney as a calibrator gene as a comparator. All qPCR used reverse transcriptase controls and no-template controls. Samples were performed in triplicates and where the replicative take off standard deviation between the triplicate values exceeded 0.6 the sample was not used for analysis. All genes of interest had their comparative concentration divided by a housekeeper gene (18s) to correct for varying amounts of RNA. Gel electrophoresis of DNA was not undertaken for CD68, CHI313 and Retnla genes because of time constraints.

3.2.4 FACS analysis of Monocyte Phenotype

Methodology for FACS analysis of circulating monocytes is covered in detail in Chapter 2 (section 2.2.6).

3.2.5 Histology: Haematoxylin and Eosin Staining (H+E)

Histology was only performed on tissues from experiment and control mice in the AD model. Mice received a terminal anaesthetic with intra-peritoneal X/K, following cardiac aspiration of blood, a loin incision was performed, the left kidney was identified, dissected free of perinephric fat and briefly washed in 0.9% saline, then placed in 10% Formalin for 48 h. After 48 h the samples were placed in 70% ethanol for storage. Subsequent steps in histological processing for H+E staining, picosirius red staining and immunohistochemistry were undertaken by the William Harvey Institute, Bart's Cancer Pathology Services.

Samples were embedded in paraffin and cut to 4µm thick sections. Kidney sections were deparaffinised and stained with Gill's II Haematoxylin.

3.2.5.1 Histological assessment of Renal Tubulointerstitial Nephritis damage.

All scoring was performed by myself blinded to diet treatment and to the genotype of mouse (WT or Gal-3 $^{-/-}$) and then validated by a Consultant Histopathologist, similarly blinded. Histological scoring methods were also discussed and agreed for describing tubulointerstitial damage, collagen scoring (picosirius red) and interstitial macrophage infiltration (F4/80 immunohistochemistry). Digital images of mounted kidney specimens were acquired using a Hamamatsu nanozoomer (Hamamatsu Phototics Hertfordshire, U.K.). Mounted digital images of kidney sections were acquired using NDPview2 software (Hamamatsu Photonics K.K. Cat no: U12388-01). 6 x40 were taken of each animal's renal cortex and medulla using NDPview2 software (Hamamatsu Photonics K.K. Cat no: U12388-01) [Fig 5]. Each image was assessed for the % of slide area with histologically 'normal' interstitium using ImageJ™ software. Histologically normal interstitium was easily distinguished from damaged interstitium by the presence of 'back to back' tubules, intact tubular lumen epithelium, non-dilated tubular lumen and lack of infiltrating cells. The AD creates 'islands' of preserved renal interstitium amongst severe tubulointerstitial damage which could be mapped out and area assessed by ImageJ™ software [Fig 15-17]. The primary focus of assessing damage was to define the extent of

tubulointerstitial damage rather than glomerular abnormalities. Glomeruli were subtracted from the total slide area being assessed to ensure the overall area assessed represented tubulointerstitium only. Each animal therefore had 6 measurements for % 'histologically normal' area in the cortex and 6 measurements for medulla. These were then averaged to give a mean % histologically normal cortex and medulla per animal.

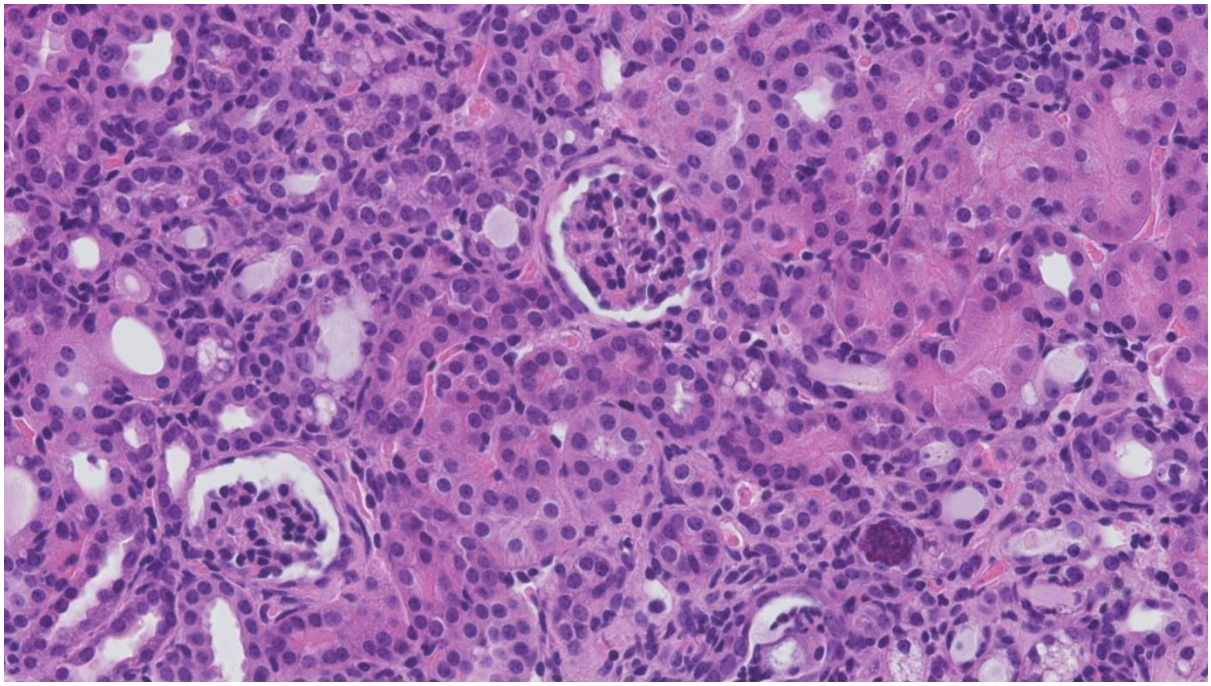

Figure 15: H+E Renal tubular interstitial damage scoring methodology 1, original image x40 magnification. This image has been digitally generated from a slide using NDPview2 software. The image is representative of renal cortex from a WT AD fed mouse. Areas of preserved tubulointerstitium are clearly visible enabling subsequent mapping and area assessment with ImageJ software™. Each animal had 6 images from cortex and 6 images from medulla.

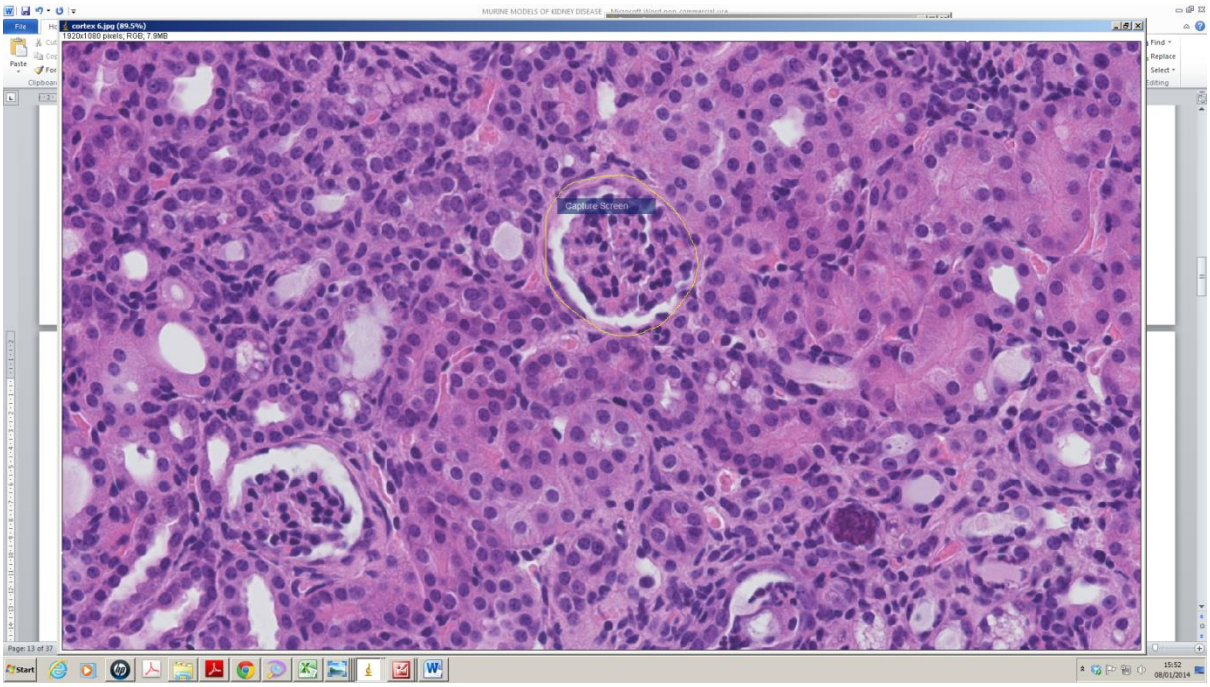

Figure 16: H+E Renal tubular interstitial damage scoring methodology 2, screen shot of H+E tubulointerstitial damage area scoring using Image J™ software. Glomeruli are identified (yellow line) and glomerular area within the yellow demarcation is measured to subtract from final area to be assessed. There are 2 glomeruli in this view which have to be measured separately.

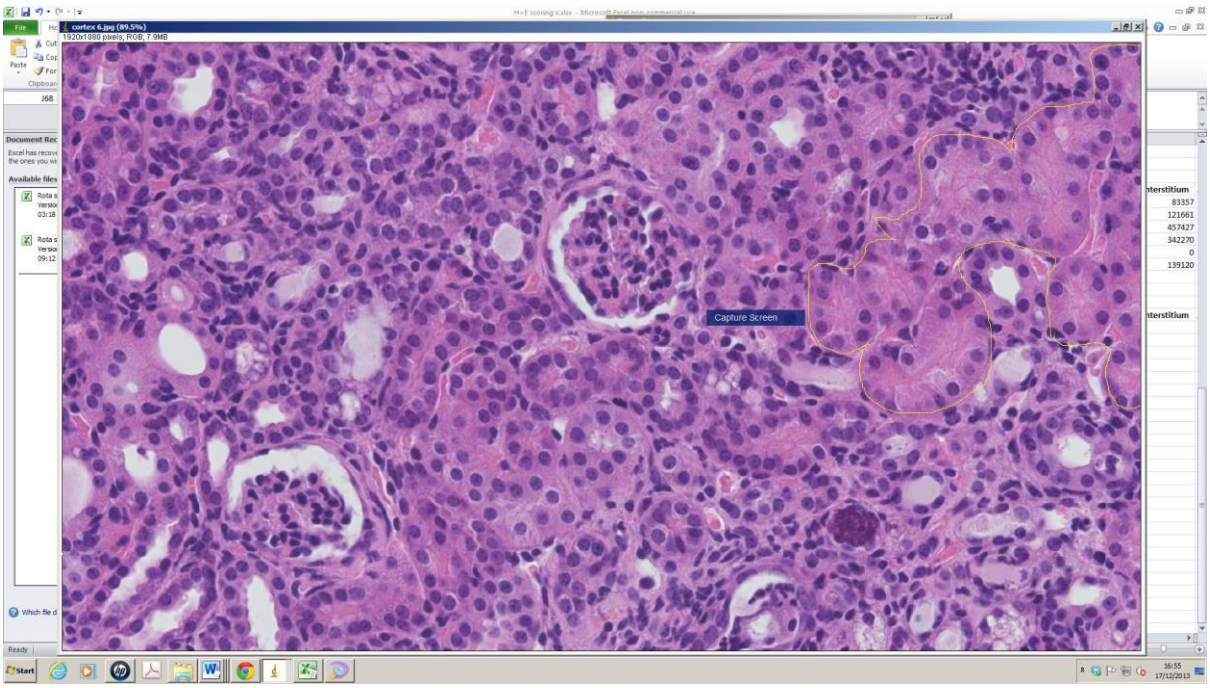

Figure 17: H+E Renal tubular interstitial damage scoring methodology 3, screen shot of H+E tubulointerstitial damage area scoring using ImageJ ™software. The area of 'normal' interstitial appearance is mapped (yellow line) and measured, then subtracted from the total slide area (minus glomerular area) and expressed as a percentage. The final % represents the % area with tubulointerstitial damage. Each mouse had 6 measurement from cortex and 6 from medulla. The mean of the 6 % values was generated to give a mean cortical and mean medullary value per mouse. The mean cortical and medullary values were combined to give an overall tubulointerstitial damage % per animal.

3.2.6 Collagen quantification by Picosirius Red stain.

The following method was used by the institute of Cancer pathology services to perform Picosirius red staining of collagen from murine kidney samples. Kidney specimens from WT and *Gal-3* $^{-/-}$ mice fed AD or SD were embedded in paraffin and cut to 4µm thick sections. The paraffin samples were de-waxed and hydrated. Hydrated specimens were then placed in picosirius red for 1 h. The samples were then sequentially washed in 2 changes of acidified water. The sample was dried by blotting then dehydrated in 3 changes of 100% ethanol before being cleared with xylene and mounted in a resinous medium. Digital images were acquired using a Hamamatsu nanozoomer (Hamamatsu Phototics). x40 slide images were then taken using NDPview2 software (Hamamatsu Photonics).

3.2.6.1 Morphometric histopathological collagen scoring using Sirius red.

Morphometric analysis was used to assess collagen content of harvested kidneys fed SD or AD at 3 weeks. The scoring methodology was discussed and agreed by Professor Mike Sheaff, a Consultant Histopathologist. Collagen staining of kidney specimens using picosirius red staining and image J software has been verified and published before.[212, 213] As mentioned earlier the assessors, both myself and Professor Sheaff, were blinded to the genotype of the mouse, WT or Gal-3 $^{-/-}$, and the treatment received AD or SD. Scoring was done for all specimens and random samples verified by Professor Sheaff. The x40 digital slide of picosirius red stained cortex or medulla was analysed using ImageJ™ software. The x40

image can be split into red, blue and green channels. The green filter is selected and red threshold is manually adjusted until intracellular contents are not present leaving extracellular collagen staining only. The area measured therefore reflects the collagen area. Because the images often had significant and variable tubular lumen sizes the actual area of tubulointerstitium was also measured by manual thresholding. The result was a value of measured area ascribed to extracellular collagen staining and a measured area of tubulointerstitium. The value of this was expressed as a percentage for each of the 6 cortical, 6 medullary images per animal.

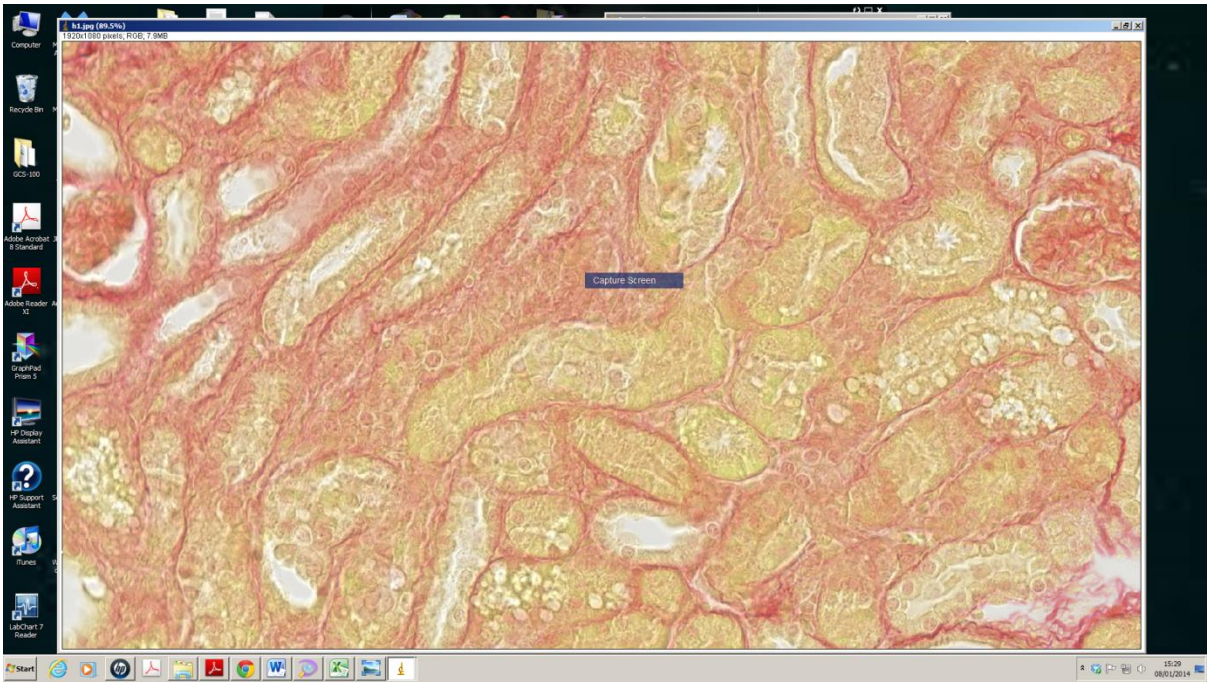

Figure 18: Histopathological renal collagen quantification methodology 1.Screen shot of original x40 image uploaded onto ImageJ™ analysis. This is a representative image of the cortex of a WT mouse fed AD and harvested at 3 weeks. The picosirius stain gives collagen (found extracellularly) a red colour and stains low collagen containing tissues yellow. ImageJ™ can filter this image into green, red and blue channels. For assessing red staining the green channel is subsequently selected.

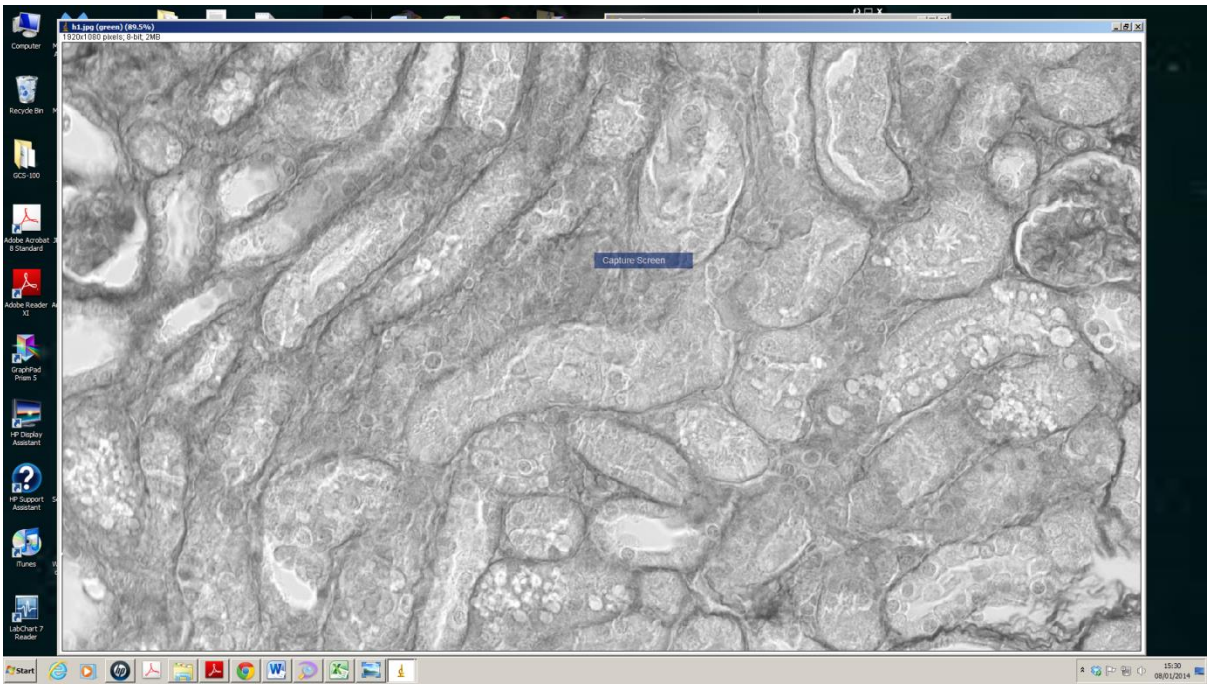

Figure 19: Histopathological renal collagen quantification methodology 2. Screen shot of original image split into a green channel

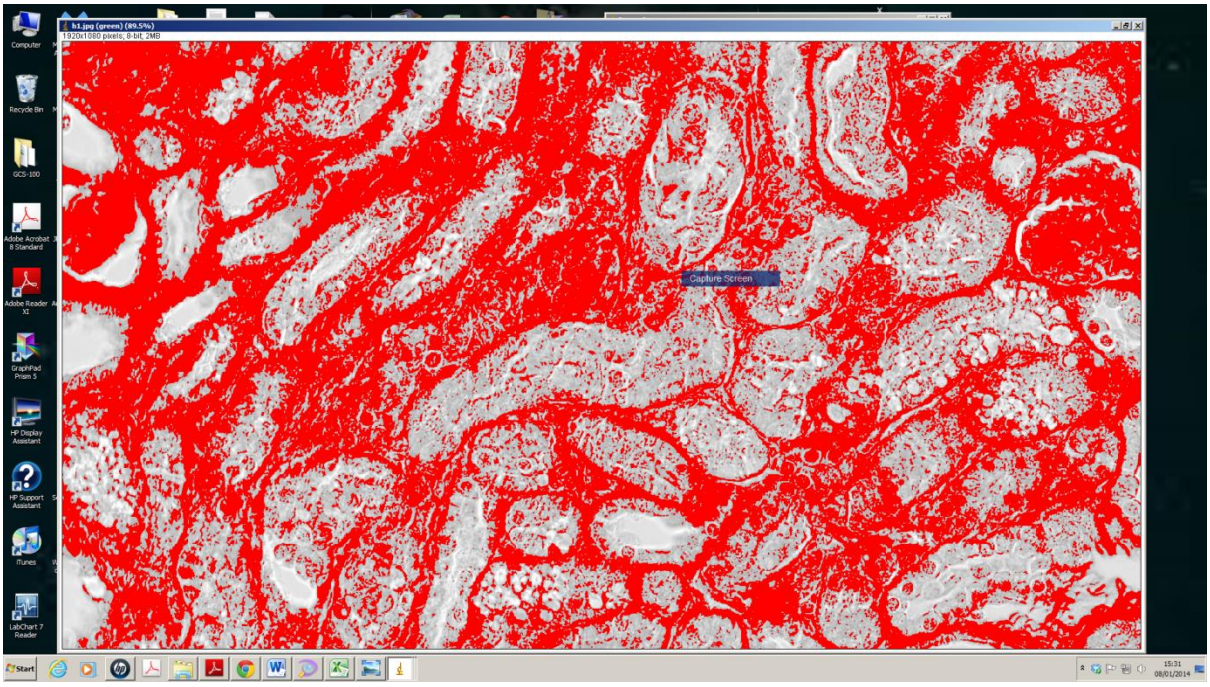

Figure 20: Histopathological renal collagen quantification methodology 3. Screen shot of automated threshold for red before manual adjustment.

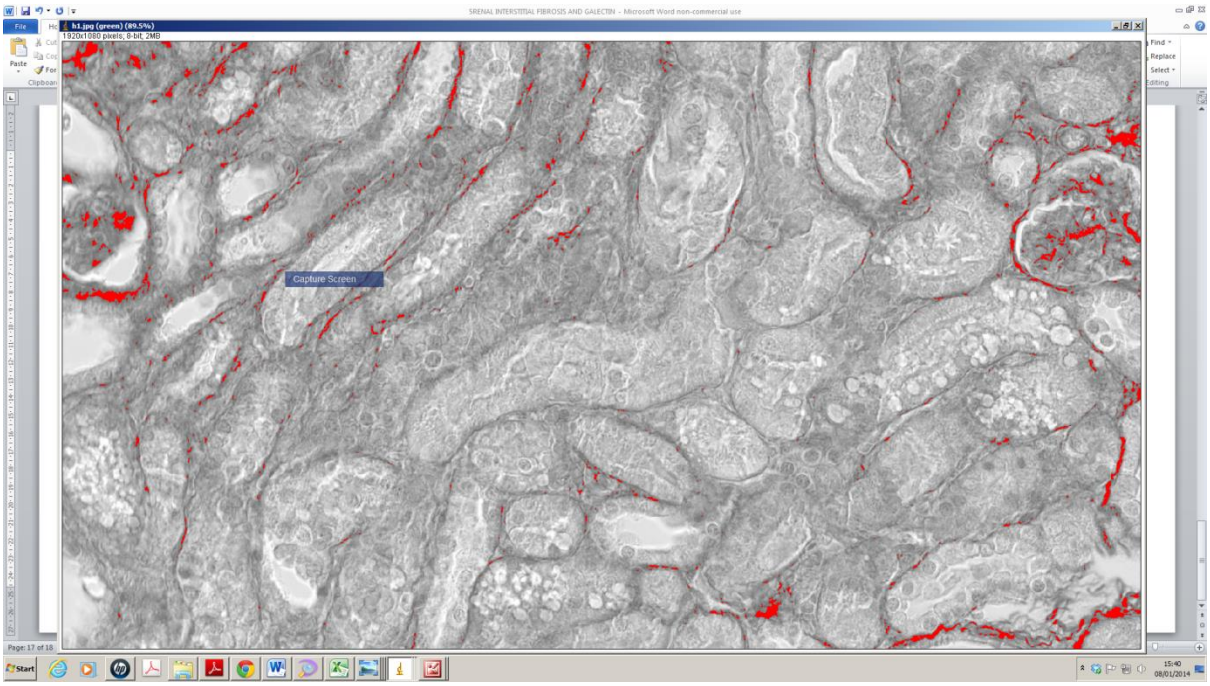

Figure 21: Histopathological renal collagen quantification methodology 4**.** Screen shot of red threshold manually adjusted to exclude nuclear staining. The area of red staining was quantified per slide and the mean % area of 6 cortical and 6 medullary slides per animal recorded.

3.2.7 Statistical Analysis

Demographic data with a 'normal' or Gaussian distribution is described using mean and standard deviation (SD) values. All data described by mean and SD values have been tested for the presence of a Gaussian distribution using the 'D'Agostino and Pearson omnibus normality test' on GraphPad Prism™ software. Where data did not have a Gaussian distribution it is described by median and interquartile range values. Tests of variance between normally distributed data in matched groups was by a 2-tailed unpaired t-test using a p value of <0.05 to infer a significant difference between groups. Where data did not have a Gaussian distribution a Mann-Whitney test was used to test the significance of

differences between the 2 groups median values and range, again a p-value of <0.05 is ascribed to be significant.

3.3 Results.

3.3.1 Reduction in weight loss in AD fed Gal-3 $^{-/-}$ mice compared to *WT* AD fed mice.

10 week old male WT and Gal-3 $^{-/-}$ mice were allocated into cages receiving either SD or AD over 3 weeks. Body weight data from the first experiment is shown in Figure 22 and subsequent data for further Gal-3 $^{-/-}$ mice used is shown in Figure 23 (a+b). Each week body weight was measured for all individuals per cage. WT and Gal-3 $^{-/-}$ mice receiving AD and SD had equivalent body weighs at the start of the diet [Fig 22, 23]. After 3 weeks WT AD fed mice had a significantly lower mean body weight than AD fed Gal-3 $^{-/-}$ mice with no significant difference between either genotype fed SD [Fig 22]. This discrepancy was apparent on visual inspection of the animals [Fig 22]. Percentage body weight loss over the 3 weeks diet was calculated by dividing the mean weight of the animals in a cage after 3 weeks with the weight at the start of the diet. The mean % weight loss was 39.89% in WT AD fed mice and 29.44% in Gal-3 $^{-/-}$ AD fed mice [Fig. 22c]. There was no % weight loss in SD fed mice of either genotype. The mean amount of diet consumed per cage did not differ significantly between the 2 AD fed groups over the 3 weeks [Fig. 23d].

3.3.2 Lower median plasma Cr in Gal-3 $^{-/-}$ mice fed AD after 3 weeks compared to WT mice.

Plasma Cr was measured at 3 weeks of AD or SD in WT and Gal-3 $^{-/-}$ mice. The experiment demonstrated an overall significantly lower Cr in Gal-3 $^{-/-}$ AD fed mice compared to WT AD fed mice [Fig 24]. It was clear that the Gal-3$^{-/-}$ mice did not have absolute protection but partial given they still had an elevated median Cr compared to both SD groups [Fig 24]. None of the data passed the normality test individually or combined. Mann Whitney was therefore used as a non-parametric test of difference between WT AD and Gal-3 $^{-/-}$ mice.

3 Wk

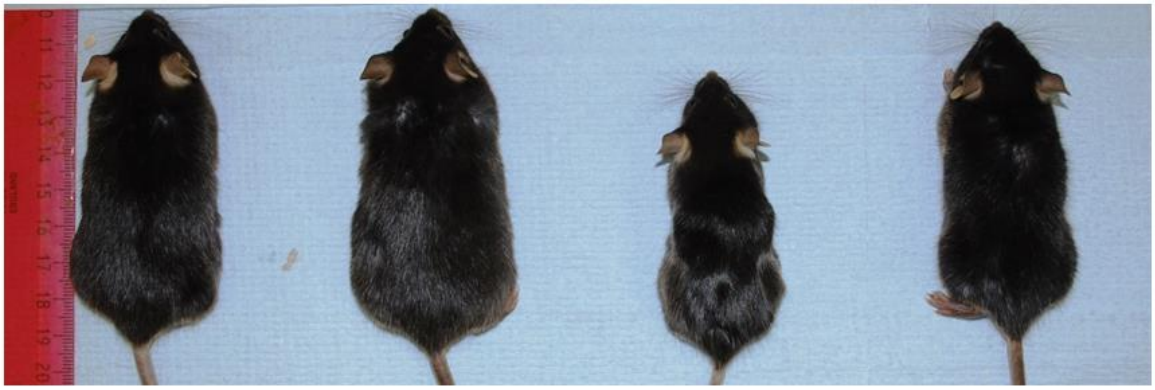

(a) WT SD | Gal-3$^{-/-}$ SD | WT AD | Gal-3$^{-/-}$ AD

(b)

Body Weight	WT		Gal-3 $^{-/-}$		p= <0.05
	SD (n=7)	AD (n=8)	SD (n=6)	AD (n=5)	
Weeks					
0	30.99 (0.81)	30.33 (0.69)	28.78 (4.11)	28.1 (3.51)	(NS)
1	31.63 (1.07)	23.71 (1.34)	26.83 (4.43)	25.88 (6.37)	(NS)
3	32.62 (1.31)	16.78 (0.41)	29.13 (4.24)	23.1 (1.61)	*

Figure 22: Body weight differences between WT and Gal-3 $^{-/-}$ mice fed AD or SD (a) Photographic images of representative anaesthetised WT and Gal-3 $^{-/-}$ mice after 3 weeks AD or SD. WT AD fed mice were noticeably smaller and on laparotomy had subjectively less adipose tissue than the matched Gal-3 $^{-/-}$ AD fed mice. (b) Body weights from 10 week old WT and Gal-3 $^{-/-}$ mice fed SD or AD for 3 weeks. Values displayed are mean weight (SD) in grams. WT AD mice had lower body weights than the Gal-3 $^{-/-}$ AD fed mice from 1 week post diet initiation but this was not significant until 3 weeks. Body weight WT AD vs Gal-3 $^{-/-}$ AD weight = 16.78 g (±0.41) vs 23.1 g (±1.61) p= 0.0043 (Mann Whitney).

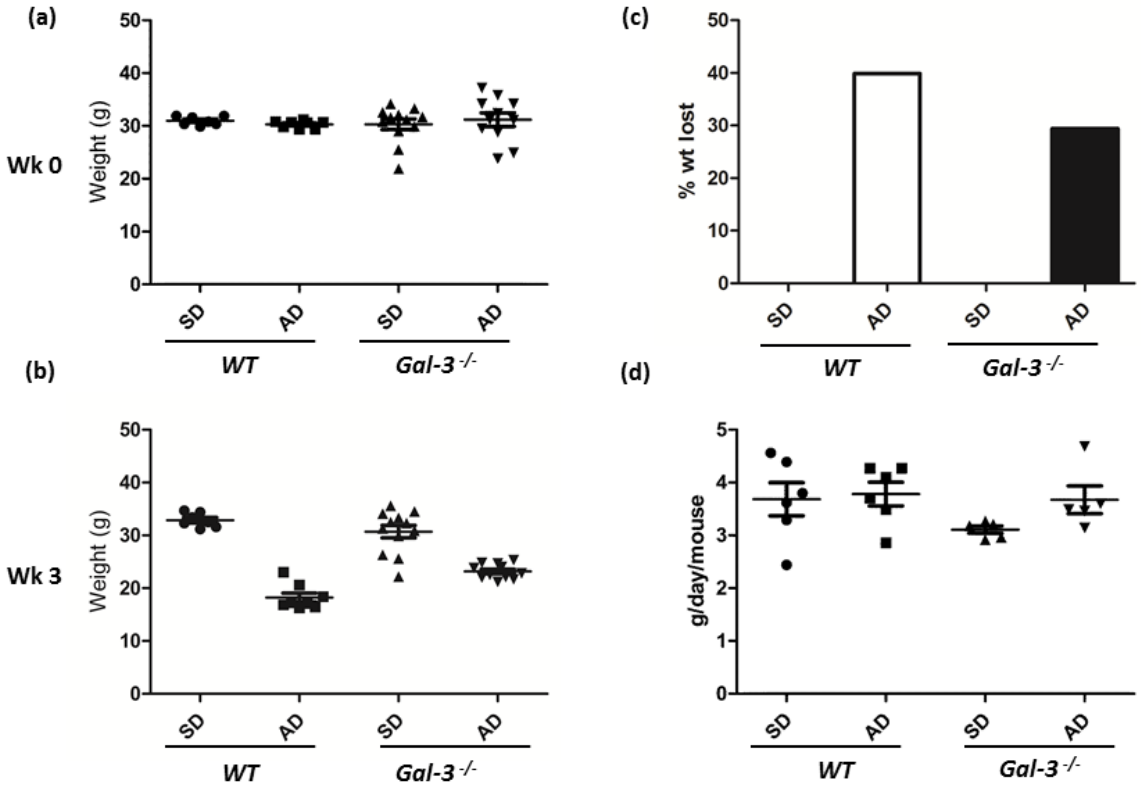

Figure 23: Body weight and diet consumed over 3 weeks of AD or SD in 10 week old WT and *Gal-3* $^{-/-}$ mice. (a) Scatter plot of individual results for body weight at Week 0 at the start of the AD with error bars showing mean body weight and standard deviation values. There were no significant differences between animals at Week 0. (b) At week 3 all mice in WT and *Gal-3* $^{-/-}$ groups fed AD have lost weight with lower body weights in the WT AD fed group. (c) % weight lost is greater in WT AD fed mice compared to *Gal-3* $^{-/-}$ AD fed mice, there was no weight loss in either SD fed group at 3 weeks. (d) Scatter plot of diet consumed over the 3 week period. Each value represents 1 cage within the group with a calculation of diet weight consumed per mouse per day over the week.

(a)

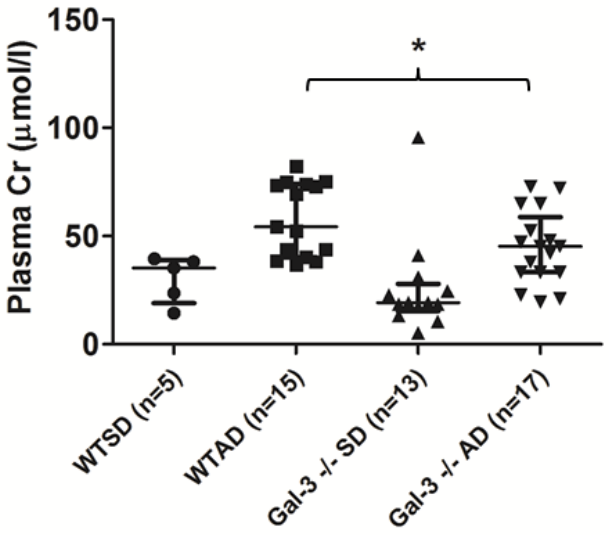

(b)

	WT		Gal-3 $^{-/-}$		p=<0.05
	SD	AD	SD	AD	
Number of animals	5	15	13	17	
Plasma Cr (µmol/L)	35.36 (10.86)	54.27 (16.93)	19.26 (22.76)	45.26 (16.92)	p= 0.0317

Figure 24: Plasma Cr in WT *vs* Gal-3 $^{-/-}$ mice fed AD in 3 repeated experiments. (a) Scatter graph of individual Cr values with the error bar showing median and interquartile range values (b) Summary table of plasma Cr from 10 week old WT and Gal-3 $^{-/-}$ mice at 3 weeks fed AD or SD. Cr values shown are median (SD). The data demonstrates a significantly lower median plasma Cr in Gal-3 $^{-/-}$ AD fed mice, 45.26 µmol/L (±16.92) vs WT AD 54.27 µmol/L (±16.93) p=0.0317 (Mann-Whitney).

3.3.3 Reduction in kidney tissue area affected by tubulointerstitial injury in Gal-3 $^{-/-}$ mice fed AD compared to WT mice

After 3 weeks AD or SD WT and Gal-3 $^{-/-}$ mice were harvested and kidneys were processed for H+E staining to assess the extent of tubulointerstitial injury. On macroscopic inspection the kidneys of both AD fed genotypes were smaller than the SD fed mice [Fig 25]. There was little difference in visual inspection between Gal-3 $^{-/-}$ and WT AD fed kidneys. Both were smaller than the SD kidneys. The dry weight of the kidneys was also equivalent between both AD fed genotypes [Fig 25b]. The renal cortex and medulla from each kidney was examined separately for each kidney. SD fed WT and Gal-3$^{-/-}$ mice had normal appearances of the interstitium with little cell infiltrate, preserved tubule epithelial cell size, structure with little intraluminal debris. Both AD fed genotypes had severe tubulointerstitial injury with intra-luminal debris, disruption of tubular architecture, an increased interstitial cell infiltrate and dilated tubular lumens. The damaged area was darker stained and easily identifiable at low power (x20) and high power (x40) light microscopic examination [Fig 26 +27]. Gal-3$^{-/-}$ AD fed mice had more identifiable 'islands' of preserved tubulointerstitium than WT AD fed mice. This was more apparent in the renal cortex than the medulla [Fig 28]. Glomeruli were not histologically formally assessed as the AD injury is primarily a tubulointerstitial injury. Formal measurement of tubulointerstitial damage was undertaken at X40 magnification by measuring the % of the image area that had evidence of tubulointerstitial damage. WT AD fed mice had significantly more %

area of tubulointerstitial damage than the Gal-3$^{-/-}$ AD fed mice in both cortex and medulla [Fig 29].

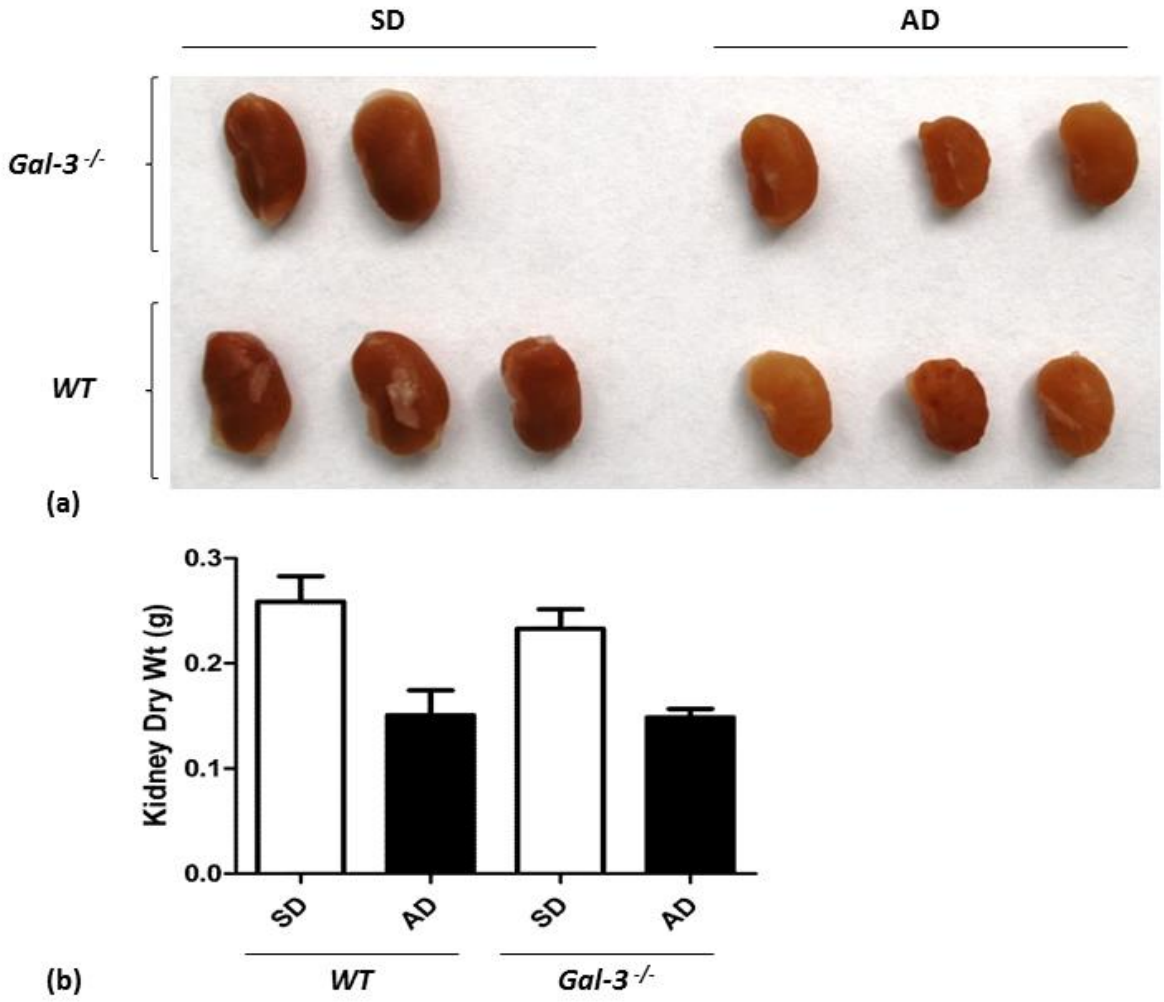

Figure 25: Photograph and dry weight of kidneys from AD and SD fed WT and Gal-3$^{-/-}$ mice at 3 weeks of diet**.** (a) Photographic image of representative harvested whole kidneys from WT and Gal-3 $^{-/-}$ mice fed AD or SD for 3 weeks. It can be seen that although WT and Gal-3$^{-/-}$ kidneys are smaller than the equivalent SD fed mice, there is little macroscopic difference between the 2 AD fed mouse genotypes. (b) Equivalent kidney dry weight between WT and Gal-3 $^{-/-}$ AD fed mice at 3 weeks.

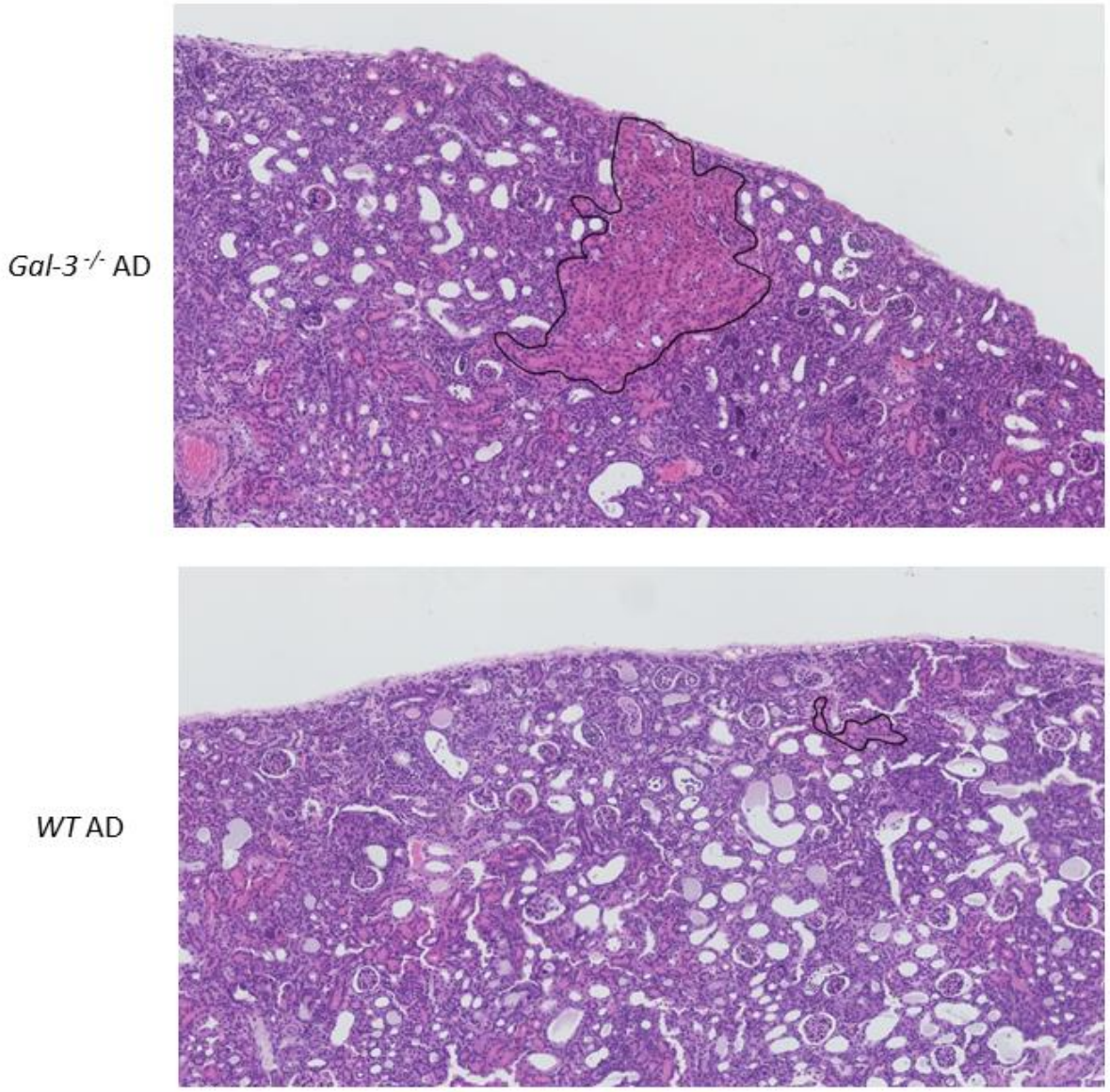

Figure 26: Representative image of x10 magnification renal cortex from AD fed WT and Gal-3 $^{-/-}$ mice. The highlighted area within a black line is preserved undamaged renal tubulointerstitium. The darker area with dilated tubular lumens is tubulointerstitial damage. Gal-3$^{-/-}$ had more areas of preserved 'normal' tubulointerstitium than WT AD fed mice which was formally assessed and quantified [Fig 29].

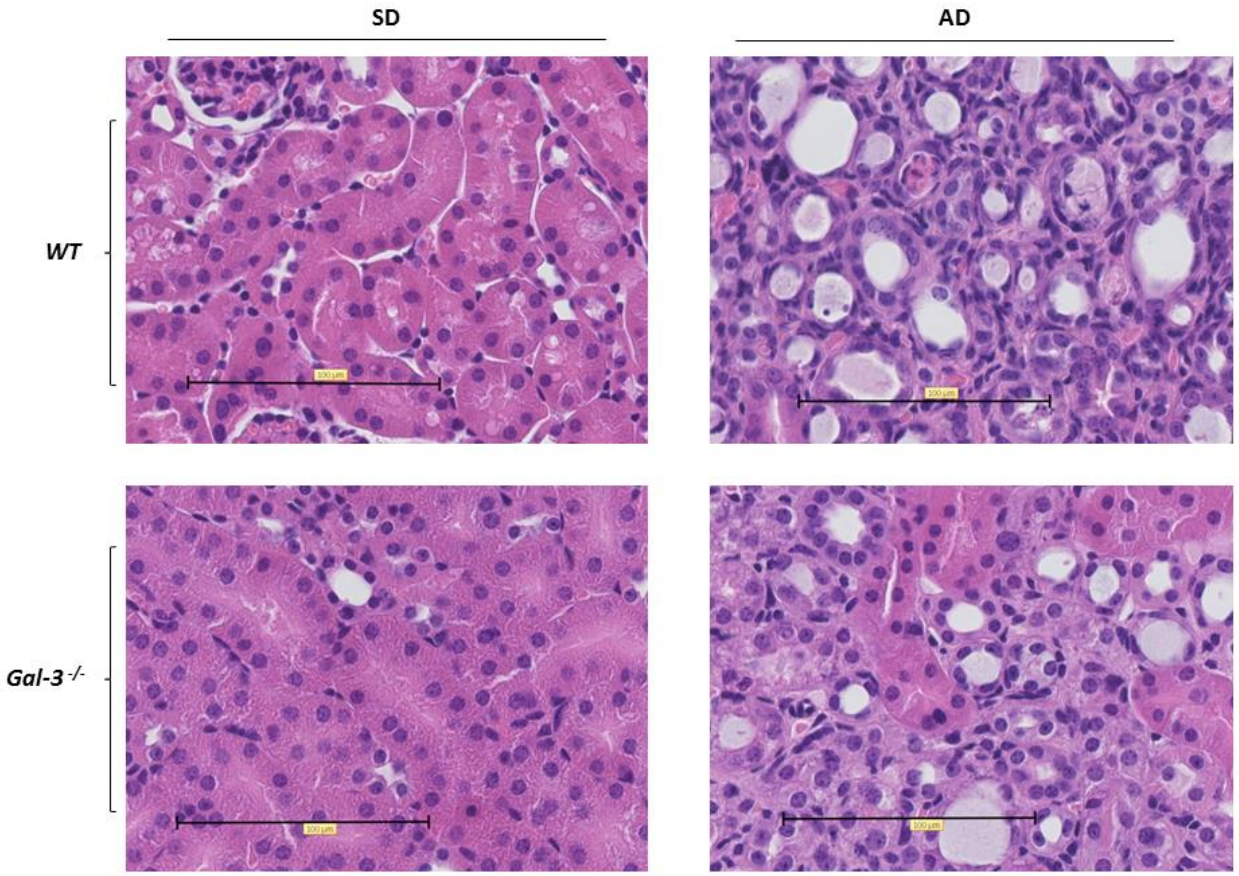

Figure 27: Representative x40 slide images of renal medullary tissue of WT and Gal-3 $^{-/-}$ mice fed SD or AD after 3 weeks. Scale bars = 100µm. Both images of SD fed mice show preserved architecture with back to back tubules, limited tubular lumen space and no inflammatory cell infiltrate. In contrast both AD groups show dilated tubular lumen with intra-luminal debris and inflammatory cell infiltrate.

	WT		Gal-3 $^{-/-}$		p= <0.05
	SD	AD	SD	AD	
Number of Animals	**2**	**3**	**3**	**5**	
Cortex					
% Affected Area	1.4 (0.53)	97.39 (0.85)	2.03 (0.59)	76.27 (6.8)	*
Medulla					
% Affected Area	0.37 (0.35)	91.92 (1.53)	1.16 (0.56)	81.98 (8.6)	*
Combined					
% Affected Area	0.88 (0.44)	94.65 (1.19)	1.6 (0.46)	79.13 (7.64)	*

(a)

(b)

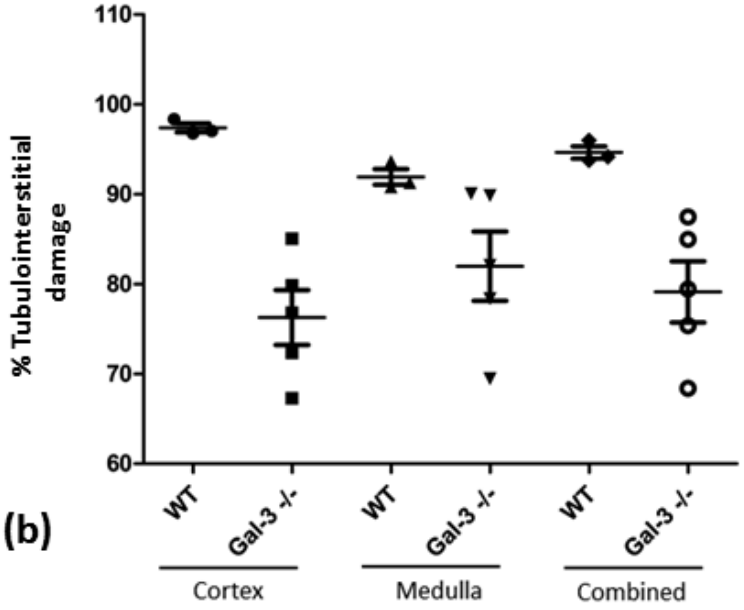

Figure 28: Histological quantification of renal tubular interstitial damage (a) Results from histological assessment of the % area of tubulointerstitial damage on kidney H+E slides. Values scored for each group refer to mean (SD) % values in each group. The p-value refers to WT AD vs Gal-3$^{-/-}$ AD comparison only, p value =0.0357 in cortex, medulla and combined comparisons respectively (Mann Whitney). (b) Scatter graph of % values with mean (SD) bar. AD fed animals only are displayed no SD data is displayed on the scatter graph.

3.3.4 Similar collagen staining in WT and Gal-3 $^{-/-}$ mice.

Collagen staining by morphometric analysis of picosirius red staining was undertaken on 10 week old WT fed SD (n=2), WT fed AD (n=6), Gal-3 $^{-/-}$ fed SD (n=2) and Gal-3 $^{-/-}$ fed AD (n=5). Kidneys were harvested after 3 weeks diet. Both AD fed genotypes had significantly more % area stained red in cortical, medullary and overall indicating more collagen deposition [Fig 29]. There were no significant differences in % area stained red between the WT AD fed mice and Gal-3$^{-/-}$ mice fed AD [Table 23].

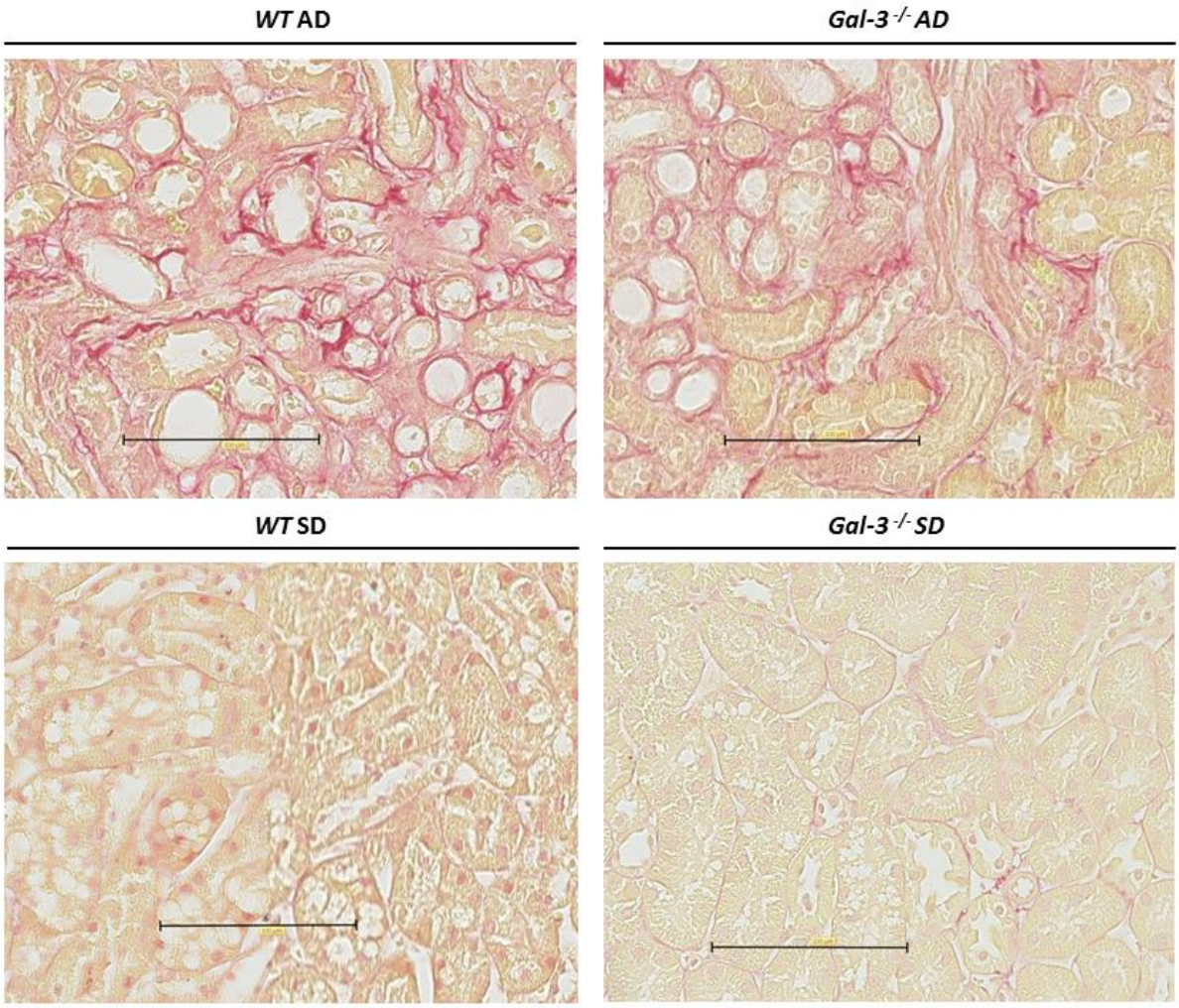

Figure 29: Representative x40 images of picosirius red staining from medullary samples in all genotype and diet groups at 3 weeks. These light microscopy images show a significant collagen deposition (red areas) in both AD fed groups. Collagen laydown has occurred extracellularly particularly around connective tissue. There were no obvious differences in collagen laydown between the WT and Gal-3 $^{-/-}$ AD fed mice. Picosirius stains non-collagen containing tissues yellow and gives a red appearance to nuclei. Distance marker = 100µm.

	WT		*Gal-3*$^{-/-}$		P=<0.05
	SD	AD	SD	AD	
Number of Animals	2	6	2	5	
Cortex	0.22 (0.15)	3.69 (0.60)	0.14 (0.01)	2.84 (0.5)	NS
Medulla	0.31 (0.14)	2.88 (0.80)	0.53 (0.4)	2.46 (0.84)	NS
Combined	0.25 (0.06)	3.4 (0.46)	0.28 (0.15)	2.70 (0.56)	NS

Table 23: Quantification of collagen staining from renal cortex and medulla in WT and Gal-3$^{-/-}$ mice fed AD or SD at 3 weeks**.** % collagen staining by picosirius red of kidney cortical, medullary and overall kidney tissue. Each mouse was fed AD or SD for 3 weeks then harvested. Kidneys were processed for histology and stained with picosirius red. 6 x40 images of cortex and 6 of medulla were taken per animal. Photometric analysis using ImageJ™ software allowed assessment of the collagen staining per image. After 6 measurements were taken the mean % was used per cortex, per medulla and combined. There were no significant differences between AD fed WT or Gal-3$^{-/-}$ mice. Data shown as median (standard deviation).

3.3.4.1 No significant difference in markers of fibrosis on qPCR

Murine kidneys from 10 week old WT and Gal-3 $^{-/-}$ mice fed SD or AD for 3 weeks were harvested and processed for qPCR. Comparative quantification analysis using a WT SD fed animal as the calibrator gene demonstrated significantly elevated procollagen (1), TGF-β and α-SMA in the WT AD fed animals compared to WT SD fed animals in both their respective genotypes. When comparing WT AD fed mice with Gal-3$^{-/-}$ AD fed mice there were no significant differences. There was a non-significant increase in procollagen (1) and α-SMA in the WT compared to Gal-3 $^{-/-}$ AD fed group and a non-significant increase in TGF-β in the Gal-3$^{-/-}$ AD group [Fig. 30]. Interestingly the Gal-3$^{-/-}$ SD fed animals had lower median gene expression than WT SD fed animals for all 3 markers of fibrosis. This did not reach significance for α-SMA and procollagen (1). Mann Whitney test of significance was not able to applied to the TGF-β PCR because the use of a WT SD fed animal as the calibrator gene meant that there were repeated values of 1.

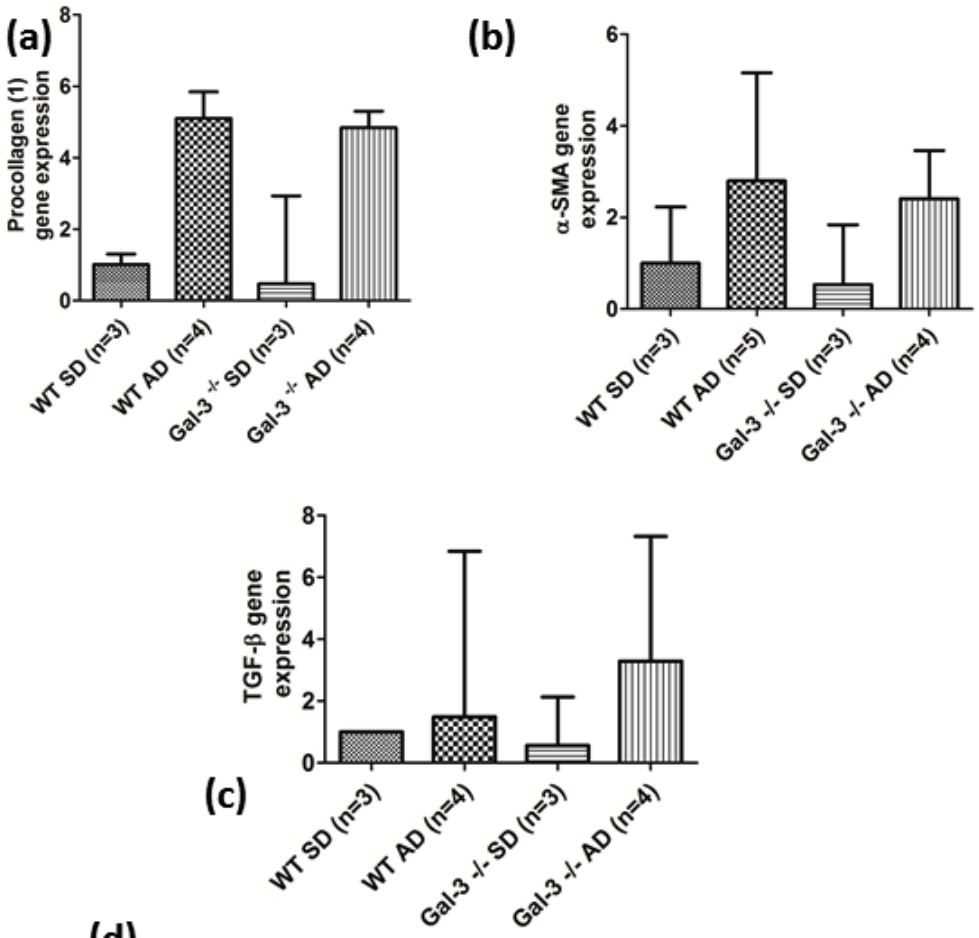

(d)

Relative Gene Expression	WT		Gal-3 $^{-/-}$		P=<0.05
	SD	AD	SD	AD	
Procollagen	1.01 (0.17)	5.1 (0.83)	0.47 (1.43)	4.84 (0.36)	NS
TGF-β	1.00	1.49 (2.68)	0.56 (0.76)	3.29 (2.63)	NS
α-SMA	1 (0.73)	2.8 (1.46)	0.53 (0.78)	2.41 (0.62)	NS

Figure 30: qPCR of fibrosis markers from kidney homogenate from 10 week old WT and Gal-3 $^{-/-}$ mice fed SD or AD. Analysis was by comparative quantitation using SD fed WT mice as the calibrator gene and 18s as a housekeeper gene. Bar charts show median (range) of relative gene expression of (a) procollagen (1), (b) α-SMA and (c) TGF-β. (d) Table of relative gene expressions showing median (standard deviation). All the markers of fibrosis had an increase in relative gene expression in AD fed animals but there were no significant differences between WT or Gal-3$^{-/-}$ mice fed an AD. Gal-3$^{-/-}$ SD fed mice had a non-significant tendency for a lower relative gene expression in all 3 genes.

3.3.5 Macrophage numbers are equivalent between WT and Gal-3 $^{-/-}$ AD fed mice at 3 weeks.

AD fed animals had more F4/80 +ve cells and CD68 gene expression than SD fed animals in both the respective genotypes. After 3 weeks diet the mice were harvested and kidneys processed for immunohistochemistry using an F4/80 primary antibody and conjugated HRP secondary antibody for immunoperoxidase staining. This resulted in 2 WT SD kidneys, 3 WT AD kidneys, 3 Gal-3 $^{-/-}$ SD kidneys and 5 Gal-3 $^{-/-}$ AD fed kidneys being available for histological analysis. The cortex only was examined due to limitations set out in Chapter 2 (2.2.7.2). F4/80+ve cells were identified predominantly amongst areas of tubulointerstitial injury in the AD fed mice of both genotypes [Fig 31]. There were more than double the mean amount of F4/80 +ve cells in AD fed mice than SD fed mice, WT SD vs WT AD= 35.84 cells/slide (±2.34) vs 110.6 (±22.18) and Gal-3 $^{-/-}$ SD vs Gal-3 $^{-/-}$ AD= 23.09 (±12.42) vs 116 (±17.84) [Fig. 32]. Whilst the AD mice had a large increase in macrophage numbers within their renal cortex compared to SD fed mice, there were no significant differences between WT AD and Gal-3$^{-/-}$ AD fed mice. WT SD and Gal-3 $^{-/-}$ SD fed mice appeared to have equivalent numbers of F4/80 +ve cells but with the small numbers available it was not possible to assess for significant differences [Fig 33].

qPCR data obtained from studying CD68 gene expression supports the immunohistochemistry F4/80 staining findings. CD68 gene expression is increased in AD fed mice regardless of genotype compared to their respective SD fed groups [Fig 33]. There is a non-significant increase in CD68 gene expression in

WT AD fed mice compared to Gal-3 $^{-/-}$ AD fed mice, relative to the WT SD CD68 gene expression (calibrator gene) WT AD vs Gal-3 $^{-/-}$ AD = 2.25 (±0.66) vs 1.35 (±0.77). The result is non-significant on Mann-Whitney testing [Fig 33].

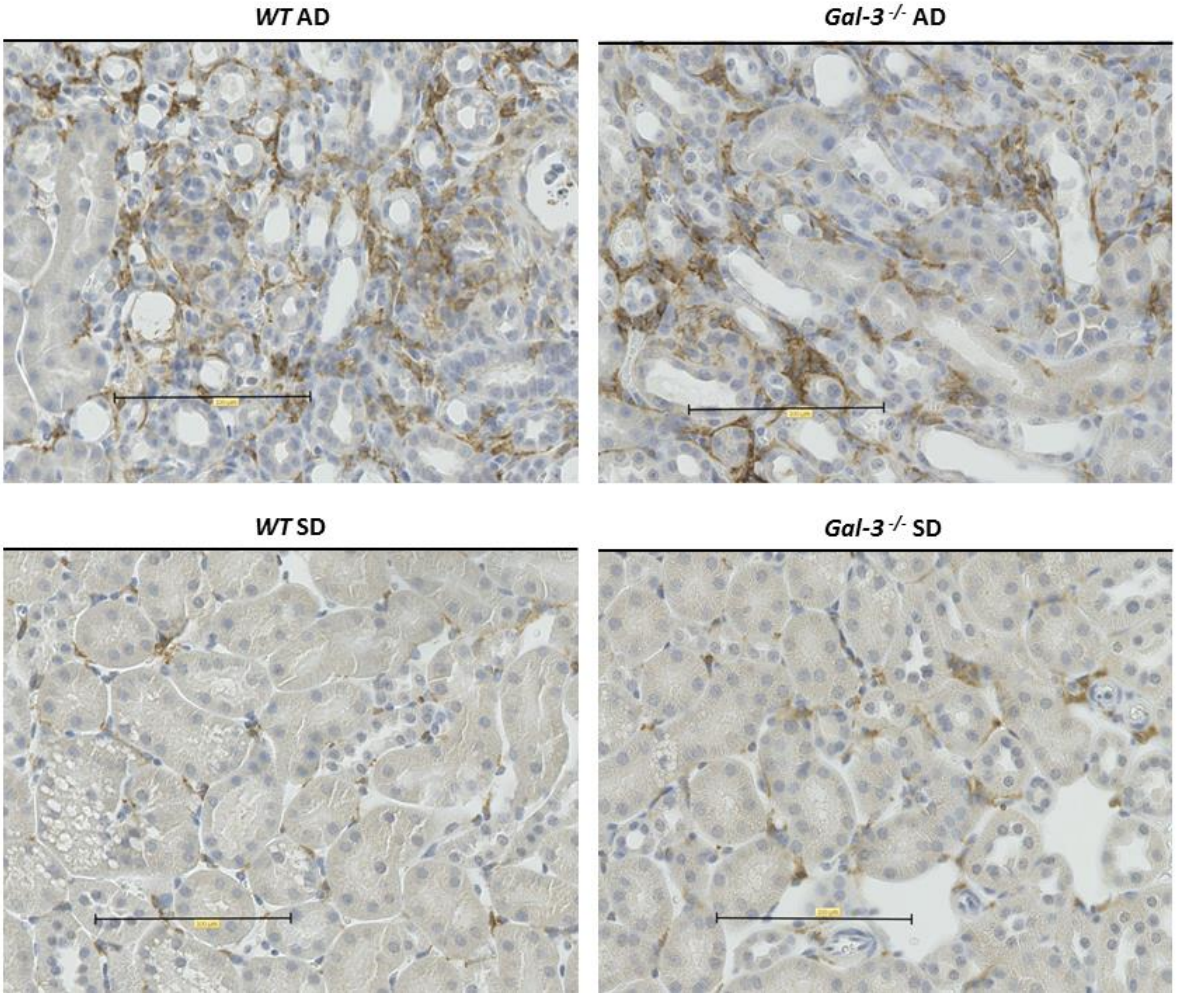

Figure 31: x40 representative images of kidney cortex with primary anti- F4/80 macrophage antibody and secondary conjugated HRP immunoperoxidase stain. Distance marker represents 100µm. F4/80 positive cells are localised to areas of tubulointerstitial damage. Due to limited histological data it was not possible to discriminate between tissue resident macrophages and infiltrating macrophages.

(a)

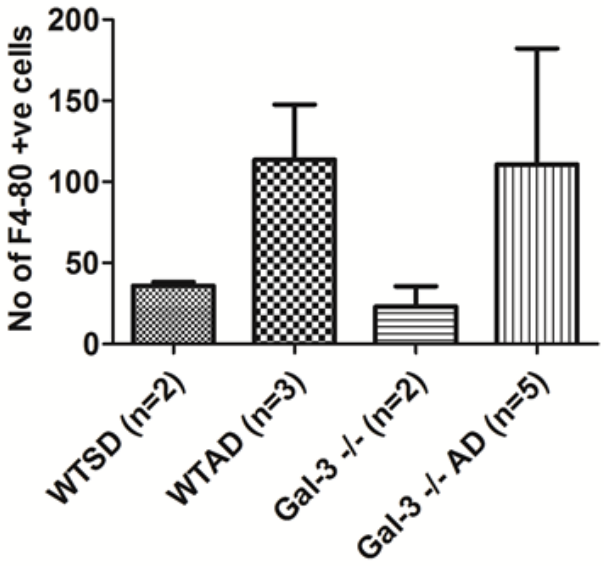

(b)

	WT		Gal-3 $^{-/-}$	
	SD	*AD*	*SD*	*AD*
No of mice	2	3	2	5
No of F4/80+ve cells	35.84 (3.3)	113.5 (38.42)	23.09 (17.56)	110.7 (39.88)

Figure 32: Relative renal cortical macrophage numbers by histological quantification. (a) bar chart of median (range) numbers of F4-80 +ve cells per x40 image. (b) Statistics of the number of F4-80+ve cells per x40 image. Median value obtained is derived from 6 x40 images per animal. Total numbers of animals analysed were too small to have confidence in normality of distribution. There were no significant difference between WT AD fed mice and Gal-3$^{-/-}$ mice. All AD fed mice had an increase in numbers of F4/80 positive cells suggesting macrophage accumulation within renal cortex.

3.3.5.2 Equivalent renal CD-68 gene expression between WT and Gal-3 $^{-/-}$ AD fed mice.

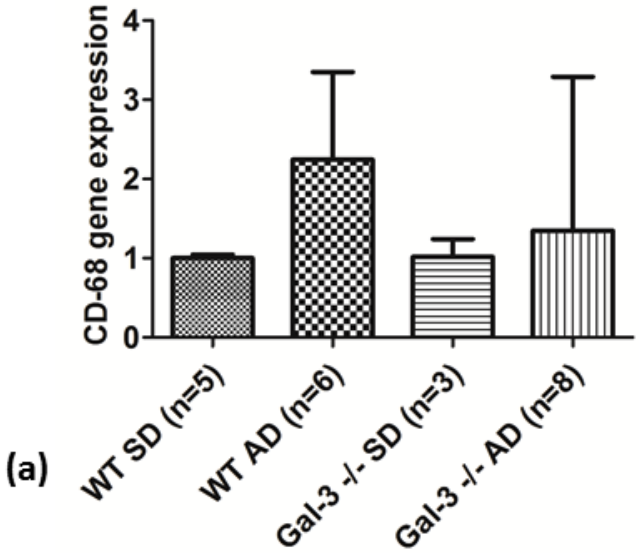

(a)

Relative Gene Expression	WT		Gal-3 $^{-/-}$		P=<0.05
	SD	AD	SD	AD	
CD68	1 (0.02)	2.25 (0.66)	1.02 (0.43)	1.35 (0.77)	NS

(b)

Figure 33: Relative CD68 gene expression by comparative quantitation using a WT SD fed mouse as a calibrator gene and 18s as a housekeeper gene. Bar chart shows median (range) and table shows median (standard deviation). The WT AD fed group had significantly more CD68 gene expression, WT SD vs WT AD, p= 0.0067. There was a non-significant increase between Gal-3 $^{-/-}$ SD and Gal-3 $^{-/-}$ AD fed animals, p= 0.08 (Mann Whitney). There was no significant difference between WT AD fed mice and Gal-3 $^{-/-}$ AD fed mice CD68 expression.

3.3.6 Circulating monocyte subset change towards a Ly6C^{low} phenotype in WT mice fed AD.

The Ly6C subset changes in experimental uraemia were examined in WT mice before including Gal-3$^{-/-}$ mice. There were 2 WT control groups used to compare data with a WT 3 Wk. AD fed mouse experiment group. The first control group were WT mice fed SD. The second control group were WT mice fed AD for 1 week. Data had previously shown 1 Wk. AD fed mice had equivalent plasma Cr, body weight and sGal-3 to SD fed mice (Chapter 2). The 1 Wk. AD fed mouse group was included to investigate if there were effects mediated by the AD independent of uraemia. In statistical analysis the control groups were combined to enable significance testing between control animals and 3 Wk. AD fed mice. The mice in all groups were harvested at the same time and circulating whole blood analysed for Gal-3 and Ly6C fluorescence according to methodology outlined in Chapter 2 (section 2.2.6.1). Monocytes were identified using FlowJo™ software using size/granularity characteristics and positivity for Ly6C [Fig 34 a+b]. The Ly6C fluorescence sorting revealed 3 distinct groups a large group with low Ly6C fluorescence similar to isotype fluorescence therefore considered Ly6C negative and not monocytes. The 2 remaining cell populations were split into Ly6C^{low} and Ly6C^{high} groups. These Ly6C^{high} and Ly6C^{low} groups could be readily identified for each animal and relative proportions as well as Ly6C MFI could be analysed [Fig. 34c]. There was no clear identification of a separate Ly6C^{int} group that could be isolated and measured. Ly6C^{int} were almost certainly present but not readily discernible. The results showed a significant reduction in the overall

Ly6C MFI of all gated monocytes from control groups (SD and 1 Wk. AD) compared to the 3 weeks AD fed mice [Table 24]. When the individual Ly6C subsets were gated and analysed it was shown that there was a sequential significant reduction in the proportion of cells gated as Ly6c^{high} and an increase in the proportion gated as Ly6C^{low} between control mice and 3 Wk. AD fed mice [Fig 35, Table 24]. There was a reduction in fluorescence intensity of Ly6c MFI within both Ly6C^{high} and Ly6C^{low} gated groups in 3 Wk. AD fed mice that reached significance [Table 24]. Both Ly6C^{high} and Ly6C^{low} monocyte populations have an increase in their Gal-3 expression at 3 weeks AD compared to (SD and 1 Wk. AD) controls [Table 24].

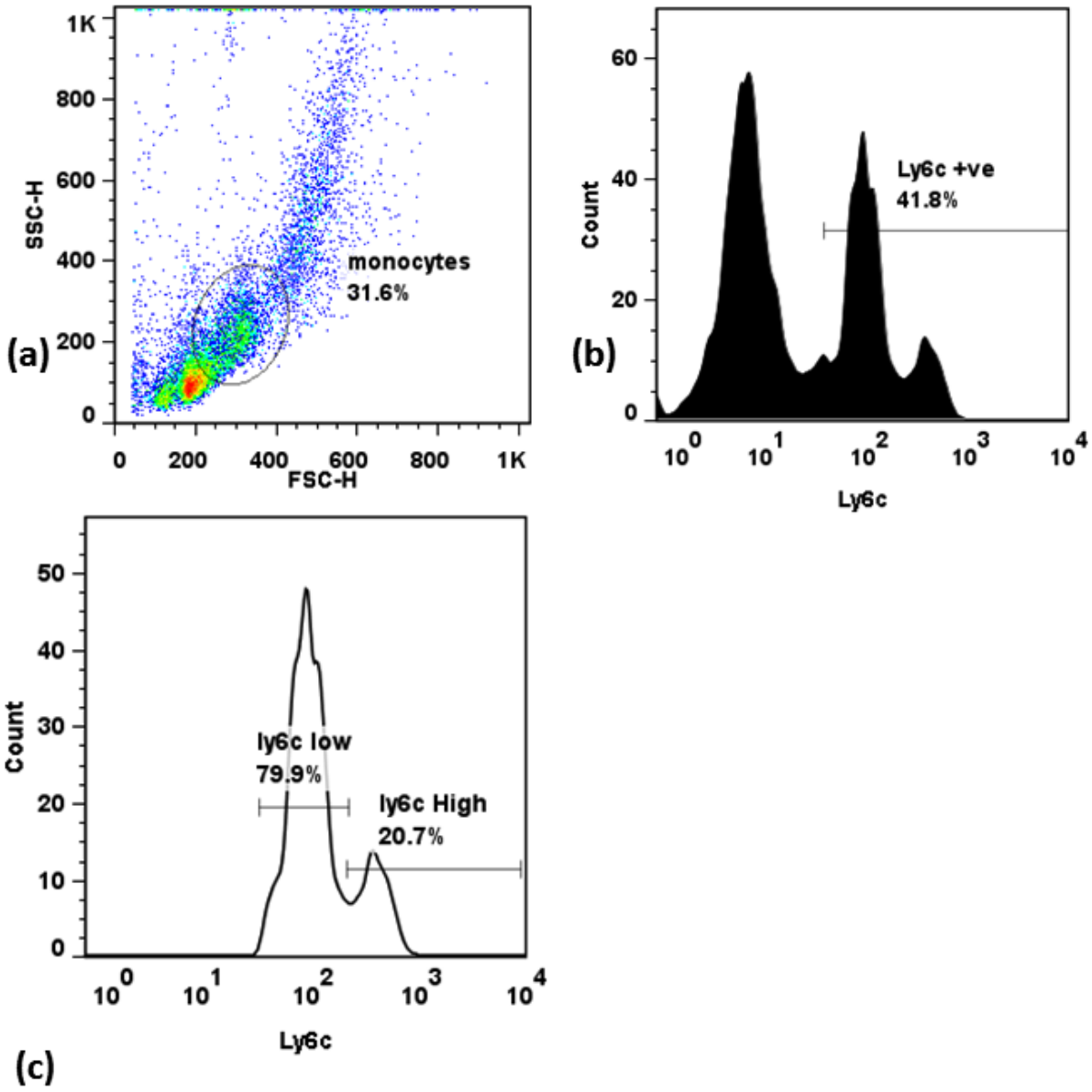

Figure 34: FACS analysis of murine whole blood, gating for monocytes (a) monocyte population identified by size and granularity (SSC/FSC) is selected from flow cytometry data using FlowJo™ software. (b) The population selected in (a) has Ly6C fluorescence measured (log scale) and uses an isotype control (not shown) to select out all events (cells) that are Ly6c +ve. (c) Ly6c +ve cells form 2 distinct groups reflecting Ly6C ^{high} and Ly6C ^{low} monocytes. These can be selected to measure Ly6C MFI and Gal-3 MFI using a Gal-3 fluorochrome. All cell populations were automatically selected in the same way.

	SD	AD (1 Wk)	AD (3 Wk)	p= <0.05
N	2	5	5	
Gal-3 MFI	519.5 (68.5)	402.6 (24.42)	797.4 (36.84)	*
Ly6c MFI	120 (11)	116.8 (2.56)	92.56 (2.67)	*
Ly6c High %	24.75 (1.25)	17.94 (1.41)	4.33 (0.77)	*
Ly6c High MFI	491 (8)	416 (3.69)	318 (9.91)	*
Ly6c High Gal-3 MFI	756.5 (349.5)	112.1 (94.72)	852.3 (215.5)	*
Ly6c Low %	62 (21.07)	82.42 (3)	95.8 (1.76)	*
Ly6c Low MFI	104.2 (10.8)	107.4 (2.23)	89.08 (2.64)	*
Ly6c Low Gal-3 MFI	502 (47)	411.8 (23.97)	794.8 (37.72)	*

Table 24: Gal-3 and Ly6C measurement of gated monocytes by FACS in WT mice fed SD, AD for 1 week and AD for 3 weeks.

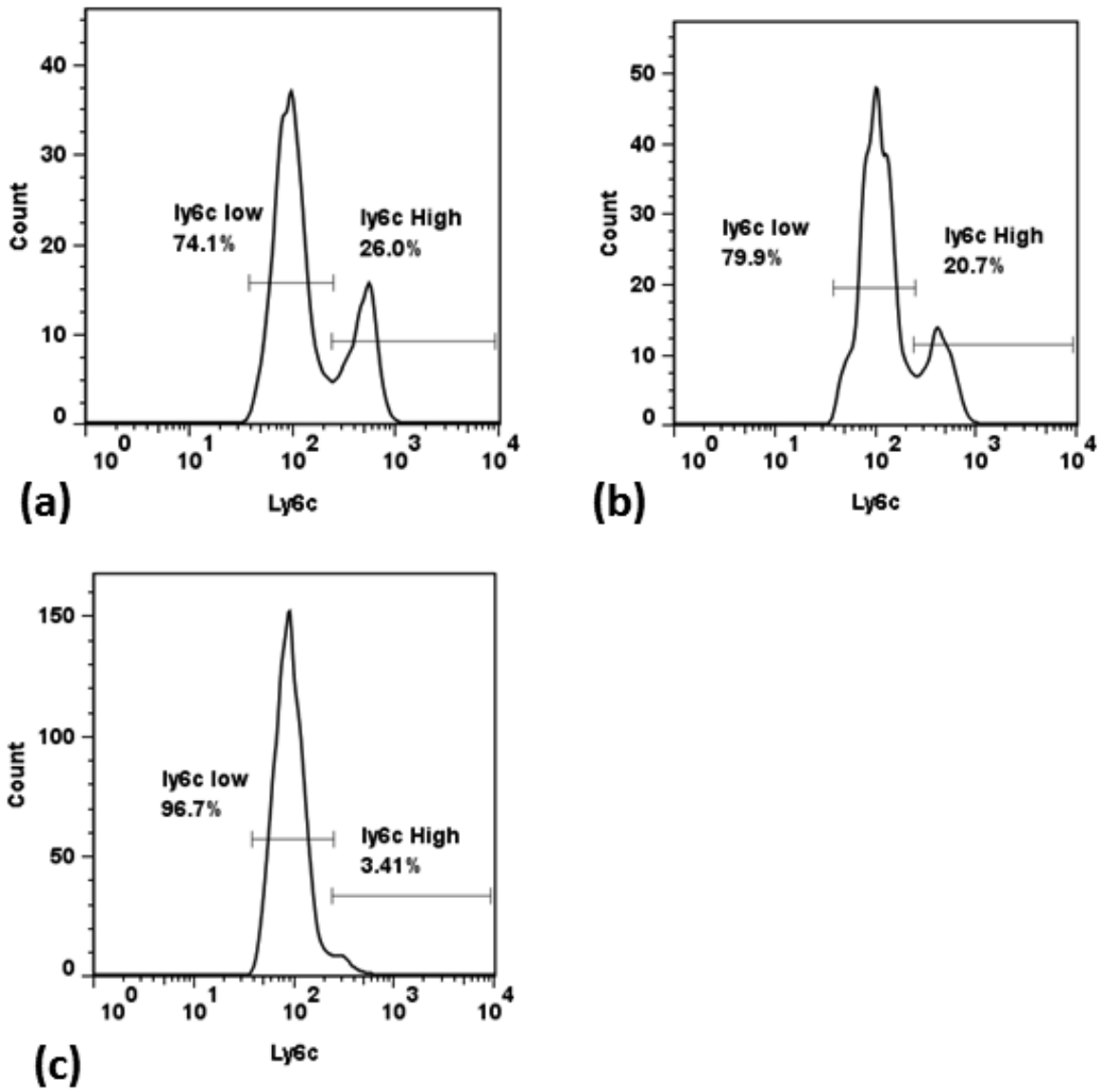

Figure 35: Ly6C ^{high} and ^{low} monocyte subsets in WT mice fed SD, AD for 1 week and AD for 3 weeks. Representative measurements of Ly6c fluorescence intensity on the X axis and cell count on the Y axis. The numbers of monocytes increase overall from (a) WT SD fed mice, (b) WT mice fed Ad for 1 week and (c) WT mice fed AD for 3 weeks. As the animals become more uraemic during the time given an AD the relative proportion of Ly6C ^{high} monocyte subset falls and the Ly6C ^{low} group increases. There is likely to be a group of Ly6C^{int} monocytes formed but the data was unable to separate a distinct grouping. Ly6C^{int} monocytes have previously been designated pro-inflammatory.

3.3.7 Gal-3$^{-/-}$ circulating monocytes resist AD uraemic phenotypic change towards a Ly6C^{low} phenotype.

FACS was performed on whole blood from 10 week old animals fed AD or SD for 3 weeks. After processing blood for FACS there were 2 WT SD animals, 5 WT AD, 3 Gal-3 $^{-/-}$ SD, and 5 Gal-3 $^{-/-}$ AD fed animals available for analysis. Live cells were gated by SSC/FSC characteristics and from this gate monocytes were gated by double positive staining for CD11B and Ly6C compared to an isotype control [Fig. 36]. There was a monocytosis observed once more for animals fed AD but with equivalent results between both AD fed groups [Table 25]. WT SD vs WT AD median % double positive events out of all gated events = 7.12 (±0.56) vs 25.26 (±8.15), Gal-3$^{-/-}$ SD vs Gal-3 $^{-/-}$ AD = 11.45 (±3.53) vs 27.42 (±6.6). In SD fed groups the Gal-3 $^{-/-}$ mice had a higher median % of gated monocytes falling within the Ly6C^{high} group and lower median % falling within the Ly6C^{low} group [Table 25, Fig 37]. Because of small numbers in the WT SD group it was not possible to test statistical significance. However, there was a non-significant reduction in the proportion of gated monocytes falling within the Ly6C^{High} monocyte subset and corresponding non-significant increase in the Ly6C^{low} group in WT AD fed mice compared to Gal-3 $^{-/-}$ mice fed AD [Table 25, Fig 38]. Given the reduction in size of the Ly6C^{high} subset and increase in Ly6c^{low} subset it could be expected that there would be a greater reduction in overall Ly6C MFI in WT mice fed AD. In fact WT AD fed mice had a significantly higher Ly6C MFI than Gal-3 $^{-/-}$ AD fed mice [Table 26]. The overall monocyte and Ly6C^{low} Ly6C MFI were both significantly higher for Gal-3$^{-/-}$ mice fed AD compared to WT AD fed mice. The WT mice had

more $Ly6C^{low}$ monocytes expressing higher Ly6C than the Gal-$3^{-/-}$ AD fed mice. The probability is that the WT mice had developed a sizeable $Ly6C^{int}$ population and the Gal-$3^{-/-}$ mice did not. The Gal-$3^{-/-}$ mice just developed a $Ly6C^{low}$ monocyte population with low levels of expressed Ly6C. However no discrete $Ly6C^{int}$ group could be identified from gating for analysis.

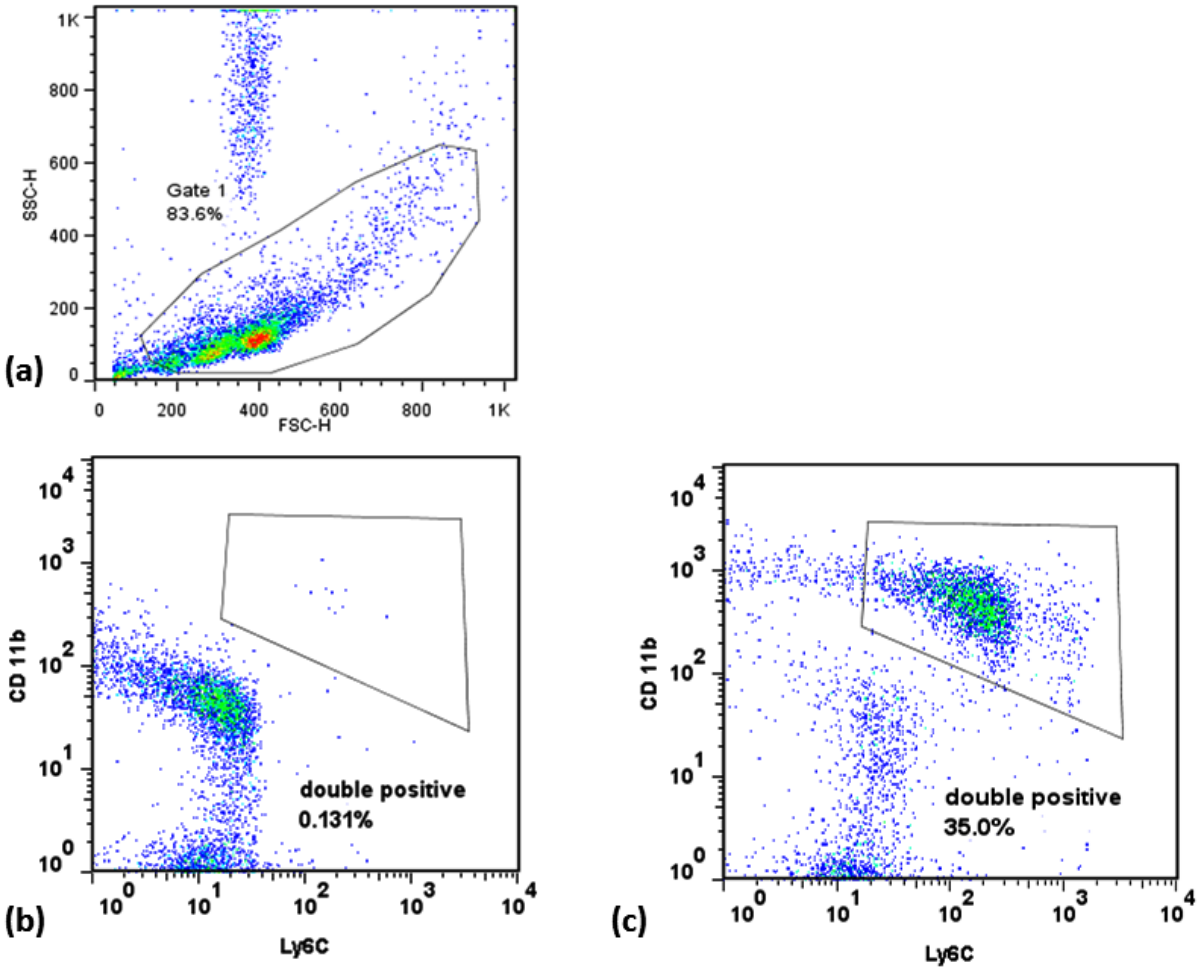

Figure 36: Gating monocytes by SSC/FSC and CD11B/Ly6C staining characteristics. Representative scatter graphs of gating techniques using FlowJo™ software. (a) Live cells including monocytes are gated using size and granularity (FSC/SSC) characteristics. (b) The selected events (cells) have their CD11B and Ly6c fluorescence measured and compared to an isotype control for both Ly6C and CD11B. (C) Representative CD11B and Ly6C fluorescence intensity scatter plot with double positive gate shown. All samples automatically had the same gating applied to them.

	WT		Gal-3 $^{-/-}$		
	SD	AD	SD	AD	p=< 0.05
No of values	2	5	3	5	
% Double Positive	7.12 (0.56)	25.26 (8.15)	11.45 (3.53)	27.42 (6.6)	NS
Ly6c MFI	175.5 (31.82)	167 (17.85)	221.7 (111.2)	129.4 (21.11)	*
Ly6c ^{High} %	24.8 (0.85)	13.0 (4.91)	40 (12.25)	18.2(6.14)	NS
Ly6c ^{High} MFI	1302 (132.2)	1044 (113.2)	1344 (79.53)	1152 (58.19)	NS
Ly6c ^{Low} %	75.2 (0.85)	87.0 (4.91)	60.0 (12.25)	81.8 (6.14)	
Ly6c ^{Low} MFI	133 (19.8)	147.8 (22.88)	91.83 (9.81)	105.7 (25.07)	*

Table 25: Relative proportions of monocytes falling into Ly6C^{high} and Ly6C^{low} groups between treatment and genotype groups. Values shown are for monocytes defined as for cells gated for positivity to both CD 11b and Ly6C. WT and Gal-3 $^{-/-}$ mice fed AD develop a monocytosis shown here by elevated double positive CD 11b and Ly6c. There are no significant differences between the 2 AD fed genotypes in the % of events being gated. The WT AD fed group had a significantly increased Ly6c expression (MFI) compared to Gal-3 $^{-/-}$ AD fed mice, 167 (±17.85) vs 129.4 (±21.11) p = 0.0317 (Mann-Whitney). Although the Ly6C MFI does significantly increase overall in double positive cells in WT AD fed mice compared to Gal-3 $^{-/-}$ this is not a uniform increase, with a reduction of both numbers and Ly6c intensity in the Ly6C^{high} group in the WT AD compared to Gal-3 $^{-/-}$ AD. The Ly6C^{low} group is the beneficiary with a non-significant increase in numbers and significant increase in MFI, 147.8 (± 22.88) vs 105.7 (±25.07) p= 0.0241 (Student t-test).

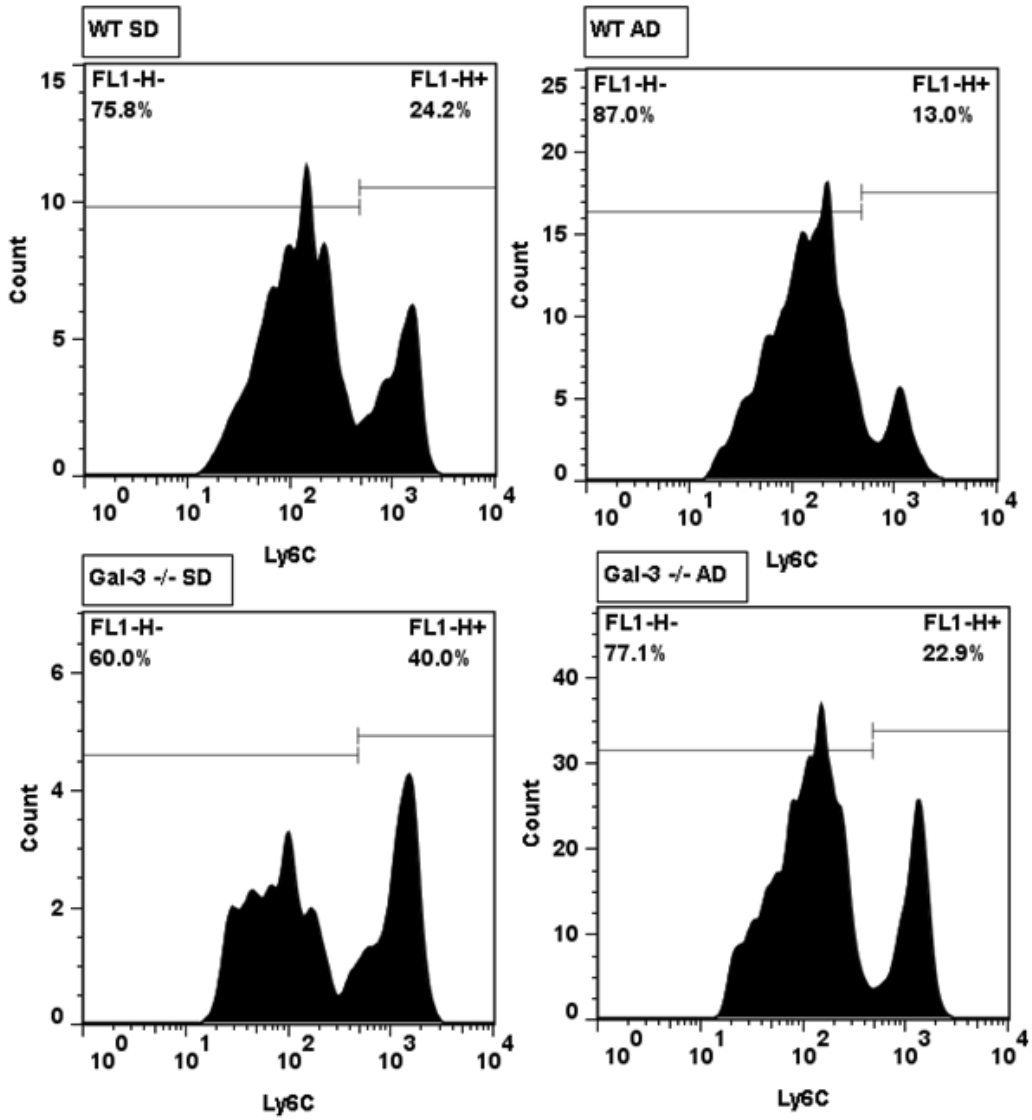

Figure 37: Representative individual mouse blood samples showing Ly6C fluorescence staining patterns of double positive (CD11B/Ly6C +ve) events. The data show an increase in overall double positive (monocyte numbers) in AD fed mice of both genotypes. There is an increase in the Ly6C^{low} (FL1-H-) monocyte population and reduction in the relative proportion of the Ly6C^{high} (FL1-H+) population in WT AD mice compared to WT SD fed mice. This increase is less in Gal-3$^{-/-}$ AD fed mice.

3.3.8 Gal-3$^{-/-}$ kidneys subject to AD have reduced CHI313 expression compared to WT AD fed mice.

Gene expression of M2 macrophage activation was assessed by qPCR. The kidneys from mice fed SD or AD for 3 weeks were processed for qPCR looking at CHI313 and Retnla gene expression and analysed by comparative quantitation using a WT SD kidney as a calibrator gene. There were 3 animals in each study group (WT SD, WT AD, Gal-3$^{-/-}$ SD and Gal-3 $^{-/-}$ AD) that had sufficient nucleic acid purity for further analysis by qPCR. CHI313 demonstrated an increase in both AD fed groups compared to their respective SD fed genotype. There was a much larger increase in relative gene expression in the WT AD groups compared to the Gal-3$^{-/-}$ group. However the variance in WT AD CHI3L3 increase (122, 45 and 20 fold) meant that there was no significance to the obvious comparison with Gal-3 $^{-/-}$ AD fed animal CHI313 increase (6.37, 3.83 and 1.91 fold) [Fig. 38 b+c]. Retnla gene expression demonstrated a reduction compared to the WT SD comparator in all the remaining study groups [Fig. 39 a+c]. WT AD fed animals had a greater median reduction in Retnla expression than Gal-3 $^{-/-}$ AD fed mice (0.14 (±0.07) vs 0.65 (±0.28)). However this was not found to be statistically significant.

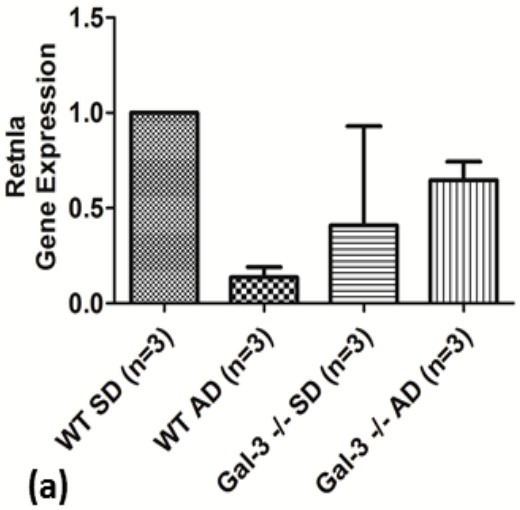

(a)

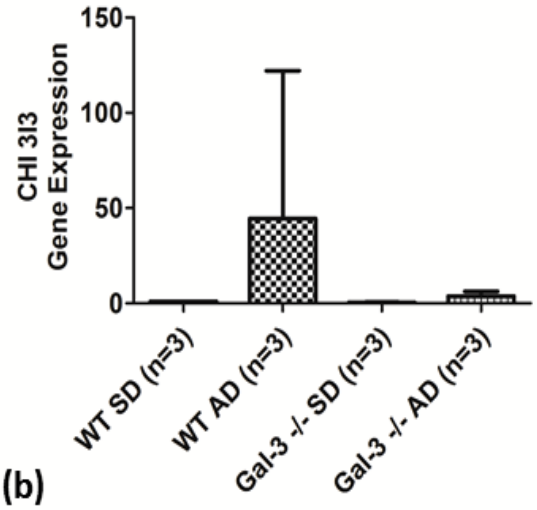

(b)

Relative Gene Expression	WT		Gal-3 $^{-/-}$		P=<0.05
	SD	AD	SD	AD	
CHI313	1 (0)	44.5 (53.21)	0.5 (0.2)	3.83 (2.24)	NS
RETNLA	1 (0)	0.14 (0.07)	0.41 (0.36)	0.65 (0.28)	NS

(c)

Figure 38: Markers of macrophage M2 differentiation from kidney homogenates after 3 weeks of AD or SD. Results show comparative quantitation analysis using a WT SD fed mouse as the calibrator gene and 18s as a housekeeper gene. Bar charts show the median (range) of comparative quantitation of gene expression using a WT SD fed animal as the calibrator gene and table gives Median (standard deviation) of values. (a+c) Retnla expression is reduced in WT AD and Gal-3 $^{-/-}$ SD and AD fed animals. (b+d) CHI313 is elevated in both AD fed groups but markedly in the WT AD fed group (relative gene expression values of 122, 45 and 20. The spread of data and the low numbers of animals studied meant that the increase was not significant on Mann Whitney analysis when compared to Gal-3 $^{-/-}$ animals fed AD (relative expression values of 6.37, 3.83 and 1.91).

3.4 Discussion

3.4.1 Gal-3 $^{-/-}$ mice have an ameliorated disease phenotype when given an AD despite evidence of equivalent amounts of fibrosis and macrophage accumulation.

Gal-3 $^{-/-}$ mice suffer significantly less weight loss and have higher plasma Cr at 3 weeks AD compared to WT controls. The variability in baseline plasma Cr values between in WT SD fed mice may reflect the variability of the Cr assay used. Because of the amount of plasma being used for analysis for a Gal-3 ELISA an 'in-house' Cr assay was used which required a lower volume of plasma (25 µl) compared to the external laboratory normally used by our laboratory (100 µl). The co-efficient of variation on samples assayed 'in-house' was performed (which were conducted in duplicate where volumes were sufficient (see Chapter 2 section 2.7.1 Table A1). WT SD and Gal-3 $^{-/-}$ SD plasma Cr values were higher than expected in group 3 compared to group 1. I would suggest this may be because of user variation in performing the 2 step assay or because of degradation of the assay. Although used within the expiry date the standard used to measure Cr against demonstrated a CV of 13.39 which suggests difference in the measured Cr standard value between assays.

3.4.2 Gal-3 $^{-/-}$ offers partial not absolute protection from the AD.

Gal-3 $^{-/-}$ AD fed mice had a partial protection as they had significantly lower creatinine than the WT controls. It is even more relevant that weight loss in Gal-3 $^{-/-}$ mice was significantly less which would lead to higher Cr levels than the low

muscle mass from WT AD fed animals. The fact that Gal-3$^{-/-}$ mice do get a CKD with the AD is reflective of the real in-vivo effect of a knockout model in the complex multifactorial process of nephrolithiasis induced interstitial fibrosis. The Gal-3$^{-/-}$ mice did consume an equivalent amount of diet. They did get equivalent crystal deposition in their tubules; the difference is in the subsequent inflammation. As described in the introduction Gal-3 is not required for any absolute function in an animal. To see real differences between WT and Gal-3 $^{-/-}$ animals in this model large numbers of animals are required. The effect of absence of Gal-3 is clearly not absolute since Gal-3 $^{-/-}$ mice still get renal fibrosis, weight loss and elevated plasma Cr. The feasibility of maintaining large colonies of Gal-3 $^{-/-}$ mice is difficult and subject to time and financial restraints.

3.4.3 Equivalent markers of fibrosis and collagen laydown between genotypes.

Renal histological assessment of the extent of tubulointerstitial damage suggests that Gal-3$^{-/-}$ mice have significant reduction in both cortical and medullary damage. However histological assessment of collagen deposition and qPCR markers of fibrosis are equivalent between WT and Gal-3$^{-/-}$ mice fed AD. At baseline the SD fed Gal-3 $^{-/-}$ mice have lower markers of fibrosis than WT SD fed mice. Both procollagen (1) and α-SMA are non-significantly elevated in WT AD fed mice compared to Gal-3$^{-/-}$ mice fed AD. The duration of the diet of 3 weeks may be too short to observe what amounts to a chronic disease process (fibrosis). Similar gene markers of fibrosis and collagen deposition in Henderson *et al.* work investigating an UUO model of renal fibrosis took 7 days to establish

significant differences between the genotypes.[60] The same model took 14 days to establish significant differences in procollagen (1) in the Okamura *et al.* paper.[121] Unlike Henderson *et al.* study (8)the Okamura paper found an increase in picosirius red staining at 14 days post UUO in the Gal-3$^{-/-}$ mice. TGF-β is non-significantly elevated in Gal-3$^{-/-}$ mice fed AD at 3 weeks. Because the PCR data comes from homogenised kidneys the cell type of origin cannot be determined. The UUO model observed a similar TGF-β gene expression between the genotypes at 14 days post-operation.[60]

3.4.2 AD induces WT circulating monocyte Ly6C subset change.

WT mice fed an AD have a reduced Ly6C^{high} population and an increased Ly6C^{low} population. No discrete Ly6C^{int} formation was found but it doesn't rule out the possible formation of this group. The increase in Ly6C number could arise from newly derived monocytes from bone marrow after initiation from the diet. There presumably must be an expansion from the bone marrow given the significantly increased numbers of monocytes at 3 weeks of AD. The increase could also come from circulating Ly6C^{high} monocytes differentiating into Ly6C^{low} monocytes. Whether renal tissue monocytes levels (transmigrated monocytes) are also Ly6c^{low} monocyte predominant remains to be examined. Previous work does suggest an increase in renal transmigrated Ly6C^{low} monocytes in the AD.[211]

3.4.3 Gal-3 $^{-/-}$ mice avoid Ly6c monocyte subset change.

Gal-3 $^{-/-}$ SD fed mice have a lower Ly6c MFI at baseline than WT SD fed mice. The functional significance of this is not known. Gal-3 $^{-/-}$ mice fed AD for 3 weeks had a non-significantly reduced Ly6C^{Low} proportional increase. Again for describing

differences in an 'optimising' molecule as opposed to an absolute molecule numbers may have to be increased to demonstrate statistical difference. However regardless of the cause or effect of Ly6C monocyte fluorescence, it is different between WT and Gal-3$^{-/-}$ mice fed SD or AD. It is tempting to hypothesize the formation of a distinct Ly6C^{int} group as demonstrated in uraemia with a human comparison.[209] However, in the work presented here no distinct subset using CD11B and Ly6c markers could be demonstrated. Further analysis using additional monocyte subset markers may be helpful in discriminating a distinct group.

3.4.4 Reduced CHI313 and elevated Retnla in Gal-3$^{-/-}$ fed AD compared to WT AD fed mice

CHI313 and Retnla are markers of alternative activation of macrophages. CHI313 was elevated in both AD fed genotypes compared to SD fed mice. It cannot be certain what the source of the CHI313 is because lymphocytes (B and T-cells), monocytes and dendritic cells also secrete these proteins in a Th2 cytokine environment.[203] The predominant infiltrating cell type observed in the AD is F4/80 +ve cells (cells of macrophage/monocyte lineage). Given the evidence that CHI313 is very highly expressed by alternatively activated macrophages It can be hypothesized that a reduction in CHI313 gene expression reflects a reduction in renal macrophage expression.[203] It may be the renal macrophage population in the *Gal-3* $^{-/-}$ mice fed AD have a reduced M2 differentiation. Further work identifying the Th1 and Th2 cytokine profile from homogenised kidneys as well as evaluation of further markers of M1 and M2 differentiation would help examine this hypothesis. There is a precedent for strongly positive CHI313

expression and downregulated Retnla below control levels in 2 models of chronic fibrotic disease predominated by alternatively activated macrophages (experimental acinomycetoma by *Nocardia brasilienis*, chronic musculoskeletal inflammation by alphavirus and acute *Trypanosoma cruzi* infection of the heart).[214-216] In these experiments, despite a Th2 cytokine rich environment and elevated CHI313 expression suggesting M2 macrophage differentiation, the Retnla levels were low and lower than the control mice indicating active downregulation. Retnla is a negative feedback mechanism for IL-13. It could be downregulation of Retnla is a mechanism to maintain chronically elevated IL-13 and persistence of the Th2 environment.

3.4.4 Concluding Remarks

Gal-$3^{-/-}$ mice have partial protection from the AD phenotype with less renal injury which is independent of collagen deposition, markers of fibrosis and macrophage accumulation. Gal-$3^{-/-}$ circulating monocytes have a non-significant reduction in the WT AD phenotypic change towards a $Ly6C^{low}$ population. That Gal-$3^{-/-}$ monocytes have a significantly lower overall Ly6C MFI despite fewer monocytes falling within the $Ly6C^{low}$ class points to the emergence of a $Ly6C^{int}$ group in WT mice that is not reflected in Gal-$3^{-/-}$ animals. Renal macrophage markers of alternative differentiation are reduced in Gal-$3^{-/-}$ kidneys fed an AD. Therefore observed partial protection in Gal-$3^{-/-}$ mice fed AD is mediated via differences in inflammation rather than fibrosis.

The influence of Gal-3 on leucocyte-endothelial interactions in extra-renal microvasculature

Chapter 4

Chapter 4: The influence of Gal-3 on leucocyte-endothelial interactions in extra-renal microvasculature.

4.1 Background

We have already determined that, whilst monocyte Gal-3 is elevated, there is not a significant difference in number of macrophages in renal cortex between Gal-3 $^{-/-}$ mice fed an AD and WT mice fed an AD (Chapter 3). The conclusion from this observation is that differences in the AD injury to WT and Gal-3$^{-/-}$ mice are independent of the numbers of monocytes transmigrating from blood to renal tissue and subsequent differentiation into macrophages. There were no differences between the AD fed genotypes used, however, both AD fed WT and Gal-3$^{-/-}$ mice did demonstrate significantly increased macrophage infiltration and a circulating monocytosis compared to SD fed mice.

The argument for elevated Gal-3 resulting in increased adhesion and leucocyte-endothelial (LEC) rolling is still compelling from earlier published data on Gal-3.[47, 56, 94, 95, 200] Vascular beds cannot be thought of as one and it may be that the intra-renal microvasculature during significant adenine induced inflammation behaves differently from other tissue microcirculation. We cannot assume that monocyte LEC are equivalent to neutrophil LEC in the AD. Leucocytes of monocyte and macrophage cell lineage are the predominant cell in the later fibrotic stages of the AD model.[170] The initial inflammatory response is characterised by neutrophil infiltration.[211] Gal-3 promotes adhesion of human neutrophils to endothelial cell monolayers, laminin and fibronectin *in vitro*.[217]

Gal-3 significantly increases the number of neutrophils, monocytes and eosinophils recruited to murine air pouches.[58] Neutrophil granulocytes do accumulate within the kidney during the AD as demonstrated by Hochst *et al*. by Ly6G (granulocyte specific) renal staining.[211] We sought to define neutrophil Gal-3 expression and LEC interactions *in vivo* during the AD in an extra-renal tissue microcirculation, the cremasteric microcirculation.

4.1.1 Intravital Microscopy

IVM has been used to describe the effects of Gal-1 on LEC but there is no published data exists using Gal-$3^{-/-}$ mice.[218] IVM is defined as the observation of a system in a living organism by microscopy. It is a useful tool to analyse and dissect complex biological and disease mechanisms *in vivo* including leucocyte recruitment and the adhesion cascade. IVM can measure each step in this cascade of leucocyte rolling, flux, rolling velocity, adhesion and emigration.[219] Small animals are frequently used, especially mice, due to the ability to use genetic manipulations. Transilluminating light microscopy can visualise vasculature and leucocytes within thin and translucent tissues (such as cremaster muscle and peritoneal membrane) without the need for contrast enhancing methods.

The microcirculation of more solid tissue can be studied using contrast enhanced epifluorescence microscopy.[220] IVM and epifluorescent microscopy enables the use of dye to identify cell populations and measure vascular permeability.

Intravenous injection of FITC-labelled Bovine Serum Albumin (BSA) allows the evaluation of vascular albumin leakage as a marker of vascular permeability.[221] Leucocytes can be labelled with dyes (rhodamine) to facilitate visualisation in thicker or opacified tissues.[222]Leucocytes can also be labelled with fluorochrome-conjugated antibodies to distinguish leucocyte subpopulations. [220] When performing IVM, inflammogens (LPS, PAF) can be added to buffer (perfusing the vasculature) or given intravenously to stimulate leucocyte recruitment so basal and inflamed measurements can be determined. Antibodies to selectins and other adhesion molecules can be given intravenously to block their effects and determine their influence on the visualised adhesion cascade. An ischaemia reperfusion model can be induced by cross clamping the superior cremasteric muscle temporarily occluding the primary artery and vein.

There are technical criticisms of IVM; it is an intricate microsurgical technique. To create suitable optical conditions necessitate surgery to the cremaster. The localised trauma of surgery can act as a local and even systemic inflammatory stimulus so microdissection techniques have to be optimised to minimise such trauma. Exposing the cremaster can cause drying which leads to microvascular dysfunction so the muscle must be continuously perfused with bicarbonate buffered saline with controlled temperature and ph. The technique is performed under anaesthesia. Anaesthetics can have effects on the macro and microcirculation. Additionally there are potentially confounding issues that may contribute to local cremasteric inflammation in a chronic uraemic animal that

could be falsely ascribed to uraemic effects. These uraemic effects include platelet dysfunction increasing the bleeding time during surgery and hence increasing the pro-inflammatory effect on LEC with local extravasation. Specific to the AD model mice are frequently half to a third the weight of their sham littermates and their testicular weights are just under half that of the shams. The cremaster appears smaller and surgical margins are closer to the viewed blood vessels potentially causing a local inflammatory stimulus and making surgery more intricate than that in larger animals.

4.2 Methods

4.2.1 IVM

IVM of the cremaster of 10 week old WT and Gal-3$^{-/-}$ fed SD or AD was performed as described by Gavins and Giddens *et al*.[223, 224] Once anaesthetised, the mouse is placed ventral side up onto a viewing stage. The right testicle covered by cremasteric muscle is exposed having blunt dissected overlying skin and fascia. Tissues are regularly perfused with bicarbonate buffered saline at 37^{0}C to prevent the tissues drying out which can elicit an inflammatory response manifest as increased leucocyte rolling. The cremasteric sack is immobilised and carefully opened by thermal cautery along the ventral axis and the use of microscissors. Once opened, the testicle is moved away and the cremaster held open for microscopic viewing with 4 hooks. The cremaster is transilluminated with a 12-V 100 W light source. Tissues are superfused with thermostated (37^{0}C) bicarbonate buffered saline. The cremaster is placed on a Plexiglas stage and mounted on a Zeiss Axioskope with a water immersion objective lens

(magnification x40) and an eyepiece (x10 magnification) [Fig 40]. Post-capillary venules can be identified from morphology and the presence of rolling leucocytes. For each animal a total of 3-5 post capillary venules should be viewed. The diameter of the venules should be between 25-50 µm. The microscope is fitted with a red blood cell optical velocimeter which measures red blood cell centreline velocity. Mean red cell velocity can then be worked out by the formula V_{mean} = centreline velocity/1.6. This enables the Wall Shear Rate (WSR) to be calculated by the formula WSR = 8000 x (V_{mean}/diameter). Post capillary venules are recorded and timed for off-line analysis. The parameters scored then include cell flux (number of leucocytes passing a fixed point/ min), rolling velocity (time for a leucocyte to travel 100 µm), number of adherent cells (stationary leucocyte on endothelium for > 30 s) and number of emigrated cells in tissue outside the vessel in a 100 x 50µm area [Fig 39].

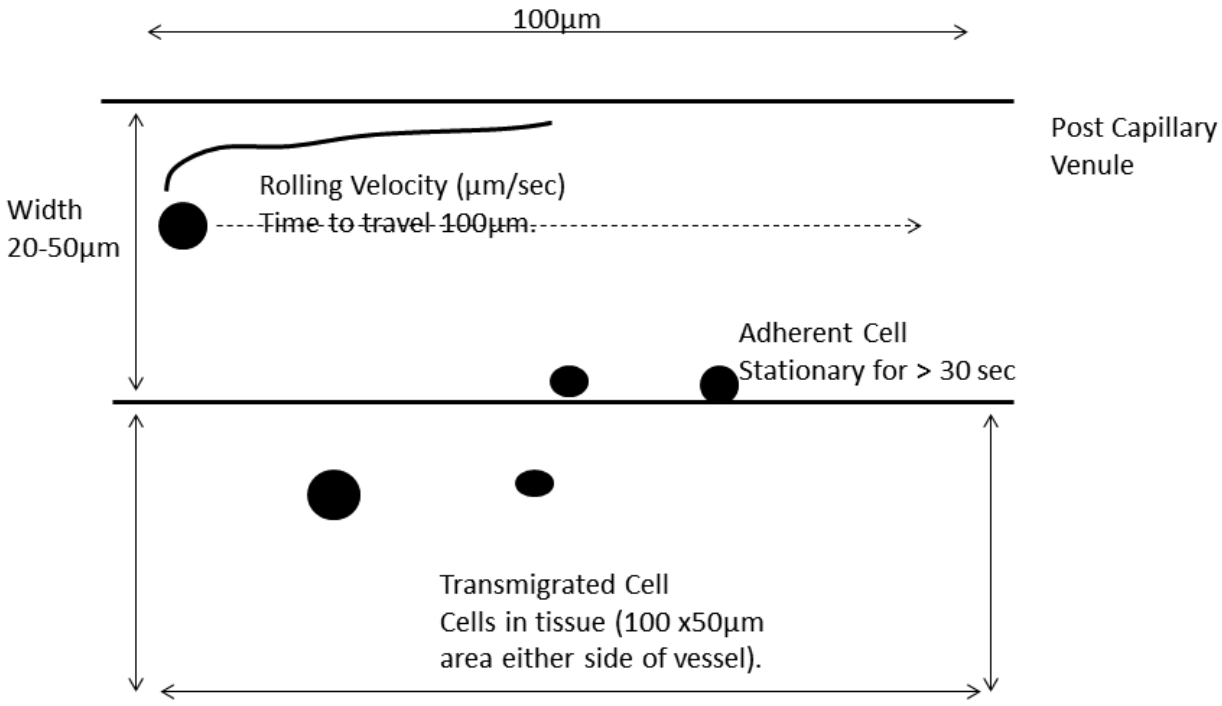

Figure 39: IVM Measurements made during off-line analysis of murine cremasteric post capillary venules. Adapted from Gavins *et al*, Journal of Pharmacological and Toxicological Methods 49 (2004) 1–14.[223]

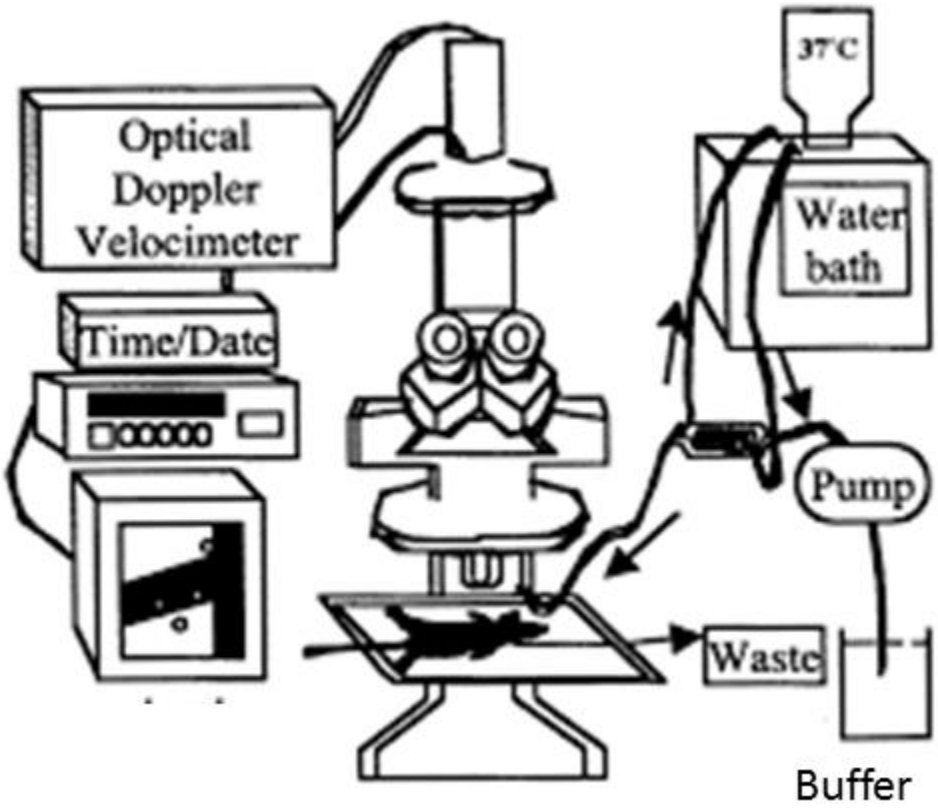

Figure 40: IVM laboratory equipment set up. A mouse with cremaster exposed is placed on a Plexiglas slide. Buffer is heated with a water bath and dripped onto the cremaster whilst a x40 image is recorded for off-line analysis later. During the procedure post capillary venules can be identified with optimum dimensions for analysis. 3-5 vessels are recorded per mouse. Adapted from Lim et al.[225]

4.2.2 Flow Cytometry

Flow cytometry of whole blood was performed as described in Chapter 3 (section 2.2.6.1). Gating of neutrophils is described in the results (4.3.1.).

4.3 Results

4.3.1 Permeabilized neutrophil Gal-3 levels are elevated after 3 weeks AD.

12 x 10 week old WT mice were used to analyse circulating neutrophil Gal-3 levels by flow cytometry. 5 mice were placed on SD for 3 weeks, 5 mice were given 1 week of AD and 5 mice given 3 weeks of AD. Only 2 of the SD fed mice had suitable processing for FACS analysis. For statistical analysis the SD fed mice and 1 Wk. AD group were considered the controls. As described before the 1 Wk. AD mice were found to have no difference in plasma Cr, weight or sGal-3. The use of the 1 Wk. AD mice was to look for direct effects of AD independent of the development of Uraemia. For statistical comparison the SD and 1 Wk. group were pooled together. All mice were harvested on the same day for flow cytometry. Permeabilized neutrophils were gated from live events by size and granularity characteristics (SSC/FSC) into a live cell gate. They were subsequently identified by SSC characteristics and negativity to Ly6c [Fig 41]. No neutrophil specific antibody was used, this was because 2 fluorochromes were already being used to analyse Ly6c and Gal-3. There was a sequential increase in Gal-3 MFI from SD fed mice (Median Gal-3 MFI = to 1 Week AD to 3 weeks AD. This was statistically significant using a Kruskall-Wallis test of the variance of the median values between the 3 groups (p= 0.0158). The low number of animals in

the WT SD group meant Mann-Whitney analysis was not able to be performed between the WTSD and WT AD 3 week groups. There was a significant increase in Gal-3 MFI between WT AD 1 week and WT AD 3 week groups, Gal-3 MFI = 288 (±67.17) vs 664 (±113), p= 0.0079 (Mann-Whitney) [Fig 42].

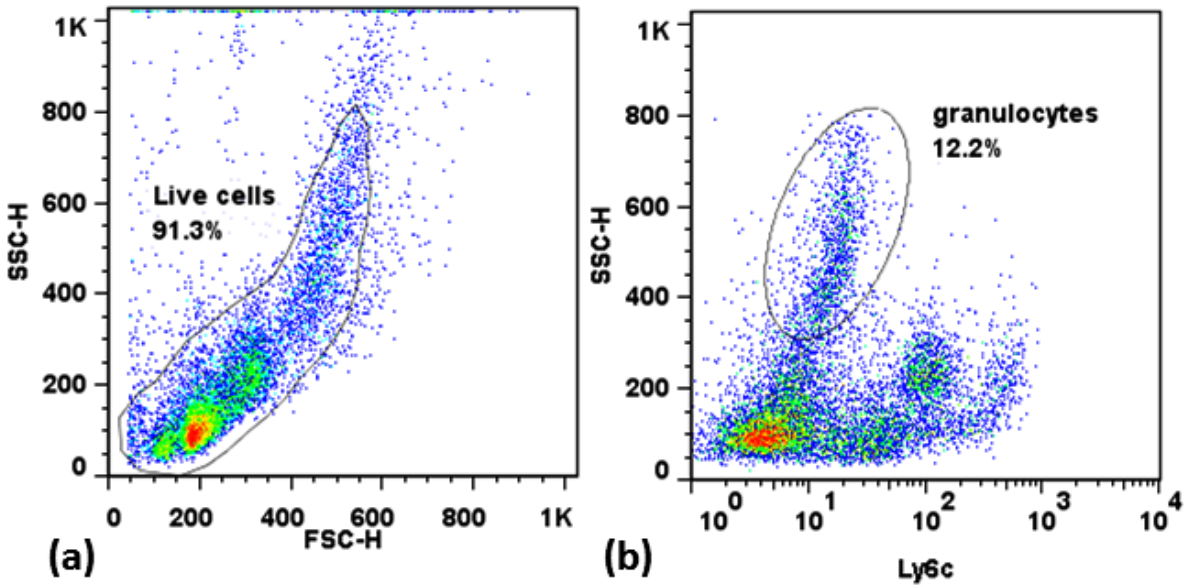

Figure 41: Selecting granulocyte populations using FACS gating. (a) Granulocytes were gated by selecting a group representing live cells. (b) Granulocytes were then selected by their ssc characteristics and negativity for Ly6c. Within this gate measurements of Gal-3 MFI were taken. All samples had the same gating automatically applied to them.

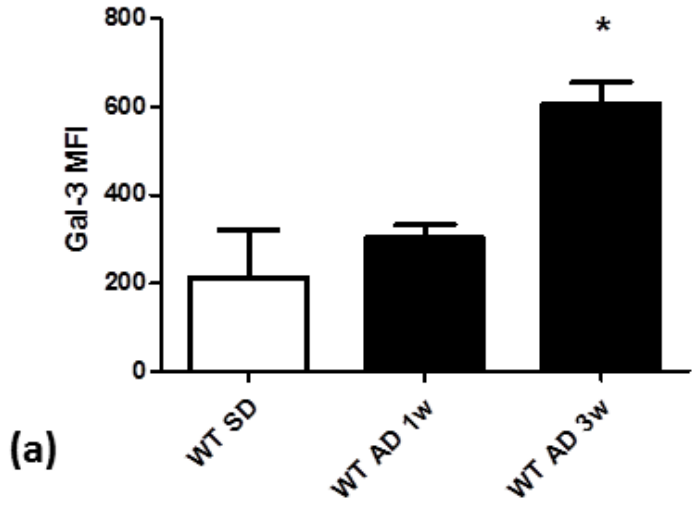

(a)

	WT		P=<0.005
	Control (SD + 1 WK AD)	3 Wk AD	
(n)	7	5	
Gal-3 MFI	288 (93.71)	664 (113)	p=0.0025

(b)

Figure 42: Measured granulocyte Gal-3 expression by FACS**.** Measured permeablised granulocyte Gal-3 MFI in 3 week AD group is significantly higher than that found in WT fed a SD and WT given AD for 1 week murine granulocytes (Kruskall-Wallis, p= 0.0158).

4.3.2 LEC adherence but not transmigration is increased in WT AD fed mice

The IVM experiments were not performed contemporaneously. Approximately 2-3 IVM preparations could be performed in a day. The subsequent availability of Gal-3 $^{-/-}$ mice meant that the IVM experiments were performed a year apart. The first experiments used WT mice only and the second experiments used both genotypes. Out of a total of 30 WT mice there were only 6 WT SD fed mice and 5 WT AD fed mice that had adequate preparations for video analysis post procedure [Fig 44]. Out of 15 Gal-3$^{-/-}$ mice only 8 were suitable (3 SD and 5 AD fed). Therefore out of 45 mice only 11 (42.2%) had adequate preparations, though the success rate was lower in the WT AD fed groups (WT AD = 27.7%). Mean blood vessel diameter was acceptable for all groups apart from the WT SD fed mice. Optimal post capillary vessel diameter is 25-50μm [Table 26]. The mean WT SD fed mouse vessel diameter was 64μm (±0.46). This resulted in a non-significantly lower mean RBC velocity and wall shear stress [Table 26]. The WT AD and both Gal-3 $^{-/-}$ groups had similar RBC velocity and wall shear stress parameters. The median number of leucocytes adherent to endothelium for > 30 s was significantly elevated in WT AD fed mice compared to WT SD fed mice and both Gal-3 $^{-/-}$ groups (Krushkall-Wallis, p=0.0115. WT AD vs Gal-3 $^{-/-}$ AD, 9.75 cells (±1.36) vs 3.13 cells (±3.13), p=0.0079 (Mann–Whitney) [Table 26]. Median leucocyte rolling velocity (the time taken for a leucocyte to roll along 100 μm of endothelium expressed as μm/s) was non-significantly reduced in WT AD compared to WT SD mice, p= 0.426 (Mann Whitney). The median rolling velocity for both Gal-3$^{-/-}$ groups was significantly lower than the WT SD fed mouse

(p=0.0456, Krushkall Wallis). The reduced rolling velocity was non-significantly reduced between WT AD and Gal-3$^{-/-}$ AD fed groups [Table 26]. There were no significant differences in numbers of transmigrated cells between the experiment groups [Table 26].

Figure 43: Representative image of IVM VHS video recording performed by author of thesis. Striated cremasteric muscle can be seen either side of a post capillary venule. Leucocytes can be visualised as circular bodies rolling along the endothelium. The dark circular black marks are to measure RBC velocity. Measurements can be drawn onto the television screen to demonstrate distance markers of 50 µm to 100µm in order to measure velocity, adhesion and transmigration.

IVM results	*WT* SD	*WT* AD	Gal-3 $^{-/-}$ SD	Gal-3 $^{-/-}$ AD
Attempted	12	18	5	10
Successful	6	5	3	5
Body Weight (g)	28.15 (1.55)	16.1 (0.43)	29.67 (3.61)	22.66 (1.20)
Blood Vessel Diameter (µm)	64 (0.46)	46 (0.22)	34 (0.08)	36 (0.14)
RBC Velocity	0.48 (0.22)	1.21 (0.92)	1.26 (0.12)	1.22 (0.07)
Wall Shear Stress	9374 (2520)	29226 (22389)	31745 (1486)	27046 (7728)
Leucocyte-endothelial adherence (no of cells)	4.02 (1.42)	9.75 (1.36)	3.89 (2.22)	3.13 (2.47)
Leucocyte rolling velocity (µm/sec)	55.13 (29.86)	36.84 (24.84)	17.84 (5.95)	17.59 (11.52)
Transmigration (no of cells)	0.64 (0.49)	1.23 (0.53)	1.11 (0.51)	1.57 (1.31)

Table 26: Intravital microscopy results from all treatment and genotype groupings. The technically challenging element of microsurgery in the cremasteric preparation for IVM meant low success rates especially in AD fed mice. Body weights of WT AD and Gal-3$^{-/-}$ mice were significantly lower than Gal-3$^{-/-}$AD fed mice and the SD fed mice. This was a confounding factor to the experiment. Leucocyte adherence to post-capillary venule endothelium was significantly elevated in WT AD fed mice compared to Gal-3 $^{-/-}$ AD fed mice 9.75 cells (±1.36) vs 3.13 cells (±2.47), p=0.0079 (Mann Whitney). Despite this, there was not an increase in numbers of transmigrated leucocytes into cremasteric tissue. Leucocyte rolling velocity appeared to be slower in Gal-3$^{-/-}$ SD and AD fed mice though this did not reach significance.

4.4 Discussion

4.4.1 Elevated neutrophil Gal-3 in the AD.

Granulocytes were selected based on size, granularity and negativity to Ly6C (defined by an isotype control) only. There was no cell-specific stain used. A distinct cell group could be identified with granularity and negativity to Ly6C. It is feasible, without using a neutrophil specific marker that other cell types could be included in the analysis. Elevated granulocyte Gal-3 could have a number of repercussions on neutrophil behaviour in the AD. Feasibly the elevated Gal-3 could increase adhesion to post-capillary venule endothelium and ECM proteins leading to the increased adherence demonstrated by IVM. Gal-3 induces oxidative burst in neutrophils, increases Il-8 production, L-selectin- shedding and it protects neutrophils from apoptosis.

4.4.2 Leucocyte-endothelial adhesion is increased in WT AD fed mice compared to Gal-3$^{-/-}$ AD fed mice but weight loss is a significant confounding factor.

As described in Chapter 2, WT AD fed mice have a significant weight loss over the 3 weeks of treatment. Their mean testicular weight was lower (data not shown). The smaller testicle size meant that the available surface to perform microsurgery was reduced. The technique was intricate and the number of animals with adequate preparation were low with only 5 WT AD fed mice out of 18 (28%) attempted resulting in acceptable cremasteric preparations. Whilst leucocyte adherence appeared to be significantly increased, the lack of elevated

transmigration may point to the adhesion originating from inflammation that occurred during surgery as opposed to that induced by systemic uraemia. To reduce the impact of surgery a rest period was observed for all animals after exposing the cremaster of 30 min to allow the post-surgical inflammation to resolve. There remains a concern that with a smaller surgical area; the probability is that some WT AD leucocyte adherence reflected surgery and not the underlying model. The cremaster also appeared more opaque in the Gal-$3^{-/-}$ mice, probably reflecting fat content, this made video analysis more difficult.

4.4.3 Lack of cell specific staining

The IVM performed by myself was pure light microscopy with no cell specific staining. It would be interesting to see if the leucocyte adherence represented granulocytes or monocytes. As already discussed there is a monocytosis associated with the AD. The monocytes also reduce their Ly6C expression towards a $Ly6C^{low}$ phenotype. This $Ly6C^{low}$ phenotype has also been observed to have 'patrolling' characteristics of rolling along post capillary endothelium. Another hypothesis would be that the leucocytes observed are neutrophils. The finding of an increase in leucocyte-endothelial adherence is interesting with the above caveats. The use of flow chambers could be a useful *in vitro* method of validating this finding.

4.4.4 Reduced rolling velocity in Gal-$3^{-/-}$ SD and AD fed mice

The findings presented here of an elevated sGal-3 and increased monocyte and granulocyte Gal-3 in the AD led to the hypothesis that rolling velocity would be

higher in Gal-3$^{-/-}$ mice. In fact, they were significantly lower compared to WT SD fed mice but not significantly changed from the WT AD fed mice. The IVM data for the WT SD fed mice does have to be viewed with some caution. The post-capillary venules in this group were larger than ideal, RBC velocity and wall shear stress were non-significantly reduced compared to all other groups.

4.4.5 Concluding Remarks

Despite limitations of this technique, one can suggest that Gal-3 is not associated with transmigration of leucocytes in the uremic milieu. Observed differences between WT and Gal-3 AD fed mice are not related to quantitative changes in numbers of leucocytes infiltrating inflamed tissue. This finding at a microcirculatory level is further validated by our data showing equivalent number of leucocytes of monocyte/macrophage lineage within the renal tissue and peritoneal in AD fed mice of both genotypes (Chapter 2.3.5).

Conclusions and future work

Chapter 5

Chapter 5 Discussion and future work

5.1 Discussion

5.1.1 Elevated sGal-3 in the AD

This thesis has described an elevated sGal-3 in the AD model of uraemia and tubulointerstitial fibrosis. A hypothesis could be that the origin of increased sGal-3 is secreted and derived from the increased circulating monocyte Gal-3 measured by FACS analysis. Most epithelial surfaces can express Gal-3 and the author did not measure endothelial expression of Gal-3 or urinary Gal-3. Gal-3 is filtered by the glomerulus so plasma levels could increase with reducing GFR. As discussed before measurement of urinary Gal-3 would be difficult to distinguish between filtered and collecting duct tubular epithelial Gal-3 which is present in the urine. To measure precise glomerular filtration of Gal-3 would require injection of a known amount of labelled sGal-3 and measured in the urine over a given time frame to determine renal clearance. Intravenous injection of sGal-3 is difficult and has not been used often as it acts as a red call agglutinin. The level of sGal-3 in the AD at 3 weeks is equivalent to levels seen in human disease.

5.1.2 Solid organ Gal-3 is elevated predominantly in the kidney during the AD.

sGal-3 is elevated at week 3 of the AD and all organs will be perfused with blood containing this increase. The solid organs (lung, heart, aorta) do not show differences between the AD and SD fed mice. The kidney does demonstrate

increased Gal-3 expression from intrinsic epithelial expression and from infiltrating cells into the interstitium. The AD model is not long enough to demonstrate some aspects of uraemia elevated (e.g. elevated PTH). The link between reduced GFR, elevated sGal-3 and the uremic cardiac fibrosis and remodelling requires more examination. Gal-3 is implicated in cardiac fibrosis and vascular fibrosis which form part of the phenotype of human CKD.[226, 227] Preferably an animal model that is longer in duration and causes hypertension with uraemia may allow further examination of the role Gal-3 may have in uremic cardiovascular disease. The 5/6 th Nx model is a chronic uremic model with hypertension and would suit. Unfortunately we were not able to reliably demonstrate uraemia in this model. A potential hypothesis linking CKD Gal-3 and cardiac fibrosis is the monocyte. Cardiac remodelling is driven by interactions between monocyte/macrophage and fibroblast.[228] We have demonstrated AD induced elevated monocyte Gal-3 and differential monocyte phenotype towards a Ly6c^{low} group in WT AD fed mice. This Ly6C^{low} group gives rise to M2 activated macrophages and correlates with fibrotic disease.[92] In my hypothesis CKD induces elevated monocyte Gal-3 and Ly6c^{low} differentiation. In the presence of hypertensive myocardial stress uraemia induced Ly6c^{low} monocytes could infiltrate myocardial tissue, differentiate into M2 activated macrophages and induce myocardial fibrosis.

5.1.3 Phenotypic differences in response to AD between WT and Gal-3$^{-/-}$ mice are independent of markers of fibrosis and monocyte/macrophage numbers.

Gal-3 has been described as an optimising molecule. Not necessary for any absolute function but required for optimal function. To see significant difference in 'optimal' as opposed to absolute function numbers have to be high. There was no doubt that Gal-3 $^{-/-}$ mice received a significant uraemia and interstitial fibrosis. The limitation of using a knockout model was the need to limit numbers to those essential in order to be efficient and not waste animals. The AD model had a high mortality so was optimised to use for 3 weeks rather than 4. This was to maximise efficiency and reduce costing whilst still being able to see differences between the genotypes. Increasing the numbers of animals may have led to a significant difference in markers of fibrosis given there was a non-significant reduction in collagen staining, Procollagen (1) and α-SMA in Gal-3$^{-/-}$ mice fed AD compared to WT. Renal monocyte /macrophage numbers were equivalent between WT and Gal-3$^{-/-}$ fed AD but there was a striking difference in markers of M2 macrophage activation with very high levels of CHI313 expressed. Because renal interstitial macrophages were not isolated for qPCR, rather the whole kidney, the source of CHI313 cannot be described as wholly macrophage derived. Dual staining on immunohistochemistry for CHI313 and CD-68 would enable co-localisation of the CHI313 to be confident of its derivation. A hypothesis could be that observed partial protection in the AD phenotype in Gal-3$^{-/-}$ mice (less weight loss and lower creatinine) is due to differences in the local inflammatory environment produced by an M2 predominant versus M1

macrophage phenotype. To further assess this hypothesis the kidneys from WT AD fed mice and Gal-3$^{-/-}$ AD fed mice could be homogenised and M1 and M2 cytokine content assessed over time. A further piece of work to describe the cause of differences would be to study the differences in granulocyte number and function over time. As previously described neutrophil function is affected by Gal-3 expression. WT AD fed mice had elevated granulocyte Gal-3 content by FACS compared to WT SD fed mice. Whilst the chronic fibrotic phase of the AD is mediated by macrophages the initial inflammatory cascade is mediated in part by granulocytes.

5.1.4 Monocyte Gal-3 as a therapeutic target

Gal-3 has useful functions that have been demonstrated in human studies. sGal-3 has an inverse relationship to glycated haemoglobin levels in diabetics and is negatively correlated to obesity.[50] The role of Gal-3 as an AGE and ALE receptor able to safely remove AGE is one that could be physiologically useful in conditions like diabetes and CKD associated with elevated AGE and ALE levels. Gal-3 is part of the normal inflammatory response and resolution. In CKD the results in this thesis would suggest that there is an inappropriate increase in Gal-3 which correlates with monocyte phenotype change and chronic renal fibrosis in a time dependent fashion during the AD. A complete therapeutic blockage of Gal-3 may have deleterious effects of an individual to mount an appropriate inflammatory response or to handle AGE and ALE accumulation in disease. A more focused therapeutic targeting of monocyte Gal-3 may have benefits in

reducing fibrosis but preserve other useful components of Gal-3 e.g. neutrophil Gal-3 response to infection.

5.2 Future work

5.2.1 Gal-3 $^{-/-}$ chimera

There is a monocytosis affected by the AD in both WT and Gal-3$^{-/-}$ mice. It is not known whether the monocyte subset change occurs in newly derived monocytes from bone marrow or whether they are pre-existing circulating monocytes. The creation of a chimera WT mouse with Gal-3$^{-/-}$ myeloid cells and Gal-3 $^{-/-}$ with WT bone marrow would enable the discovery of whether it is the myeloid local environment that induces monocyte Ly6C change or the circulating plasma environment.

5.2.2 In vitro signalling and fibroblast work

Dissecting the intracellular signalling pathways of Gal-3 in cells of the monocyte/macrophage lineage could enable further understanding of why this galectin is elevated in CKD. It is feasible that the initial inflammatory phase of the AD may have different pathways triggering an appropriate Gal-3 response and then an inappropriate elevated Gal-3 expression occurs subsequently through a different pathway. Cell signalling pathways would have to be reviewed at different times during the AD *in vivo*.

5.2.3 Measurement of Gal-3$^{-/-}$ monocyte ly6C phenotype exposed to recombinant Gal-3

Could Gal-3$^{-/-}$ monocytes exposed to recombinant Gal-3 exhibit similar Ly6C changes in the AD as WT monocytes? The answer to this would inform about whether the Gal-3 monocyte subset difference is inherent, at the level of myeloid development or whether it is the local circulating environment that contributes to Ly6C subset change. This would enable targeted therapy towards myeloid development or towards the current situation of intravenous Gal-3 antagonism.

Appendices

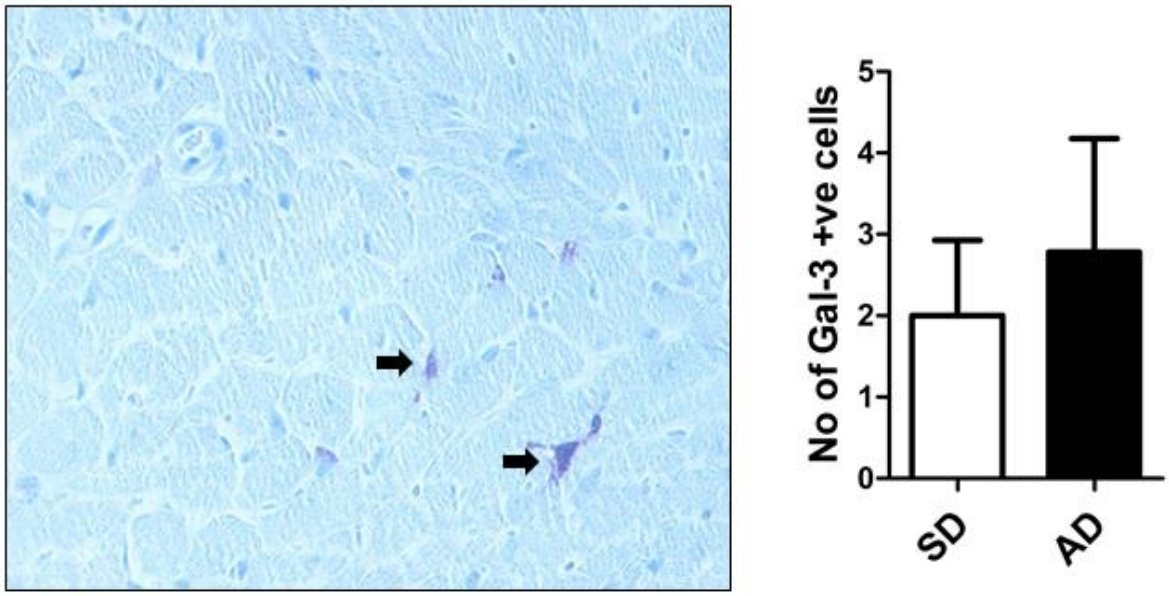

Figure A1: Myocardial Gal-3 expression by immunohistochemistry. Gal-3 positive cells (arrows) in WT myocardial section at x40 magnification and bar chart of number of Gal-3 positive cells per x40 section (6 section per animals) n= 3 in each group. No significant differences between the SD fed mice, median number of Gal-3 +ve cells per x40 slide = 2.17 (±0.93) vs 3.5 (±1.4) p. = 0.4 (Mann Whitney).

Creatinine assay
Co-efficient of Variation

	Number of Duplicates /Assays	CV (%)
Intra-assay	14	14.1 (9.78)
Inter-assay	5	13.39

Table A1 : Inter and Intra assay Coefficient of variation for the Quantichrom™ Cr assay.The intra-assay CV has a mean CV of 14 duplicates within the same assay and gives the SD in brackets. The Inter-assay CV has the overall CV for 5 different Cr assays hence does not have a SD.

Gal-3 Plasma ELISA					
Intra-assay Coefficient of Variation	16/09/2011	14/12/2011	19/12/2011	31/12/2011	09/01/2
Number of values	32	6	24	25	14
Mean CV	12.59 (9.78)	9.554 (8.67)	25.88 (13.53)	14.77 (8.08)	11.38 (9

Gal-3 Tissue ELISA		
Intra-assay Coefficient of Variation	16/03/2011	22/03/2011
Number of values	11	29
Mean CV	6.18 (7.59)	14.53 (10.35)

Table A2: Intra-assay Coefficient of Variation for commercial Gal-3 ELISA performed on plasma and tissue samples.

Subsequent to these data – any sample with a Co-efficient of Variation greater than 20% was excluded from analysis.

Gal-3 Standards	Gal-3 (pg/ml)	16/11/2011	14/12/2011	19/12/2011	31/12/2011	09/01/2012	CV (%)
1	0	0.01	0.015	0.013	0.015	0.024	33.93
2	15.6	0.051	0.046	0.052	0.076	0.066	21.34
3	31.3	0.096	0.076	0.087	0.116	0.099	15.67
4	62.5	0.194	0.118	0.147	0.162	0.132	19.46
5	125	0.222	0.289	0.25	0.241	0.22	11.44
6	250	0.428	0.446	0.401	0.419	0.428	3.85
7	500	0.705	0.719	0.602	0.574	0.541	12.68
8	1000	1.026	0.887	0.755	0.677	0.619	20.75

Table A3: Interassay coefficient of variation using Gal-3 Standards results from 5 different ELISA's on mouse plasma samples.

Plasma Gal-3 (ng/ml) at 0 weeks AD + SD	
Centrifuge >800 *g*	Centrifuge <800 *g*
19.845	4.02
26.985	10.89
34.46	6.4

Table A4: Elevated plasma Gal-3 on centrifugation of mouse whole blood > 800 *g* in the process of separating plasma.

7. References

1. Barondes, S.H., et al., *Galectins: a family of animal beta-galactoside-binding lectins.* Cell, 1994. **76**(4): p. 597-8.
2. Mody, R., S. Joshi, and W. Chaney, *Use of lectins as diagnostic and therapeutic tools for cancer.* J Pharmacol Toxicol Methods, 1995. **33**(1): p. 1-10.
3. Gorelik, E., U. Galili, and A. Raz, *On the role of cell surface carbohydrates and their binding proteins (lectins) in tumor metastasis.* Cancer Metastasis Rev, 2001. **20**(3-4): p. 245-77.
4. Cooper, D.N. and S.H. Barondes, *God must love galectins; he made so many of them.* Glycobiology, 1999. **9**(10): p. 979-84.
5. Sharon, N. and H. Lis, *History of lectins: from hemagglutinins to biological recognition molecules.* Glycobiology, 2004. **14**(11): p. 53R-62R.
6. Minko, T., *Drug targeting to the colon with lectins and neoglycoconjugates.* Adv Drug Deliv Rev, 2004. **56**(4): p. 491-509.
7. Bouckaert, J., et al., *Receptor binding studies disclose a novel class of high-affinity inhibitors of the Escherichia coli FimH adhesin.* Mol Microbiol, 2005. **55**(2): p. 441-55.
8. Kerrigan, A.M. and G.D. Brown, *C-type lectins and phagocytosis.* Immunobiology, 2009. **214**(7): p. 562-75.
9. Drickamer, K., *Increasing diversity of animal lectin structures.* Curr Opin Struct Biol, 1995. **5**(5): p. 612-6.
10. Kasai, K. and J. Hirabayashi, *Galectins: a family of animal lectins that decipher glycocodes.* J Biochem, 1996. **119**(1): p. 1-8.
11. Barondes, S.H., et al., *Galectins. Structure and function of a large family of animal lectins.* J Biol Chem, 1994. **269**(33): p. 20807-10.
12. Sato, S., et al., *Galectins in innate immunity: dual functions of host soluble beta-galactoside-binding lectins as damage-associated molecular patterns (DAMPs) and as receptors for pathogen-associated molecular patterns (PAMPs).* Immunol Rev, 2009. **230**(1): p. 172-87.
13. Hart, G.W., et al., *Glycosylation in the nucleus and cytoplasm.* Annu Rev Biochem, 1989. **58**: p. 841-74.
14. Liu, F.T., R.J. Patterson, and J.L. Wang, *Intracellular functions of galectins.* Biochim Biophys Acta, 2002. **1572**(2-3): p. 263-73.
15. Elola, M.T., et al., *Galectins: matricellular glycan-binding proteins linking cell adhesion, migration, and survival.* Cell Mol Life Sci, 2007. **64**(13): p. 1679-700.
16. Teichberg, V.I., et al., *A beta-D-galactoside binding protein from electric organ tissue of Electrophorus electricus.* Proc Natl Acad Sci U S A, 1975. **72**(4): p. 1383-7.
17. Hirabayashi, J. and K. Kasai, *The family of metazoan metal-independent beta-galactoside-binding lectins: structure, function and molecular evolution.* Glycobiology, 1993. **3**(4): p. 297-304.
18. Leffler, H., et al., *Introduction to galectins.* Glycoconj J, 2004. **19**(7-9): p. 433-40.
19. Dodd, R.B. and K. Drickamer, *Lectin-like proteins in model organisms: implications for evolution of carbohydrate-binding activity.* Glycobiology, 2001. **11**(5): p. 71R-9R.
20. Liu, F.T. and G.A. Rabinovich, *Galectins: regulators of acute and chronic inflammation.* Ann N Y Acad Sci, 2010. **1183**: p. 158-82.
21. Lobsanov, Y.D., et al., *X-ray crystal structure of the human dimeric S-Lac lectin, L-14-II, in complex with lactose at 2.9-A resolution.* J Biol Chem, 1993. **268**(36): p. 27034-8.
22. Hirabayashi, J., et al., *Oligosaccharide specificity of galectins: a search by frontal affinity chromatography.* Biochim Biophys Acta, 2002. **1572**(2-3): p. 232-54.
23. Leppanen, A., et al., *Dimeric galectin-1 binds with high affinity to alpha2,3-sialylated and non-sialylated terminal N-acetyllactosamine units on surface-bound extended glycans.* J Biol Chem, 2005. **280**(7): p. 5549-62.
24. Liu, F.T., *Molecular biology of IgE-binding protein, IgE-binding factors, and IgE receptors.* Crit Rev Immunol, 1990. **10**(3): p. 289-306.
25. Woo, H.J., et al., *Carbohydrate-binding protein 35 (Mac-2), a laminin-binding lectin, forms functional dimers using cysteine 186.* J Biol Chem, 1991. **266**(28): p. 18419-22.

26. Nieminen, J., et al., *Visualization of galectin-3 oligomerization on the surface of neutrophils and endothelial cells using fluorescence resonance energy transfer.* J Biol Chem, 2007. **282**(2): p. 1374-83.
27. Ahmad, N., et al., *Galectin-3 precipitates as a pentamer with synthetic multivalent carbohydrates and forms heterogeneous cross-linked complexes.* J Biol Chem, 2004. **279**(12): p. 10841-7.
28. Takenaka, Y., et al., *Nuclear export of phosphorylated galectin-3 regulates its antiapoptotic activity in response to chemotherapeutic drugs.* Mol Cell Biol, 2004. **24**(10): p. 4395-406.
29. Hughes, R.C., *Secretion of the galectin family of mammalian carbohydrate-binding proteins.* Biochim Biophys Acta, 1999. **1473**(1): p. 172-85.
30. Patterson, R.J., W. Wang, and J.L. Wang, *Understanding the biochemical activities of galectin-1 and galectin-3 in the nucleus.* Glycoconj J, 2004. **19**(7-9): p. 499-506.
31. Ochieng, J., V. Furtak, and P. Lukyanov, *Extracellular functions of galectin-3.* Glycoconj J, 2004. **19**(7-9): p. 527-35.
32. Dagher, S.F., J.L. Wang, and R.J. Patterson, *Identification of galectin-3 as a factor in pre-mRNA splicing.* Proc Natl Acad Sci U S A, 1995. **92**(4): p. 1213-7.
33. Barondes, S.H., et al., *Multiple soluble vertebrate galactoside-binding lectins.* Biochimie, 1988. **70**(11): p. 1627-32.
34. Than, N.G., et al., *Galectins: Double-edged Swords in the Cross-roads of Pregnancy Complications and Female Reproductive Tract Inflammation and Neoplasia.* J Pathol Transl Med, 2015. **49**(3): p. 181-208.
35. Poirier, F., *Roles of galectins in vivo.* Biochem Soc Symp, 2002(69): p. 95-103.
36. Norling, L.V., M. Perretti, and D. Cooper, *Endogenous galectins and the control of the host inflammatory response.* J Endocrinol, 2009. **201**(2): p. 169-84.
37. Henderson, N.C. and T. Sethi, *The regulation of inflammation by galectin-3.* Immunol Rev, 2009. **230**(1): p. 160-71.
38. Ho, M.K. and T.A. Springer, *Mac-2, a novel 32,000 Mr mouse macrophage subpopulation-specific antigen defined by monoclonal antibodies.* J Immunol, 1982. **128**(3): p. 1221-8.
39. Lotan, R., et al., *Expression of galectins on microvessel endothelial cells and their involvement in tumour cell adhesion.* Glycoconj J, 1994. **11**(5): p. 462-8.
40. Truong, M.J., et al., *Human neutrophils express immunoglobulin E (IgE)-binding proteins (Mac-2/epsilon BP) of the S-type lectin family: role in IgE-dependent activation.* J Exp Med, 1993. **177**(1): p. 243-8.
41. Liu, F.T., et al., *Expression and function of galectin-3, a beta-galactoside-binding lectin, in human monocytes and macrophages.* Am J Pathol, 1995. **147**(4): p. 1016-28.
42. Joo, H.G., et al., *Expression and function of galectin-3, a beta-galactoside-binding protein in activated T lymphocytes.* J Leukoc Biol, 2001. **69**(4): p. 555-64.
43. Moutsatsos, I.K., et al., *Endogenous lectins from cultured cells: nuclear localization of carbohydrate-binding protein 35 in proliferating 3T3 fibroblasts.* Proc Natl Acad Sci U S A, 1987. **84**(18): p. 6452-6.
44. Koch, A., et al., *Galectin-3, a novel centrosome-associated protein, required for epithelial morphogenesis.* Mol Biol Cell, 2010. **21**(2): p. 219-31.
45. Yu, F., et al., *Galectin-3 translocates to the perinuclear membranes and inhibits cytochrome c release from the mitochondria. A role for synexin in galectin-3 translocation.* J Biol Chem, 2002. **277**(18): p. 15819-27.
46. Paz, I., et al., *Galectin-3, a marker for vacuole lysis by invasive pathogens.* Cell Microbiol, 2010. **12**(4): p. 530-44.
47. Kuwabara, I. and F.T. Liu, *Galectin-3 promotes adhesion of human neutrophils to laminin.* J Immunol, 1996. **156**(10): p. 3939-44.
48. Nio, J., et al., *Immunohistochemical and in situ hybridization analysis of galectin-3, a beta-galactoside binding lectin, in the urinary system of adult mice.* Histochem Cell Biol, 2006. **126**(1): p. 45-56.
49. Wanninger, J., et al., *Systemic and hepatic vein galectin-3 are increased in patients with alcoholic liver cirrhosis and negatively correlate with liver function.* Cytokine, 2011. **55**(3): p. 435-40.
50. Weigert, J., et al., *Serum galectin-3 is elevated in obesity and negatively correlates with glycosylated hemoglobin in type 2 diabetes.* J Clin Endocrinol Metab, 2010. **95**(3): p. 1404-11.

51. Winyard, P.J., et al., *Epithelial galectin-3 during human nephrogenesis and childhood cystic diseases.* J Am Soc Nephrol, 1997. **8**(11): p. 1647-57.
52. Bullock, S.L., et al., *Galectin-3 modulates ureteric bud branching in organ culture of the developing mouse kidney.* J Am Soc Nephrol, 2001. **12**(3): p. 515-23.
53. Colnot, C., et al., *Embryonic implantation in galectin 1/galectin 3 double mutant mice.* Dev Dyn, 1998. **211**(4): p. 306-13.
54. Bichara, M., et al., *Exploring the role of galectin 3 in kidney function: a genetic approach.* Glycobiology, 2006. **16**(1): p. 36-45.
55. Nomoto, K., et al., *Disrupted galectin-3 causes non-alcoholic fatty liver disease in male mice.* J Pathol, 2006. **210**(4): p. 469-77.
56. Colnot, C., et al., *Maintenance of granulocyte numbers during acute peritonitis is defective in galectin-3-null mutant mice.* Immunology, 1998. **94**(3): p. 290-6.
57. Farnworth, S.L., et al., *Galectin-3 reduces the severity of pneumococcal pneumonia by augmenting neutrophil function.* Am J Pathol, 2008. **172**(2): p. 395-405.
58. Sano, H., et al., *Human galectin-3 is a novel chemoattractant for monocytes and macrophages.* J Immunol, 2000. **165**(4): p. 2156-64.
59. Chen, H.Y., et al., *Role of galectin-3 in mast cell functions: galectin-3-deficient mast cells exhibit impaired mediator release and defective JNK expression.* J Immunol, 2006. **177**(8): p. 4991-7.
60. Henderson, N.C., et al., *Galectin-3 expression and secretion links macrophages to the promotion of renal fibrosis.* Am J Pathol, 2008. **172**(2): p. 288-98.
61. Saravanan, C., et al., *Detection of differentially expressed wound-healing-related glycogenes in galectin-3-deficient mice.* Invest Ophthalmol Vis Sci, 2009. **50**(12): p. 5690-6.
62. Cao, Z., et al., *Galectins-3 and -7, but not galectin-1, play a role in re-epithelialization of wounds.* J Biol Chem, 2002. **277**(44): p. 42299-305.
63. Vlassara, H., et al., *Identification of galectin-3 as a high-affinity binding protein for advanced glycation end products (AGE): a new member of the AGE-receptor complex.* Mol Med, 1995. **1**(6): p. 634-46.
64. Iacobini, C., et al., *Role of galectin-3 in diabetic nephropathy.* J Am Soc Nephrol, 2003. **14**(8 Suppl 3): p. S264-70.
65. Li, Y., et al., *Galectin-3 is a negative regulator of lipopolysaccharide-mediated inflammation.* J Immunol, 2008. **181**(4): p. 2781-9.
66. Mey, A., et al., *The animal lectin galectin-3 interacts with bacterial lipopolysaccharides via two independent sites.* J Immunol, 1996. **156**(4): p. 1572-7.
67. Sano, H., et al., *Critical role of galectin-3 in phagocytosis by macrophages.* J Clin Invest, 2003. **112**(3): p. 389-97.
68. Craig, S.S., et al., *Immunoelectron microscopic localization of galectin-3, an IgE binding protein, in human mast cells and basophils.* Anat Rec, 1995. **242**(2): p. 211-9.
69. Flotte, T.J., T.A. Springer, and G.J. Thorbecke, *Dendritic cell and macrophage staining by monoclonal antibodies in tissue sections and epidermal sheets.* Am J Pathol, 1983. **111**(1): p. 112-24.
70. Sato, S. and R.C. Hughes, *Regulation of secretion and surface expression of Mac-2, a galactoside-binding protein of macrophages.* J Biol Chem, 1994. **269**(6): p. 4424-30.
71. Yamaoka, A., et al., *A human lectin, galectin-3 (epsilon bp/Mac-2), stimulates superoxide production by neutrophils.* J Immunol, 1995. **154**(7): p. 3479-87.
72. Kadrofske, M.M., K.P. Openo, and J.L. Wang, *The human LGALS3 (galectin-3) gene: determination of the gene structure and functional characterization of the promoter.* Arch Biochem Biophys, 1998. **349**(1): p. 7-20.
73. Hsu, D.K., et al., *Human T lymphotropic virus-I infection of human T lymphocytes induces expression of the beta-galactoside-binding lectin, galectin-3.* Am J Pathol, 1996. **148**(5): p. 1661-70.
74. Dong, S. and R.C. Hughes, *Galectin-3 stimulates uptake of extracellular Ca2+ in human Jurkat T-cells.* FEBS Lett, 1996. **395**(2-3): p. 165-9.
75. Frigeri, L.G., R.I. Zuberi, and F.T. Liu, *Epsilon BP, a beta-galactoside-binding animal lectin, recognizes IgE receptor (Fc epsilon RI) and activates mast cells.* Biochemistry, 1993. **32**(30): p. 7644-9.

76. Karlsson, A., et al., *Galectin-3 functions as an opsonin and enhances the macrophage clearance of apoptotic neutrophils.* Glycobiology, 2009. **19**(1): p. 16-20.
77. MacKinnon, A.C., et al., *Regulation of alternative macrophage activation by galectin-3.* J Immunol, 2008. **180**(4): p. 2650-8.
78. Bernardes, E.S., et al., *Toxoplasma gondii infection reveals a novel regulatory role for galectin-3 in the interface of innate and adaptive immunity.* Am J Pathol, 2006. **168**(6): p. 1910-20.
79. Meuret, G., J. Bammert, and G. Hoffmann, *Kinetics of human monocytopoiesis.* Blood, 1974. **44**(6): p. 801-16.
80. Passlick, B., D. Flieger, and H.W. Ziegler-Heitbrock, *Identification and characterization of a novel monocyte subpopulation in human peripheral blood.* Blood, 1989. **74**(7): p. 2527-34.
81. Heine, G.H., et al., *CD14(++)CD16+ monocytes but not total monocyte numbers predict cardiovascular events in dialysis patients.* Kidney Int, 2008. **73**(5): p. 622-9.
82. Waterhouse, D.F., et al., *Prediction of calculated future cardiovascular disease by monocyte count in an asymptomatic population.* Vasc Health Risk Manag, 2008. **4**(1): p. 177-87.
83. Khan, H.A., et al., *Significant increases in monocyte counts and serum creatine kinase in acute myocardial infarction versus general infections.* Indian J Pathol Microbiol, 2012. **55**(4): p. 474-7.
84. Maekawa, Y., et al., *Prognostic significance of peripheral monocytosis after reperfused acute myocardial infarction:a possible role for left ventricular remodeling.* J Am Coll Cardiol, 2002. **39**(2): p. 241-6.
85. Audoy-Remus, J., et al., *Rod-Shaped monocytes patrol the brain vasculature and give rise to perivascular macrophages under the influence of proinflammatory cytokines and angiopoietin-2.* J Neurosci, 2008. **28**(41): p. 10187-99.
86. Auffray, C., et al., *Monitoring of blood vessels and tissues by a population of monocytes with patrolling behavior.* Science, 2007. **317**(5838): p. 666-70.
87. Rogacev, K.S., et al., *CD14++CD16+ monocytes and cardiovascular outcome in patients with chronic kidney disease.* Eur Heart J, 2011. **32**(1): p. 84-92.
88. Dietz, A.B., et al., *Maturation of human monocyte-derived dendritic cells studied by microarray hybridization.* Biochem Biophys Res Commun, 2000. **275**(3): p. 731-8.
89. Helming, L. and S. Gordon, *Macrophage fusion induced by IL-4 alternative activation is a multistage process involving multiple target molecules.* Eur J Immunol, 2007. **37**(1): p. 33-42.
90. Holscher, C., et al., *A protective and agonistic function of IL-12p40 in mycobacterial infection.* J Immunol, 2001. **167**(12): p. 6957-66.
91. Louis, J., et al., *Regulation of protective immunity against Leishmania major in mice.* Curr Opin Immunol, 1998. **10**(4): p. 459-64.
92. Gordon, S., *Alternative activation of macrophages.* Nat Rev Immunol, 2003. **3**(1): p. 23-35.
93. Munder, M., et al., *Th1/Th2-regulated expression of arginase isoforms in murine macrophages and dendritic cells.* J Immunol, 1999. **163**(7): p. 3771-7.
94. Sato, S., et al., *Role of galectin-3 as an adhesion molecule for neutrophil extravasation during streptococcal pneumonia.* J Immunol, 2002. **168**(4): p. 1813-22.
95. Nieminen, J., et al., *Role of galectin-3 in leukocyte recruitment in a murine model of lung infection by Streptococcus pneumoniae.* J Immunol, 2008. **180**(4): p. 2466-73.
96. Jin, R., et al., *Human monocytes recognize porcine endothelium via the interaction of galectin 3 and alpha-GAL.* J Immunol, 2006. **177**(2): p. 1289-95.
97. Hsu, D.K., et al., *Targeted disruption of the galectin-3 gene results in attenuated peritoneal inflammatory responses.* Am J Pathol, 2000. **156**(3): p. 1073-83.
98. Darrow, A.L. and R.V. Shohet, *Galectin-3 deficiency exacerbates hyperglycemia and the endothelial response to diabetes.* Cardiovasc Diabetol, 2015. **14**: p. 73.
99. Pugliese, G., et al., *Accelerated diabetic glomerulopathy in galectin-3/AGE receptor 3 knockout mice.* FASEB J, 2001. **15**(13): p. 2471-9.
100. Pugliese, G., et al., *The diabetic milieu modulates the advanced glycation end product-receptor complex in the mesangium by inducing or upregulating galectin-3 expression.* Diabetes, 2000. **49**(7): p. 1249-57.

101. Zhu, W., et al., *The role of galectin-3 in endocytosis of advanced glycation end products and modified low density lipoproteins.* Biochem Biophys Res Commun, 2001. **280**(4): p. 1183-8.
102. Nachtigal, M., et al., *Galectin-3 expression in human atherosclerotic lesions.* Am J Pathol, 1998. **152**(5): p. 1199-208.
103. MacKinnon, A.C., et al., *Inhibition of galectin-3 reduces atherosclerosis in apolipoprotein E-deficient mice.* Glycobiology, 2013. **23**(6): p. 654-63.
104. Iacobini, C., et al., *Galectin-3/AGE-receptor 3 knockout mice show accelerated AGE-induced glomerular injury: evidence for a protective role of galectin-3 as an AGE receptor.* FASEB J, 2004. **18**(14): p. 1773-5.
105. Nishiyama, J., et al., *Up-regulation of galectin-3 in acute renal failure of the rat.* Am J Pathol, 2000. **157**(3): p. 815-23.
106. Sasaki, S., Q. Bao, and R.C. Hughes, *Galectin-3 modulates rat mesangial cell proliferation and matrix synthesis during experimental glomerulonephritis induced by anti-Thy1.1 antibodies.* J Pathol, 1999. **187**(4): p. 481-9.
107. Kikuchi, Y., et al., *Galectin-3-positive cell infiltration in human diabetic nephropathy.* Nephrol Dial Transplant, 2004. **19**(3): p. 602-7.
108. Sun, Z.L., et al., *Effects of advanced glycosylation end products and rosiglitazone on the expression and secretion of galectin-3 in human renal mesangial cells.* Chin Med J (Engl), 2009. **122**(9): p. 1067-71.
109. Iacobini, C., et al., *Advanced lipoxidation end-products mediate lipid-induced glomerular injury: role of receptor-mediated mechanisms.* J Pathol, 2009. **218**(3): p. 360-9.
110. Agrwal, N., J.L. Wang, and P.G. Voss, *Carbohydrate-binding protein 35. Levels of transcription and mRNA accumulation in quiescent and proliferating cells.* J Biol Chem, 1989. **264**(29): p. 17236-42.
111. Rosenberg, I.M., et al., *Structure of the murine Mac-2 gene. Splice variants encode proteins lacking functional signal peptides.* J Biol Chem, 1993. **268**(17): p. 12393-400.
112. Gritzmacher, C.A., V.S. Mehl, and F.T. Liu, *Genomic cloning of the gene for an IgE-binding lectin reveals unusual utilization of 5' untranslated regions.* Biochemistry, 1992. **31**(40): p. 9533-8.
113. Schreck, R., K. Albermann, and P.A. Baeuerle, *Nuclear factor kappa B: an oxidative stress-responsive transcription factor of eukaryotic cells (a review).* Free Radic Res Commun, 1992. **17**(4): p. 221-37.
114. Bierhaus, A., et al., *Understanding RAGE, the receptor for advanced glycation end products.* J Mol Med (Berl), 2005. **83**(11): p. 876-86.
115. Yeh, C.H., et al., *Requirement for p38 and p44/p42 mitogen-activated protein kinases in RAGE-mediated nuclear factor-kappaB transcriptional activation and cytokine secretion.* Diabetes, 2001. **50**(6): p. 1495-504.
116. Kim, K., E.P. Mayer, and M. Nachtigal, *Galectin-3 expression in macrophages is signaled by Ras/MAP kinase pathway and up-regulated by modified lipoproteins.* Biochim Biophys Acta, 2003. **1641**(1): p. 13-23.
117. Nangaku, M., *Mechanisms of tubulointerstitial injury in the kidney: final common pathways to end-stage renal failure.* Intern Med, 2004. **43**(1): p. 9-17.
118. Wynn, T.A., *Fibrotic disease and the T(H)1/T(H)2 paradigm.* Nat Rev Immunol, 2004. **4**(8): p. 583-94.
119. Sharma, U.C., et al., *Galectin-3 marks activated macrophages in failure-prone hypertrophied hearts and contributes to cardiac dysfunction.* Circulation, 2004. **110**(19): p. 3121-8.
120. Henderson, N.C., et al., *Galectin-3 regulates myofibroblast activation and hepatic fibrosis.* Proc Natl Acad Sci U S A, 2006. **103**(13): p. 5060-5.
121. Okamura, D.M., et al., *Galectin-3 preserves renal tubules and modulates extracellular matrix remodeling in progressive fibrosis.* Am J Physiol Renal Physiol, 2011. **300**(1): p. F245-53.
122. Kasper, M. and R.C. Hughes, *Immunocytochemical evidence for a modulation of galectin 3 (Mac-2), a carbohydrate binding protein, in pulmonary fibrosis.* J Pathol, 1996. **179**(3): p. 309-16.
123. Nishi, Y., et al., *Role of galectin-3 in human pulmonary fibrosis.* Allergol Int, 2007. **56**(1): p. 57-65.
124. van Kimmenade, R.R., et al., *Utility of amino-terminal pro-brain natriuretic peptide, galectin-3, and apelin for the evaluation of patients with acute heart failure.* J Am Coll Cardiol, 2006. **48**(6): p. 1217-24.
125. Lok, D.J., et al., *Prognostic value of galectin-3, a novel marker of fibrosis, in patients with chronic heart failure: data from the DEAL-HF study.* Clin Res Cardiol, 2010. **99**(5): p. 323-8.

126. Lin, Y.H., et al., *The relationship between serum galectin-3 and serum markers of cardiac extracellular matrix turnover in heart failure patients.* Clin Chim Acta, 2009. **409**(1-2): p. 96-9.
127. Ho, J.E., et al., *Galectin-3, a marker of cardiac fibrosis, predicts incident heart failure in the community.* J Am Coll Cardiol, 2012. **60**(14): p. 1249-56.
128. Levey, A.S., et al., *Chronic kidney disease: common, harmful and treatable--World Kidney Day 2007.* Am J Nephrol, 2007. **27**(1): p. 108-12.
129. *K/DOQI clinical practice guidelines for chronic kidney disease: evaluation, classification, and stratification.* Am J Kidney Dis, 2002. **39**(2 Suppl 1): p. S1-266.
130. *KDOQI Clinical Practice Guideline for Diabetes and CKD: 2012 Update.* Am J Kidney Dis, 2012. **60**(5): p. 850-86.
131. Collins, A.J., et al., *'United States Renal Data System 2011 Annual Data Report: Atlas of chronic kidney disease & end-stage renal disease in the United States.* Am J Kidney Dis, 2012. **59**(1 Suppl 1): p. A7, e1-420.
132. Coresh, J., et al., *Prevalence of chronic kidney disease and decreased kidney function in the adult US population: Third National Health and Nutrition Examination Survey.* Am J Kidney Dis, 2003. **41**(1): p. 1-12.
133. Go, A.S., et al., *Chronic kidney disease and the risks of death, cardiovascular events, and hospitalization.* N Engl J Med, 2004. **351**(13): p. 1296-305.
134. Shah, R.V., et al., *Galectin-3, cardiac structure and function, and long-term mortality in patients with acutely decompensated heart failure.* Eur J Heart Fail, 2010. **12**(8): p. 826-32.
135. Felker, G.M., et al., *Galectin-3 in ambulatory patients with heart failure: results from the HF-ACTION study.* Circ Heart Fail, 2012. **5**(1): p. 72-8.
136. de Boer, R.A., et al., *The fibrosis marker galectin-3 and outcome in the general population.* J Intern Med, 2012. **272**(1): p. 55-64.
137. van der Velde, A.R., et al., *Prognostic Value of Changes in Galectin-3 Levels Over Time in Patients With Heart Failure: Data From CORONA and COACH.* Circ Heart Fail, 2013. **6**(2): p. 219-26.
138. Gopal, D.M., et al., *Relationship of plasma galectin-3 to renal function in patients with heart failure: effects of clinical status, pathophysiology of heart failure, and presence or absence of heart failure.* J Am Heart Assoc, 2012. **1**(5): p. e000760.
139. Sarnak, M.J. and A.S. Levey, *Cardiovascular disease and chronic renal disease: a new paradigm.* Am J Kidney Dis, 2000. **35**(4 Suppl 1): p. S117-31.
140. Tyralla, K. and K. Amann, *Morphology of the heart and arteries in renal failure.* Kidney Int Suppl, 2003(84): p. S80-3.
141. Diez, J., *Mechanisms of cardiac fibrosis in hypertension.* J Clin Hypertens (Greenwich), 2007. **9**(7): p. 546-50.
142. de Almeida, E.A., et al., *Diastolic function in several stages of chronic kidney disease in patients with autosomal dominant polycystic kidney disease: a tissue Doppler imaging study.* Kidney Blood Press Res, 2007. **30**(4): p. 234-9.
143. Ahmed, A., et al., *Chronic kidney disease associated mortality in diastolic versus systolic heart failure: a propensity matched study.* Am J Cardiol, 2007. **99**(3): p. 393-8.
144. Chapman, C.M., et al., *Monocyte count, but not C-reactive protein or interleukin-6, is an independent risk marker for subclinical carotid atherosclerosis.* Stroke, 2004. **35**(7): p. 1619-24.
145. Grau, A.J., et al., *Leukocyte count as an independent predictor of recurrent ischemic events.* Stroke, 2004. **35**(5): p. 1147-52.
146. Johnsen, S.H., et al., *Monocyte count is a predictor of novel plaque formation: a 7-year follow-up study of 2610 persons without carotid plaque at baseline the Tromso Study.* Stroke, 2005. **36**(4): p. 715-9.
147. Liu, Y., *Renal fibrosis: new insights into the pathogenesis and therapeutics.* Kidney Int, 2006. **69**(2): p. 213-7.
148. Boor, P., et al., *Treatment targets in renal fibrosis.* Nephrol Dial Transplant, 2007. **22**(12): p. 3391-407.

149. Miyata, T., et al., *Accumulation of albumin-linked and free-form pentosidine in the circulation of uremic patients with end-stage renal failure: renal implications in the pathophysiology of pentosidine.* J Am Soc Nephrol, 1996. **7**(8): p. 1198-206.
150. Miyata, T., et al., *Autoxidation products of both carbohydrates and lipids are increased in uremic plasma: is there oxidative stress in uremia?* Kidney Int, 1998. **54**(4): p. 1290-5.
151. Meng, J., et al., *Evidence for a link between glycoxidation and lipoperoxidation in patients with chronic renal failure.* Clin Nephrol, 1999. **51**(5): p. 280-9.
152. Niwa, T., et al., *Elevated serum levels of 3-deoxyglucosone, a potent protein-cross-linking intermediate of the Maillard reaction, in uremic patients.* Nephron, 1995. **69**(4): p. 438-43.
153. Odani, H., et al., *Increase in three alpha,beta-dicarbonyl compound levels in human uremic plasma: specific in vivo determination of intermediates in advanced Maillard reaction.* Biochem Biophys Res Commun, 1999. **256**(1): p. 89-93.
154. Miyata, T., et al., *Implication of an increased oxidative stress in the formation of advanced glycation end products in patients with end-stage renal failure.* Kidney Int, 1997. **51**(4): p. 1170-81.
155. Stadtman, E.R. and C.N. Oliver, *Metal-catalyzed oxidation of proteins. Physiological consequences.* J Biol Chem, 1991. **266**(4): p. 2005-8.
156. Miyata, T., *Alterations of non-enzymatic biochemistry in uremia, diabetes, and atherosclerosis ("carbonyl stress").* Bull Mem Acad R Med Belg, 2002. **157**(3-4): p. 189-96; discussion 196-8.
157. Glomb, M.A. and V.M. Monnier, *Mechanism of protein modification by glyoxal and glycolaldehyde, reactive intermediates of the Maillard reaction.* J Biol Chem, 1995. **270**(17): p. 10017-26.
158. Yeung, J.H., *Effects of glycerol-induced acute renal failure on tissue glutathione and glutathione-dependent enzymes in the rat.* Methods Find Exp Clin Pharmacol, 1991. **13**(1): p. 23-8.
159. Canestrari, F., et al., *Erythrocyte redox state in uremic anemia: effects of hemodialysis and relevance of glutathione metabolism.* Acta Haematol, 1994. **91**(4): p. 187-93.
160. Newlaczyl, A.U. and L.G. Yu, *Galectin-3--a jack-of-all-trades in cancer.* Cancer Lett, 2011. **313**(2): p. 123-8.
161. Platt, D. and A. Raz, *Modulation of the lung colonization of B16-F1 melanoma cells by citrus pectin.* J Natl Cancer Inst, 1992. **84**(6): p. 438-42.
162. Pienta, K.J., et al., *Inhibition of spontaneous metastasis in a rat prostate cancer model by oral administration of modified citrus pectin.* J Natl Cancer Inst, 1995. **87**(5): p. 348-53.
163. Hsieh, T.C. and J.M. Wu, *Changes in cell growth, cyclin/kinase, endogenous phosphoproteins and nm23 gene expression in human prostatic JCA-1 cells treated with modified citrus pectin.* Biochem Mol Biol Int, 1995. **37**(5): p. 833-41.
164. Hayashi, A., A.C. Gillen, and J.R. Lott, *Effects of daily oral administration of quercetin chalcone and modified citrus pectin on implanted colon-25 tumor growth in Balb-c mice.* Altern Med Rev, 2000. **5**(6): p. 546-52.
165. Nangia-Makker, P., et al., *Inhibition of human cancer cell growth and metastasis in nude mice by oral intake of modified citrus pectin.* J Natl Cancer Inst, 2002. **94**(24): p. 1854-62.
166. Chauhan, D., et al., *A novel carbohydrate-based therapeutic GCS-100 overcomes bortezomib resistance and enhances dexamethasone-induced apoptosis in multiple myeloma cells.* Cancer Res, 2005. **65**(18): p. 8350-8.
167. Streetly, M.J., et al., *GCS-100, a novel galectin-3 antagonist, modulates MCL-1, NOXA, and cell cycle to induce myeloma cell death.* Blood, 2010. **115**(19): p. 3939-48.
168. Glinsky, V.V. and A. Raz, *Modified citrus pectin anti-metastatic properties: one bullet, multiple targets.* Carbohydr Res, 2009. **344**(14): p. 1788-91.
169. Eddy, A.A., *Progression in chronic kidney disease.* Adv Chronic Kidney Dis, 2005. **12**(4): p. 353-65.
170. Tamura, M., et al., *Progressive renal dysfunction and macrophage infiltration in interstitial fibrosis in an adenine-induced tubulointerstitial nephritis mouse model.* Histochem Cell Biol, 2009. **131**(4): p. 483-90.
171. Engle, S.J., et al., *Adenine phosphoribosyltransferase-deficient mice develop 2,8-dihydroxyadenine nephrolithiasis.* Proc Natl Acad Sci U S A, 1996. **93**(11): p. 5307-12.

172. Stockelman, M.G., et al., *Chronic renal failure in a mouse model of human adenine phosphoribosyltransferase deficiency.* Am J Physiol, 1998. **275**(1 Pt 2): p. F154-63.
173. Kamatani, N., et al., *Genetic and clinical studies on 19 families with adenine phosphoribosyltransferase deficiencies.* Hum Genet, 1987. **75**(2): p. 163-8.
174. Nasr, S.H., et al., *Crystalline nephropathy due to 2,8-dihydroxyadeninuria: an under-recognized cause of irreversible renal failure.* Nephrol Dial Transplant, 2010. **25**(6): p. 1909-15.
175. Edvardsson, V., et al., *Clinical features and genotype of adenine phosphoribosyltransferase deficiency in iceland.* Am J Kidney Dis, 2001. **38**(3): p. 473-80.
176. Benedetto, B., et al., *Adenine phosphoribosyltransferase deficiency and renal allograft dysfunction.* Am J Kidney Dis, 2001. **37**(5): p. E37.
177. Kaartinen, K., et al., *Adenine phosphoribosyltransferase deficiency as a rare cause of renal allograft dysfunction.* J Am Soc Nephrol, 2014. **25**(4): p. 671-4.
178. Greenwood, M.C., et al., *Renal failure due to 2,8-dihydroxyadenine urolithiasis.* Eur J Pediatr, 1982. **138**(4): p. 346-9.
179. Wada, T., et al., *Up-regulation of monocyte chemoattractant protein-1 in tubulointerstitial lesions of human diabetic nephropathy.* Kidney Int, 2000. **58**(4): p. 1492-9.
180. Myllymaki, J.M., et al., *Severity of tubulointerstitial inflammation and prognosis in immunoglobulin A nephropathy.* Kidney Int, 2007. **71**(4): p. 343-8.
181. Yokoyama, H., et al., *Urinary levels of chemokines (MCAF/MCP-1, IL-8) reflect distinct disease activities and phases of human IgA nephropathy.* J Leukoc Biol, 1998. **63**(4): p. 493-9.
182. Ding, L., et al., *Mycophenolate mofetil combined with prednisone for diffuse proliferative lupus nephritis: a histopathological study.* Lupus, 2004. **13**(2): p. 113-8.
183. Anders, H.J., V. Vielhauer, and D. Schlondorff, *Chemokines and chemokine receptors are involved in the resolution or progression of renal disease.* Kidney Int, 2003. **63**(2): p. 401-15.
184. Segerer, S., P.J. Nelson, and D. Schlondorff, *Chemokines, chemokine receptors, and renal disease: from basic science to pathophysiologic and therapeutic studies.* J Am Soc Nephrol, 2000. **11**(1): p. 152-76.
185. Vielhauer, V., et al., *Obstructive nephropathy in the mouse: progressive fibrosis correlates with tubulointerstitial chemokine expression and accumulation of CC chemokine receptor 2- and 5-positive leukocytes.* J Am Soc Nephrol, 2001. **12**(6): p. 1173-87.
186. Rodriguez-Iturbe, B., et al., *Role of immunocompetent cells in nonimmune renal diseases.* Kidney Int, 2001. **59**(5): p. 1626-40.
187. Abbate, M., C. Zoja, and G. Remuzzi, *How does proteinuria cause progressive renal damage?* J Am Soc Nephrol, 2006. **17**(11): p. 2974-84.
188. Sean Eardley, K. and P. Cockwell, *Macrophages and progressive tubulointerstitial disease.* Kidney Int, 2005. **68**(2): p. 437-55.
189. Yokozawa, T., et al., *Animal model of adenine-induced chronic renal failure in rats.* Nephron, 1986. **44**(3): p. 230-4.
190. Santana, A.C., et al., *Thalidomide suppresses inflammation in adenine-induced CKD with uraemia in mice.* Nephrol Dial Transplant, 2013.
191. Santana, A.C., et al., *Thalidomide suppresses inflammation in adenine-induced CKD with uraemia in mice.* Nephrol Dial Transplant, 2013. **28**(5): p. 1140-9.
192. Jia, T., et al., *A novel model of adenine-induced tubulointerstitial nephropathy in mice.* BMC Nephrol, 2013. **14**: p. 116.
193. Shobeiri, N., M.A. Adams, and R.M. Holden, *Vascular calcification in animal models of CKD: A review.* Am J Nephrol, 2010. **31**(6): p. 471-81.
194. Liu, F.T., et al., *Expression and function of an IgE-binding animal lectin (epsilon BP) in mast cells.* Immunopharmacology, 1993. **26**(3): p. 187-95.
195. Pilette, C., et al., *Increased galectin-3 expression and intra-epithelial neutrophils in small airways in severe COPD.* Eur Respir J, 2007. **29**(5): p. 914-22.
196. Pini, M., et al., *Rosiglitazone improves survival and hastens recovery from pancreatic inflammation in obese mice.* PLoS One, 2012. **7**(7): p. e40944.

197. Bustin, S.A., et al., *The MIQE guidelines: minimum information for publication of quantitative real-time PCR experiments.* Clin Chem, 2009. **55**(4): p. 611-22.
198. Levey, A.S., *Measurement of renal function in chronic renal disease.* Kidney Int, 1990. **38**(1): p. 167-84.
199. Song, S., et al., *Serum cystatin C in mouse models: a reliable and precise marker for renal function and superior to serum creatinine.* Nephrol Dial Transplant, 2009. **24**(4): p. 1157-61.
200. Danella Polli, C., et al., *Monocyte Migration Driven by Galectin-3 Occurs through Distinct Mechanisms Involving Selective Interactions with the Extracellular Matrix.* ISRN Inflamm, 2013. **2013**: p. 259256.
201. Hesse, M., et al., *Differential regulation of nitric oxide synthase-2 and arginase-1 by type 1/type 2 cytokines in vivo: granulomatous pathology is shaped by the pattern of L-arginine metabolism.* J Immunol, 2001. **167**(11): p. 6533-44.
202. Nair, M.G., et al., *Chitinase and Fizz family members are a generalized feature of nematode infection with selective upregulation of Ym1 and Fizz1 by antigen-presenting cells.* Infect Immun, 2005. **73**(1): p. 385-94.
203. Raes, G., et al., *FIZZ1 and Ym as tools to discriminate between differentially activated macrophages.* Dev Immunol, 2002. **9**(3): p. 151-9.
204. Chang, N.C., et al., *A macrophage protein, Ym1, transiently expressed during inflammation is a novel mammalian lectin.* J Biol Chem, 2001. **276**(20): p. 17497-506.
205. Falcone, F.H., et al., *A Brugia malayi homolog of macrophage migration inhibitory factor reveals an important link between macrophages and eosinophil recruitment during nematode infection.* J Immunol, 2001. **167**(9): p. 5348-54.
206. Welch, J.S., et al., *TH2 cytokines and allergic challenge induce Ym1 expression in macrophages by a STAT6-dependent mechanism.* J Biol Chem, 2002. **277**(45): p. 42821-9.
207. Loke, P., et al., *IL-4 dependent alternatively-activated macrophages have a distinctive in vivo gene expression phenotype.* BMC Immunol, 2002. **3**: p. 7.
208. Nair, M.G., D.W. Cochrane, and J.E. Allen, *Macrophages in chronic type 2 inflammation have a novel phenotype characterized by the abundant expression of Ym1 and Fizz1 that can be partly replicated in vitro.* Immunol Lett, 2003. **85**(2): p. 173-80.
209. Clements, M., et al., *Differential Ly6C Expression after Renal Ischemia-Reperfusion Identifies Unique Macrophage Populations.* J Am Soc Nephrol, 2015.
210. Gibbons, M.A., et al., *Ly6Chi monocytes direct alternatively activated profibrotic macrophage regulation of lung fibrosis.* Am J Respir Crit Care Med, 2011. **184**(5): p. 569-81.
211. Hochst, B., et al., *Differential induction of Ly6G and Ly6C positive myeloid derived suppressor cells in chronic kidney and liver inflammation and fibrosis.* PLoS One, 2015. **10**(3): p. e0119662.
212. Farris, A.B., et al., *Morphometric and visual evaluation of fibrosis in renal biopsies.* J Am Soc Nephrol, 2011. **22**(1): p. 176-86.
213. Hadi, A.M., et al., *Rapid quantification of myocardial fibrosis: a new macro-based automated analysis.* Cell Oncol (Dordr), 2011. **34**(4): p. 343-54.
214. Meester, I., A.G. Rosas-Taraco, and M.C. Salinas-Carmona, *Retnla down-regulation and IL-13-rich environment correlate with inflammation severity in experimental actinomycetoma by Nocardia brasiliensis.* Pathog Dis, 2013. **67**(3): p. 214-20.
215. Stoermer, K.A., et al., *Genetic ablation of arginase 1 in macrophages and neutrophils enhances clearance of an arthritogenic alphavirus.* J Immunol, 2012. **189**(8): p. 4047-59.
216. Cuervo, H., et al., *Myeloid-derived suppressor cells infiltrate the heart in acute Trypanosoma cruzi infection.* J Immunol, 2011. **187**(5): p. 2656-65.
217. Cooper, D., et al., *The effect of galectins on leukocyte trafficking in inflammation: sweet or sour?* Ann N Y Acad Sci, 2012. **1253**: p. 181-92.
218. Cooper, D., L.V. Norling, and M. Perretti, *Novel insights into the inhibitory effects of Galectin-1 on neutrophil recruitment under flow.* J Leukoc Biol, 2008. **83**(6): p. 1459-66.
219. Springer, T.A., *Traffic signals for lymphocyte recirculation and leukocyte emigration: the multistep paradigm.* Cell, 1994. **76**(2): p. 301-14.

220. Hulstrom, D. and E. Svensjo, *Intravital and electron microscopic study of bradykinin-induced vascular permeability changes using FITC-dextran as a tracer.* J Pathol, 1979. **129**(3): p. 125-33.
221. Kubes, P. and J.P. Gaboury, *Rapid mast cell activation causes leukocyte-dependent and -independent permeability alterations.* Am J Physiol, 1996. **271**(6 Pt 2): p. H2438-46.
222. Baatz, H., et al., *Kinetics of white blood cell staining by intravascular administration of rhodamine 6G.* Int J Microcirc Clin Exp, 1995. **15**(2): p. 85-91.
223. Gittens, B.R., R.D. Wright, and D. Cooper, *Methods for assessing the effects of galectins on leukocyte trafficking.* Methods Mol Biol, 2015. **1207**: p. 133-51.
224. Gavins, F.N. and B.E. Chatterjee, *Intravital microscopy for the study of mouse microcirculation in anti-inflammatory drug research: focus on the mesentery and cremaster preparations.* J Pharmacol Toxicol Methods, 2004. **49**(1): p. 1-14.
225. Lim, L.H., B.S. Bochner, and E.M. Wagner, *Leukocyte recruitment in the airways: an intravital microscopic study of rat tracheal microcirculation.* Am J Physiol Lung Cell Mol Physiol, 2002. **282**(5): p. L959-67.
226. Lopez, B., et al., *Myocardial fibrosis in chronic kidney disease: potential benefits of torasemide.* Kidney Int Suppl, 2008(111): p. S19-23.
227. Disthabanchong, S., *Vascular calcification in chronic kidney disease: Pathogenesis and clinical implication.* World J Nephrol, 2012. **1**(2): p. 43-53.
228. Shinagawa, H. and S. Frantz, *Cellular immunity and cardiac remodeling after myocardial infarction: role of neutrophils, monocytes, and macrophages.* Curr Heart Fail Rep, 2015. **12**(3): p. 247-54.